TECHNO SCIENCE ACADEMY
The International Open Access Publisher

IJSRST

**National Conference
on
"Smart Materials and Devices for
Sustainable Technologies"
NCSMDST-2022**

Organized By
Department of Physics & IQAC
Shri Lal Bahadur Shastri Degree College, Gonda, U.P.
(Affiliated to Dr. R.M.L. Avadh University Ayodhya, U.P.)
Co-Sponsored by
Satya Saroj Foundation, Gonda
&
State Bank of India, Main Branch, Gonda

INTERNATIONAL JOURNAL OF SCIENTIFIC

RESEARCH IN SCIENCE AND TECHNOLOGY

National Conference on 'Smart Materials and Devices for Sustainable Technologies' (NCSMDST-2022)

20th and 21st June, 2022

Organised by

(The International Open Access Publisher)

website: www.technoscienceacademy.com

Chief Patron
Prof. Akhilesh Kumar Singh
Vice Chancellor
Dr. R.M.L. Avadh University, Ayodhya

Patron
Dr. Ujjwal Kumar
President
DM, Gonda

Co-Patron
Varsha Singh
Vice President
Shri Umesh Shah, Secretary

President
Prof. R. K. Pandey
Principal

Convenor
Prof. Jitendra Singh
Head Department of physics

Co-Convenor
Prof. S. N. Mishra
Director - Research Center

Prof. R. S. Singh
IQAC Coordinator

Prof. S. K. Pandey
Head, Deptt. of Mathematics

Prof. Mukul Sinha
Head, Deptt. of Zoology

Prof. S. K. Srivastava
Head, Deptt. of Botany

Dr. S. C. Mishra
Head, Deptt. of Chemistry

Organizing Secretary
Santosh Kumar Srivastava
Assistant Professor, Deptt. of Physics
Mobile No.: 7318541875

Organizing Committee
Dr. Rekha Sharma, Deptt. of Botany
Dr. Pushyamitra Mishra, Deptt. of Chemistry
Sri Manish Sharma, Deptt. of Mathematics
Sri Shishir Tripathi, Deptt. of Zoology
Dr. Dev Narayan Pandey, Deptt. of Physics
Dr. Ankit Maurya, Deptt. of Mathematics

Inaugural Lecture
by

Prof. S. N. Shukla
Department Of Physics
Dr. R.M.L. Avadh University Ayodhya

Prof D. K. Dwivedi
Dean of Faculty Affairs
MMMUT, Gorakhpur

Prof S. K. Tripathi
Dean Research and
Consultancy
Mahatma Gandhi
Central University
Motihari Bihar

Prof. R.S. Singh
OSD, Maha Yogi Guru Shri
Gorakshanath Shodh Peeth
and
Department of Physics,
DDU Gorakhpur University

Dr A. K. Maurya
Department of Physics,
School of Physical and
Decision Sciences
Babasaheb Bhimrao
Ambedkar University, Lucknow

SUB-THEMES OF THE CONFERENCE
- Carbon nanostructure modified life Po4 cathodes for lithium-ion battery applications.
- Failure analysis of bubble canopy: MiG-29 Aircraft.
- Effect of additives on gelation of methylcellulose based ophthalmic thermo-responsive in situ gels.
- Surface plasmon resonance for C-reactive protein detection in human plasma.
- Sustainable waste water treatment plants networks design through multi-objective optimization.
- Magnesium ferrite/polyvinyl alcohol nanocomposites fabrication and characterization.
- Single crystal silicon nanomembrane molecular sieves.
- Robust sustainable infrastructure using smart materials and technologies.
- Carbon based smart organic devices and bio product derived sustainable technology application.
- Eco friendly nanomaterials for flexible sensors, opto-electronics and solar energy harvesting.
- Effects of porosity distribution on properties of multifunctional foam structure.
- Wheat bran fiber as resources for industries.
- Optoelectronic diffusion waves in semiconductors: carrier lifetime chronotomography imaging of Si solar cells.
- Power, Energy, Efficient resource management, and Energy Harvesting
- Things to Cloud: Computation and Communication Gateways
- Semantic technologies: Information and data models for interoperability
- Other concerning topics are also accepted.

CONTENTS

A Role of GST in Sustainable Technology

Nitin Kumar Sharma[1], BinodPratap Singh[2]
[1]Ph.D. Research Scholar, Dr. R. M. L. Awadh University, Ayodhya, Uttar Pradesh, India
[2]Department of Commerce, Shri Lal Bahadur Shastri Degree Collage, Gonda, Uttar Pradesh, India

ABSTRACT

I. INTRODUCTION

The GST tax legislation is one of the methods used by the government to achieve its goal of long-term growth in all sectors, including sustainable technology gadgets. The purpose of this study is to learn more about the Goods and Services Tax (GST) and its consequences for the long-term growth of sustainable technologies, as well as to figure out what role GST plays as a tax reform. The worldwide community is presented with a number of essential long-term concerns in today's world. Under the new concept of sustainable development with sustainable technology, the settlement of which is relevant to each country, embracing technology will have an influence on organizations' top line and bottom line now that we are in the digitalization era. Technology provides for a re-examination of the business process as well as automation when it comes to GST compliance. The basics of revamping the domestic tax system to make it more ecologically friendly are examined. New characteristics for energy systems have evolved from the use of digital technology in the generation and use of power. According to the article, a comprehensive strategy to change current taxation in line with sustainable development is necessary.

II. MEANING OF SUSTAINABLE TECHNOLOGY

Sustainable technology is defined as innovation that considers natural resources while also promoting economic and social progress. These technologies aim to provide a sustainable product while substantially reducing the dangers to the environment and ecology.

There are several ways to describe sustainability in technology: Substitution: The method encourages a switch in the manufacture of the product from non-biodegradable to biodegradable ingredients. Technology that is sustainable has already found its way into general usage and innovation. The following are some examples of sustainable technology and innovations:

- Public and electric transportation are also available.
- Light-emitting diode (LED) technology
- Solar energy
- Technologies for carbon capture and storage

- Buildings and construction techniques that are self-sufficient and LEED certified

III. GST WITH SUSTAINABLE TECHNOLOGY

The Goods and Services Tax (GST) system's technological foundation has modified a few features on its portal during the past month to strengthen the system and enable a glitch-free tax payment facility. The GST is a single tax that replaces all other indirect taxes. This will completely alter the tax system, including tax rates, how prices are determined, and how taxes are paid. One of the most pressing topics on everyone's mind, besides the biggest change that will occur, is how technology will be applied to facilitate corporate and governmental operations. Because many taxes are complicated, the government is now unable to identify tax evasion. By implementing GST, the Indian government hopes to simplify and streamline the tax system. The largest problem, though, is preserving a record of the millions of invoices that taxpayers will be uploading each month. It is critical to use solid technology to simplify the entire taxation process, including invoice generation, uploading, paying, and filing taxes. In addition to reducing fraud, it should also cut down on claim duplication. Everything will be achievable without the need to use physical Labour. GSTN will also include additional techniques to eliminate duplication as well as alerting capabilities, offline functionality, mobile and tablet interfaces, and other features.Technology is assisting tax administrations in reducing tax risks and increasing efficiency. A number of concerns must be resolved to provide taxpayers with a smooth experience. Any firm must keep up with the latest technological developments. Innovation and the use of cutting-edge technologies are more important than ever. The time has come to embrace technology, whether it be for automated processes or remote operations. These days, technology permeates every aspect of business and trade. Technology and innovation are redefining the many stages of production in both developed and emerging countries. They are encouraging new opportunities for communication and corporate communication in addition to providing cost-effective solutions. In order to provide a hassle-free experience, taxation is also progressively using novel technological integration strategies.

IV. TECHNOLOGY MADE GST SIMPLER

The Goods and Services Tax (GST) has elevated India to the world arena, making it one of the most attractive countries for international investment. However, in order to improve this rating, the government is continually working to make compliance easier and to lower the average time it takes a firm to file tax returns, forms, and other documents. The decision to convert all compliances to a faceless schema also helps to improve the compliance experience. The E-way bill system and the E-invoicing system are both classic instances of the government's desire to transition from paper to paperless E-compliances. It's hard for a taxpayer to avoid employing technology while complying with rules in a country where the government is moving toward tech-based compliance.

In terms of technology usage, corporations and governments throughout the world are well ahead of India. Despite the fact that India is late to the game, we are rapidly gaining ground. The necessity of investing in tax

technology has been recognized by Indian conglomerates, which have begun to regard taxation as much more than a back-office duty. Enterprise Resource Planning, or ERP, as it is popularly known, is the primary and essential pre-requisite for taking the initial steps toward GST compliance. The ERP function, which was previously primarily used in accounting, is now widely employed in the tax function as well. Transactions and invoices in large companies are massive. Manually submitting taxes and uploading invoices are common issues for such Organisations. The ERP enablers and connectors have saved the day in this situation. ERP enablers and connectors have come to the rescue of Organisations in this situation. ERP Connectors synchronize data and change it to a format that is GST compliant.

Digital firms are gaining traction in a wide range of industries throughout the world. As a result of the increase in digitalization, businesses are reorienting themselves to developing technologies in taxes, particularly in terms of legal rules and procedural elements. Today, a methodical framework is required to address the technical complexity of taxes. While tax authorities are digitizing tax administration, including data sharing and reconciliation between income tax, GST, and customs, resulting in more transactional inspection, there is unfair pressure on businesses to cut costs within the tax function. Integration of indirect tax procedures with modern-day technology in GST has opened up new vistas for taxpayers and the government, resulting in a slew of advantages.

V. CONCLUSION

Technology will also enable efficient tax administration for registration, return filing, data exchange, and effective inquiry, monitoring, auditing, and performance analysis with little or no human involvement. However, if processes are streamlined, the two major goals – reducing tax evasion and boosting tax collection while making it easier for taxpayers to comply – will be realized. Though changing technology may appear to some as a disruption, it can only be described as a chance. It comes with a slew of advantages that can only be realized if the technology is put into place and put to use. It's also important to have an open mind about technology; otherwise, it'll appear to be an intruder, which it isn't. The launch has rekindled expectations that India's fiscal reform agenda could gain traction and broaden the economy. On the other hand, there are concerns about disruption, which are rooted in what is seen as a hasty transition that may not be in the country's best interests. Nobody can deny that the future of taxation would be unthinkable without technological advancements. The digital age began a few years ago, but there has been little shift until lately. In recent years, the rise of technology, combined with e-governance, has given tech-based compliance the impetus it requires. As a result, the only path forward is forward. A technological revolution in tax compliance is expected in the future, which will undoubtedly revolutionize the way compliance is handled. It will also have a variety of user-friendly features, such as offline functionality, alerts, a mobile and tablet interface, and more data duplication protection mechanisms. Businesses will face a number of obstacles during the early phases of implementation because this tax structure is being introduced for the first time in India.

VI. REFERENCES

[1].   https://www.rubicon.com/sustainability-hub/articles/what-is-sustainable-technology/

[2].   https://www.taxmann.com/research/gst-new/top-story/105010000000021653/gst-and-technology-all-you-need-to-know-experts-opinion

[3].   https://www.cygnetgsp.in/adopting-changes-under-gst-got-easier-with-technology/

[4].   GST Impact of Sustainable Development in Indian Economy Dr. Kasthuri Assistant Professor in Economics, A. D. M College for women (Autonomous), Nagapattinam, Tamil Nadu, India

[5].   https://markitsolutions.in/why-is-technology-the-epicentre-of-gst-implementation/

A Theoretical Study of Half- Heusler Compound LaPtSb

Pallavi, Chandravir Singh

Department of Physics, Agra College Agra 282002, Uttar Pradesh, India

ABSTRACT

As a result of the severe energy crisis and environmental degradation in the world, the demand for a sustainable and clean energy source is growing. Thermoelectric materials can convert waste heat directly into energy, and they've gotten a lot of attention from the scientific and industrial worlds. LaPtSb, a half-Heusler compound, being studied for its electrical and transport properties, by using first-principles computations in conjunction with semi-classical Boltzmann theory , the theory of deformation potential .When LaPtSb compared with other half-Heusler compounds, at room temperature, the power factor is clearly higher ,especially for the n-type system. In addition to the low heat conductivity of the lattice, the thermoelectric figure of merit (ZT) of LaPtSb can be optimised to a new high value of 2.2 by fine-tuning the carrier concentration.

Keywords: Half Heusler, Thermoelectric, LaPtSb, Deformation Potential.

I. INTRODUCTION

Due to their thermal stability, mechanical toughness, and moderate ZT, half-Heusler (HH) thermoelectric (TE) materials have garnered a great deal of research interest over the past 20 years. This material system has the potential to be used in applications requiring medium to high temperatures, which is in the same range as the majority of industrial waste heat sources. We succinctly cover the most recent developments and improvements in HH thermoelectric materials in this mini-review essay. Some efficient methods are currently accessible, such as HH nanocomposites, which use bigger atomic mass and size differences to boost phonon scattering and hence reduce heat conductivity even further by producing ternary systems[1-5]. The vast amount of waste heat that is dissipated in industrial applications and vehicle exhaust gas can be scavenged by thermoelectric (TE) materials in a less expensive and ecologically friendly manner. Medium-high temperature TE materials are preferred for waste heat recovery applications due to the relative high temperature (500 C) of exhaust gas in the hot side. PbTe , skutterudites and half-Heuslers have received the greatest attention among the TE material options for medium-high temperature applications[6-9]. Skutterudites, on the other hand, primarily suffer from their low thermal stability, whereas PbTe materials are known for their toxicity and inadequate mechanical strength for large-scale industrial application reasons. Due to current research efforts, half-Heusler materials display respectable performance metrics and lack the aforementioned shortcomings of their competitors, which means they are promising thermoelectric for medium to high temperature. Bulk TE materials having a dimensionless figure of merit (ZT) greater than 1

are preferred for TE technology to become competitive. The formula for ZT is $(S^2 \sigma/k)T$, where S, s, k, and T stand for the Seebeck coefficient, electrical conductivity, thermal conductivity, and absolute working temperature, respectively. As a result, we choose low thermal conductivity and high electrical conductivity and Seebeck coefficient. Due to their comparatively high thermal conductivity, p-type and n-type half-Heuslers' measured peak ZT previously was only around 0.5 and 0.8, respectively [10-14]. Our group has recently achieved ZT 1.0 for both p- and n-type half-Heuslers by effectively implementing the nanocomposite technique into the half-Heusler material system[15-19].

The need for sustainable and clean energy sources is growing in importance as a result of the severe energy crisis and environmental pollution. Thermoelectric materials, which are capable of directly converting waste heat into energy, have drawn a lot of interest from both the scientific and business communities[20,21]. The dimensionless figure of merit, which takes into account the Seebeck coefficient, electrical conductivity, absolute temperature, lattice structure, and electronic thermal conductivity, is typically used to assess the performance of thermoelectric materials. In order to increase power factor and/or limit thermal conductivity , a thermoelectric material must behave as a phonon-glass electron-crystal (PGEC). Although these transport coefficients are typically connected to one another, it is still a fantastic idea [22]. Because of their narrow band gaps, great temperature stability, significant Seebeck coefficients, and moderate electrical conductivities, certain of the intermetallic compounds in the ternary half-Heusler (HH) system have the potential to be thermoelectric materials. However, it was shown that the majority of HH compounds have greater thermal conductivities, on the order of 10 W/mK, which is not ideal for high performance thermoelectric materials . However, these ZT values of HH compounds remain low compared with the desired value of roughly 3.0, which can compete with the efficiency of traditional freezers or power generators. The thermoelectric properties of a few HH compounds have been widely studied during the past two decades. Searching for thermoelectric materials with intrinsically low thermal conductivity is an effective way to increase ZT value [23]. The thermal conductivities of numerous HH compounds were recently theoretically examined by Carrete et al., who discovered that the compound LaPtSb had a particularly low lattice thermal conductivity of 1.72 W/mK at ambient temperature[24]. Therefore, it is intriguing to inquire as to whether such a molecule can demonstrate improved thermoelectric performance. In this study, multiscale calculations that incorporate first-principles calculations, Boltzmann theory, and deformation potential theory are used to predict the thermoelectric properties of LaPtSb. We show that a maximum ZT value of 2.2 for an n-type system at room temperature can be obtained by carefully controlling the carrier concentration of LaPtSb, making it a very interesting option for high performance thermoelectric materials[25].

II. COMPUTATIONAL METHODS

The projector-augmented wave (PAW) approach , as used in the Vienna ab initio simulation package (VASP), is used for LaPtSb's structure optimization and electronic structure computations. Perdew-Burke-Ernzerhof (PBE) with the generalised gradient approximation is used to treat exchange and correlation energy (GGA).

To act on the La 5d and Pt 5d states, it is important to include a Hubbard-type term U , which can considerably enhance PBE quality and provide the proper electronic structure .

III. OBSERVATIONS AND CONCLUSIONS

HH compounds crystallise in the space group F m 43 cubic MgAgAs-type structure. In Wyckoff coordinates, the La atoms are at location 4a(0,0,0), the Pt atoms are at position 4c(1/4,1/4,1/4), and the Sb atoms are at position 4b(1/2,1/2,1/2) in the unit cell of the HH compound LaPtSb shown in Figure 1. The structure can also be thought of as four interpenetrating fcc lattices, each of which has a lattice of vacancies as well as a lattice of La, Pt, Sb, and Sb atoms. A rock salt structure is created by the La and Sb atoms. LaPtSb's optimised lattice constant is 6.87. The primitive cell's total valence electron count (VEC) meets the VEC=18 requirement, which is typically found in HH compounds. As illustrated in Figure 2 along the high-symmetry lines of the irreducible Brillouin zone, we initially concentrate on the electronic band structure of LaPtSb (IBZ). We can see that the direct band gap is 0.23 eV since the valence band maximum (VBM) and conduction band minimum (CBM) are both situated at the same place. LaPtSb compound's derived relaxation times for both p- and n-type carriers can also be observed from the dispersion relations around CBM and VBM in Fig. 2, it is evident that electrons have a far longer relaxation period than holes, which is mostly due to the latter's substantially larger density-of-states effective mass. Remember that other systems like few-layer black phosphorus and phosphorene have also been discovered to have such a large variation in the relaxation period between electrons and holes. However, unlike common thermoelectric materials like Bi_2Te_3 and MoS_2 , the relaxation times of both electrons and holes are longer, indicating that LaPtSb compound has better thermoelectric performance. Knowing the thermal conductivity, which incorporates the contributions from both phonons (l) and charge carriers (e), is necessary to calculate the ZT value of the LaPtSb complex. The electronic thermal conductivity may be easily calculated using the Wiedemann-Franz Law is displayed as a function of carrier concentration at ambient temperature. We can see that e's behaviour resembles with that electrical conductivity in Fig. 3 . This makes sense given that there is little variation in the Lorenz number as determined with respect to carrier concentration. For the phonon component, we use the conclusion reached by Carrete et al., who found that by solving the phonon Boltzmann transport equation, a thermal conductivity of 1.72 W/mK at ambient temperature could be expected. When compared to other HH compounds, a thermal conductivity with such a low value is highly desirable for thermoelectric applications. By entering all the transport coefficients into Equation, we can now assess the thermoelectric performance of the compound LaPtSb . The room temperature ZT values are presented in Figure 4 as a function of carrier concentration. At 1.2×10^{19} cm^{-3}, a maximal ZT of 1.3 is observed for the p-type system. When the carrier concentration is tuned to 3.3×10^{19} cm-3, the ZT value for the n-type system can be further increased to 2.2. In particular, the typical (Ti, Zr, and Hf)NiSn-based and (Ti, Zr, and Hf)CoSb-based HH compounds have ZT values that are higher than many other good thermoelectric materials. LaPtSb is one of numerous rare-earth based HH compounds that have had their thermoelectric properties experimentally recorded , despite the fact that there is currently no study on LaPtSb (Ln=Ho, Er, Dy), ScMSb (M=Ni, Pd, Pt),

YMSb (M=Ni, Pd, Pt), ErPdX (X=Sb, Bi), PtYSb, and YNi .These HH compounds have substantially smaller power factors and higher lattice thermal conductivities than the LaPtSb predicted in the current work. The thermoelectric performances are consequently inferior to those of LaPtSb.

IV. Summary

In conclusion, our theoretical study shows that the HH compound LaPtSb could be tuned to exhibit very strong thermoelectric performance. This performance is thought to be aided by the comparatively large power factor and low lattice thermal conductivity. The room temperature ZT value for an n-type system can be increased to as high as 2.2 at a moderate carrier concentration of 3.3×10^{19} cm-3, which is higher than that of the HH compounds previously reported. Our calculations indicate that the n-type LaPtSb is an extremely promising thermoelectric material, and significant efforts should be put toward producing the more efficient p-type LaPtSb in order to construct functional thermoelectric modules based on this HH compound.
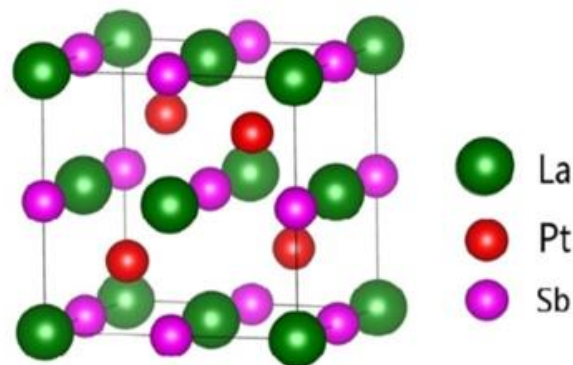

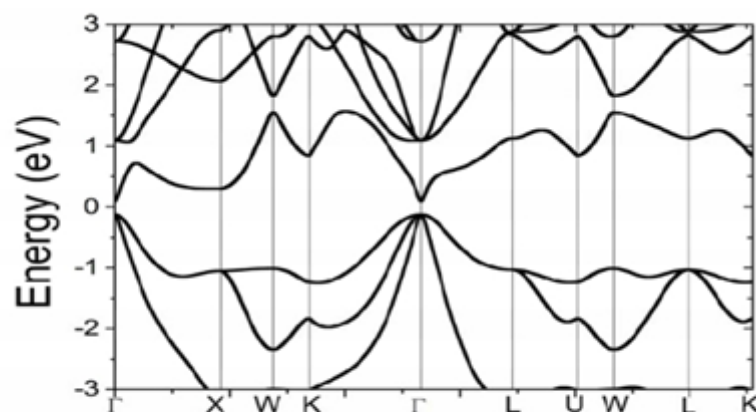**Figure 1** (Color online) The unit cell of the half-Heusler compound LaPtSb.
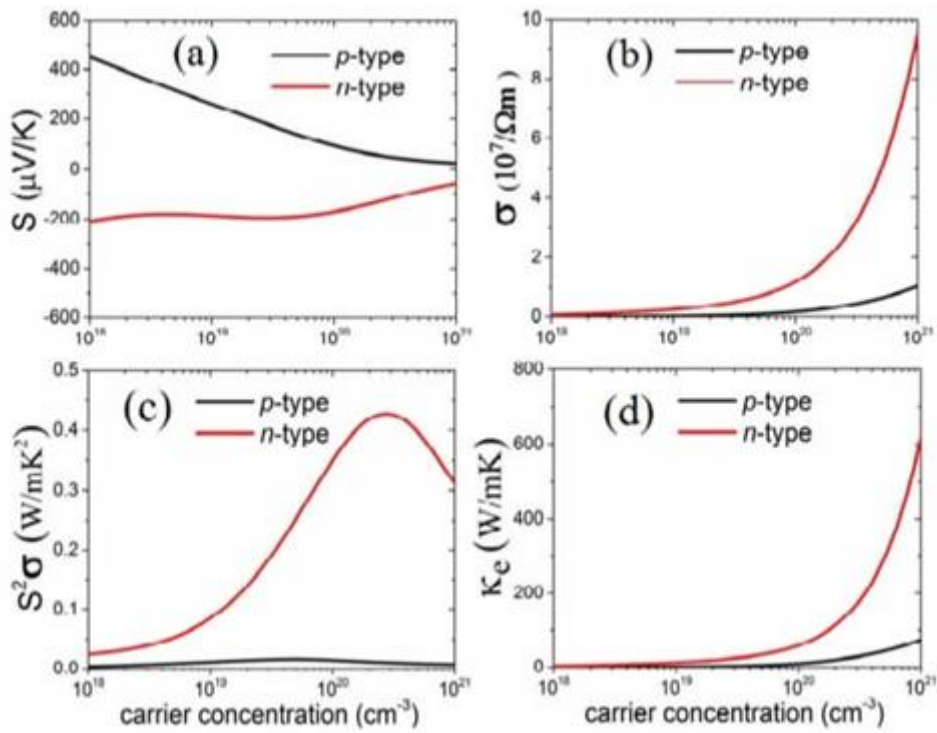

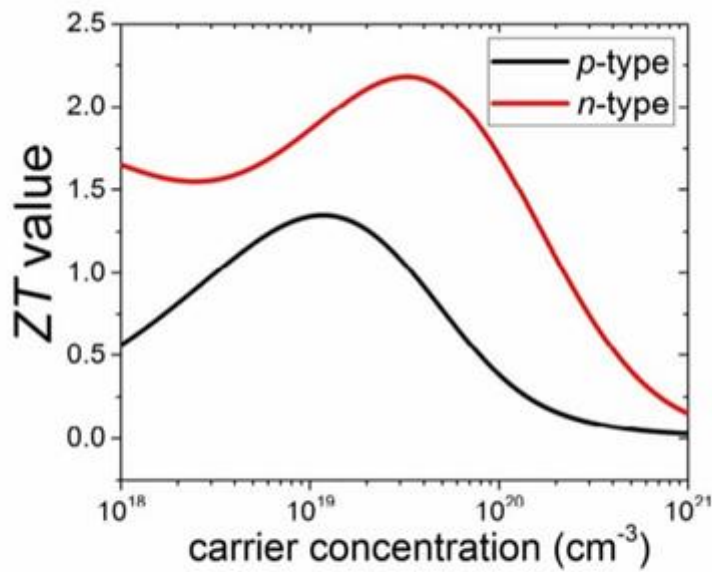**Figure 2** The calculated energy band structure of LaPtSb.

Figure 3

Figure 4 The calculated ZT values of LaPtSb as a function of carrier concentration at room temperature.

V. REFERENCES

[1]. L.E. Bell, Science 321 (2008) 1457.

[2]. J.H. Yang, F.R. Stabler, J. Electron. Mater. 38 (2009) 1245.

[3]. J.P. Heremans, V. Jovovic, E.S. Toberer, A. Saramat, K. Kurosaki, A. Charoenphakdee, S. Yamanaka, G.J. Snyder, Science 321 (2008) 554.

[4]. Y.Z. Pei, X.Y. Shi, A. LaLonde, H. Wang, L.D. Chen, G.J. Snyder, Nature 473 (2011) 66.

[5]. B.C. Sales, D. Mandrus, R.K. Williams, Science 272 (1996) 1325.

[6]. C. Uher, J. Yang, S. Hu, D.T. Morelli, G.P. Meisner, Phys. Rev. B 59 (1999) 8615.

[7]. S.J. Poon, Recent trends in thermoelectric materials research II, in: T.M. Tritt (Ed.), Semi-conductors and Semimetals, vol. 70, Academic, New York, 2001, pp. 37.

[8]. S.R. Culp, J.W. Simonson, S.J. Poon, V. Ponnambalam, J. Edwards, T.M. Tritt, Appl. Phys. Lett. 93 (2008) 022105.

[9]. S.R. Culp, S.J. Poon, N. Hickman, T.M. Tritt, J. Blumm, Appl. Phys. Lett. 88 (2006) 042106.

[10]. X. Yan, G. Joshi, W.S. Liu, Y.C. Lan, H. Wang, S. Lee, J.W. Simonson, S.J. Poon, T.M. Tritt, G. Chen, Z.F. Ren, Nano Lett. 11 (2011) 556.

[11]. G. Joshi, X. Yan, H.Z. Wang, W.S. Liu, G. Chen, Z.F. Ren, Adv. Energy Mater. 1 (2011) 643.

[12]. X. Yan, W.S. Liu, H. Wang, S. Chen, J. Shiomi, K. Esfarjani, H.Z. Wang, D.Z. Wang, G. Chen, Z.F. Ren, Energy Environ. Sci 5 (2012) 7543.

[13]. G. Joshi, T. Dahal, S. Chen, H.Z. Wang, J. Shiomi, G. Chen, Z.F. Ren, Nano Energy 2 (2013) 82.

[14]. S. Chen, K.C. Lukas, W.S. Liu, C.P. Opeil, G. Chen, Z.F. Ren, Adv. Energy Mater. 3 (2013) 1210.

[15]. X. Yan, W.S. Liu, S. Chen, H. Wang, Q. Zhang, G. Chen, Z.F. Ren, Adv. Energy Mater. 3 (2013) 1195.

[16]. G. Joshi, R. He, M. Engber, G. Samsonidze, T. Pantha, E. Dahal, K. Dahal, J. Yang, Y. C. Lan, B. Kozinsky, Z.F. Ren, Energy Environ. Sci. 7 (2014) 4070.

[17]. R. He, H.S. Kim, Y.C. Lan, D.Z. Wang, S. Chen, Z.F. Ren, RSC Adv. 4 (2014) 64711.

[18]. S.J. Poon, D. Wu, S. Zhu, W.J. Xie, T.M. Tritt, P. Thomas, R. Venkatasubramanian, J. Mater. Res. 26 (2011) 2795.

[19]. W.S. Liu, X. Yan, G. Chen, Z.F. Ren, Nano Energy 1 (2012) 42.

[20]. A. Xie, X.F. Tang, Q.J. Zhang, J. Poon, T.M. Tritt, Nanomaterials 2 (2012) 379.

[21]. S. Chen, Z.F. Ren, Mater. Today 16 (2013) 387.

[22]. W. Jeischko, Metall. Trans. 1 (1970) 3159.

[23]. Y. Xia, S. Bhattacharya, V. Ponnambalam, A.L. Pope, S.J. Poon, T.M. Tritt, J. Appl. Phys. 2000 (1952) 88.

[24]. K. Sekimoto, H. Muta, S. Yamanaka, J. Alloys Compd. 407 (2006) 326.

[25]. T. Wu, W. Jiang, X.Y. Li, Y.F. Zhou, L.D. Chen, J. Appl. Phys. 102 (2007) 103705.

Analysis of Resistance and Noise Measurement of P3HT Based Photovoltaic Cell: Organic Solar Cell

Kishun Bir

Department of Physics, Kisan PG College, Bahraich-271801, Uttar Pradesh, India

ABSTRACT

Noise studies constitute an important approach to study polymer based organic photovoltaic cell from the perspective for device application. Poly (3-hexylthiophene) is the most studied polymer for organic photovoltaic cell. We investigated the thermal noise power spectral density of polymer: P3HT based photovoltaic cells at 300 K with different input voltages. The power spectral density for P3HT material is in order of 10-21(V2Hz-1). We investigate the random errors in signal and observed frequency dependency phenomenon (1/f noise) and the resistance fluctuations of P3HT based photovoltaic cell as a function of frequency and from the result we can say the existence of noise comes in picture

Keywords: Photovoltaic cell, Power spectral density, Electrical noise

I. INTRODUCTION

Precision electronic measurements are present in modern physics. The lock-in is an extremely versatile measurement tool, and the ideas behind lock-in detection are often used in experimental physics. The purpose of using lock-in amplifier is to measure the resistance fluctuation and systematic errors present in device due to external sources at low frequency with respect to different input voltages[1].An important parameter for electrical transport is the fluctuations in resistance (or as it is called electrical "noise"), which can arise from fundamental reasons. The study of electrical noise is also important from the point of view of applications[2].

II. THE MEASUREMENT TECHNIQUE: LOCK-IN DETECTION

The lock-in amplifier is based on the cross-connection signal detection. The basic lock-in amplifier consists of a reference signal, an amplifier, a phase sensitive detector and a low pass filter. This signal is amplified to a level adequate for Phase sensitive detector, which multiplies it by internal reference[3]. Then filtering the ac frequencies and only keeping the dc component in signal, and the resultant signal that has exactly same frequency and phase as the reference signal can be measured[4].
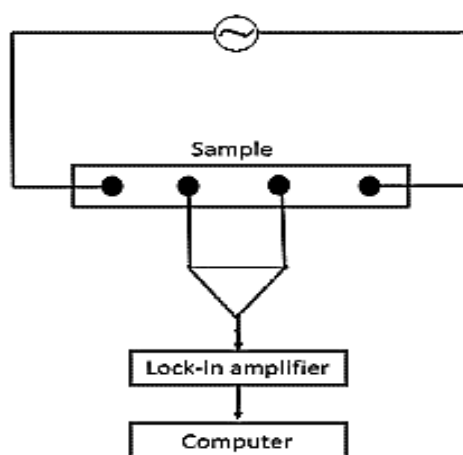
Fig1.1 Circuit used for 4 probe measurement

In fig 1.1 shows the circuit diagram which we used for this experiment.

III. BACKGROUND: ELECTRICAL NOISE

Noise in electronic devices mainly comes in picture due to many sources like instrument setup, environment etc. The most common noise is Nyquist noise which is mainly because of thermal fluctuations and flicker noise is occurs in any transistor through which a current is passing display a voltage fluctuation which contains spectrum goes as $1/f^\alpha$ where α is a constant and the value of α is in between 0.8-1.2[5]. In general, if the relaxation is occurring over a time scale τ, the autocorrelation function of the fluctuation $C(\tau)$ is an exponential function and the corresponding power spectral density $S(f)$ of the fluctuations is a Lorentzian given by-

S (f) $\propto 2\tau / 1+(2\pi f\tau)^2$ ....(1.1)

For $f_\tau >> 1$, the power spectrum $\propto 1/f^2$ while for $f_\tau << 1$ the power spectrum is white.

IV. SAMPLE PREPARATION

P3HT based π-conjugated polymer was synthesized by Prof. Sanjib Kumar Patra's research group (department of Chemistry, IIT Kharagpur) and PC61BM was obtained from Sigma Aldrich and used as received.P3HT (~8mg/ml) and PC61BM (~8mg/ml) were dissolved in a mixture of orthodichlorobenzene and 1,2,3,4-tetrahydronaphtalene with a donor to acceptor ratio of 1:1 in weight[6].The whole sample preparation took place in argon atmosphere. Devices were fabricated on Indium tin oxide (ITO) coated glass substrates from Macwin India. A PEDOT-PSS (1.3 wt.% dispersed in H_2O, Sigma Aldrich) layer of ~25 nm was spin coated onto the ITO at 4000 rpm for 30sec and then baked on a Si oil bath under vacuum at 120°C for 1 h. Solutions (P3HT and PC61BM mixture) were spin coated (~100 nm) onto the PEDOT-PSS coated ITO substrates at

1000 rpm for 60 sec[7]. The spin coated films were solvent annealed for 10 min at 100℃ on a Si oil bath under vacuum. Finally, an Al (~100 nm) layer was deposited by thermal Poly(3,4-ethylenedioxythiophene)poly(styrenesulfonate) abbreviated PEDOT:PSS is a polymer mixture of two ionomers[6] and The fullerene derivative [6,6]-phenyl-C61-butyric acid methyl ester (PCBM) has been an attractive electron acceptor material in photovoltaic cells and mostly used in conjunction with an electron donor material such as P3HT[15].

V. RESULT AND DISCUSSION

First we have investigated the absorption spectra of P3HT and P3HT: PCBM heterojunction in the wavelength range 200-1100 nm to compare the spectral response of the devices. From fig1.3 we can say that the devices shows significant absorption in the wavelength range 290-795 nm with

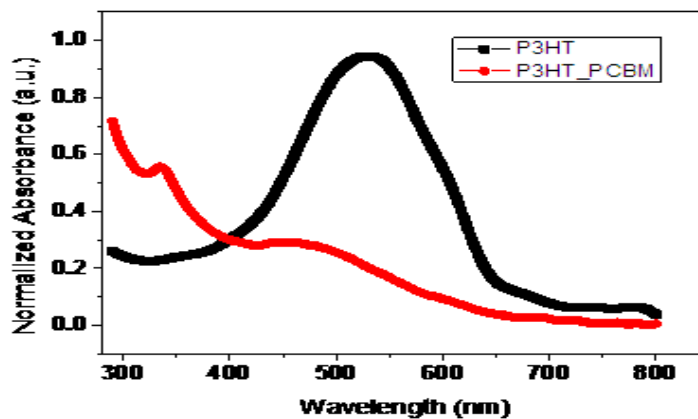peak at ~535 nm and 420 nm respectively.

Fig 1.3 Shows the absorption spectra of P3HT and P3HT:PCBM device.
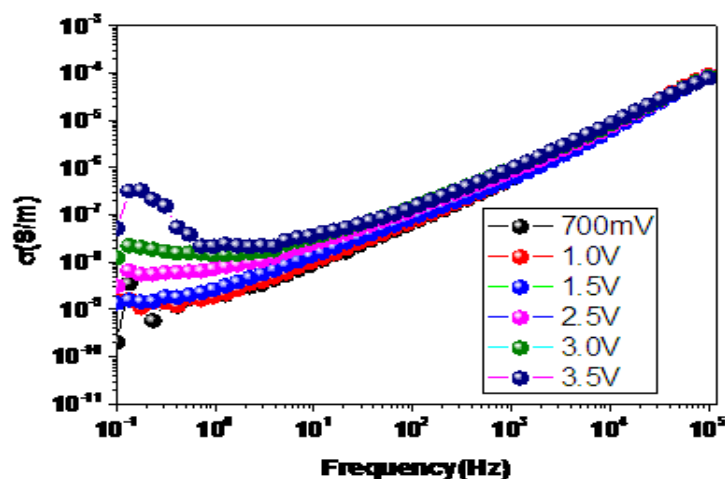
Fig1.4Conductivity response with respect to frequency

In fig 1.4 the conductivity increases with frequency which is a characteristic to the ω^n (n is the exponential). The conductivity ($\sigma(\omega)$) is found to be frequency independent in the lower frequency region ($\omega < \omega_p$), suggesting that the ionic diffusion is random less, i.e. the ions perform correlated forward-backward motions, While the frequency exceeds hopping frequency ω_p, $\sigma(\omega)$increases with frequency following proper law of dispersion $\sigma(\omega) \propto \omega^n$, (where n < 1).

Resistance as a function of frequency with respect to input voltages

We measure for both P3HT: PCBM is used for the experiment which gives resistance about 623.For the voltage fluctuation and noise measurement associated with the output signal take a R_{series} = 10kΩ and make a connection with lock-in amplifier by using co-axial cable. Then we measured unknown resistance value of the sample.
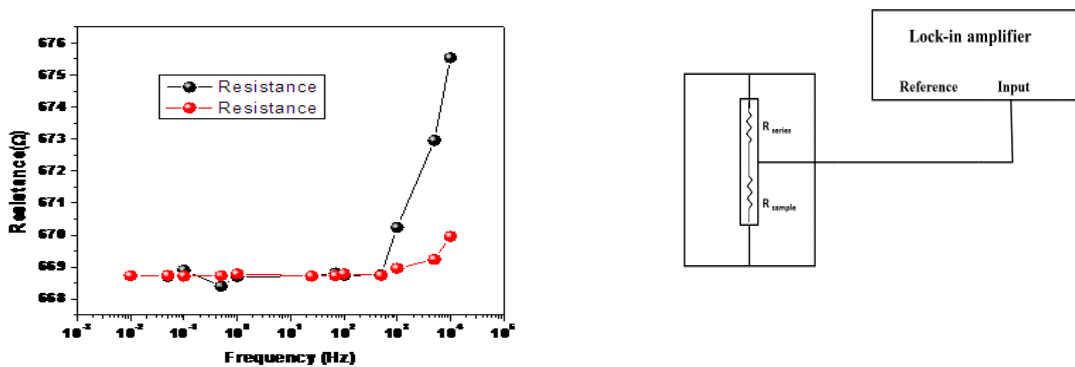
Fig.1.5 (a) Resistance as a function of frequency and 1.5(b) The circuit we used for this experiment

Measurement of thermal noise voltage and power spectral density of thermal noise:

We measure the thermal noise voltage and power spectral density of thermal noise measurement of both the devices. We use 4-probe noise measurement technique shown in fig1.The sample is biased by an ac carrier signal from an SR830 dual-channel lock-in-amplifier at a frequency f_0. The voltage developed across the sample is amplified by a preamplifier whose output is detected by the lock-in-amplifier.. The voltage output we get from the lock in amplifier is voltage fluctuation then we take the Fourier transform of voltage fluctuation and we get the power spectral density of thermal noise and take the under root of power spectral density and we get thermal noise associated with the devices.
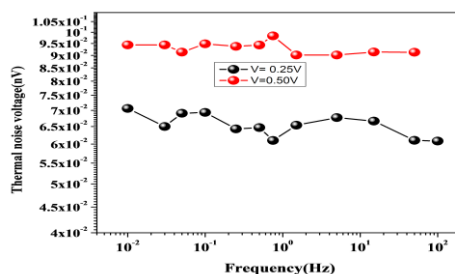
Fig1.6 Thermal noise voltage fluctuation as a function of frequency with respect to input voltages

Power spectral density measurement for thermal noise:

The power spectral density is defined as the Fourier transformation of voltage fluctuation and also mathematical expression for thermal noise power spectral density is defined as-

$S_V = 4K_BTR$ ....(1.2)

From the result in fig1.7 we can say this is frequency independent. The power spectral density for thermal noise is temperature dependent. We get power spectral density for P3HT: PCBM is in order of 10^{-21}.
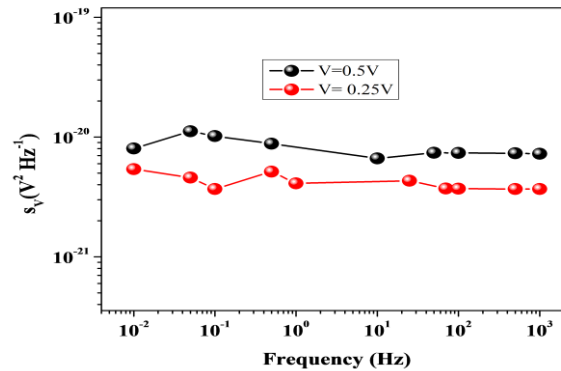
Fig 1.7 Power spectral density curve with respect to input voltages

VI. REFERENCES

[1]. K. G. Libbrecht et.al. "Basic undergraduate laboratory experiment for lock-in amplifier" American association of physics teachers

[2]. Arindam Ghosh, Swastik Kar, Aveek Bid and A. K. Raychaudhuri, "A set-up for measurement of low frequency conductance fluctuation (noise) using digital signal processing techniques", condmat, arXiv:condmat/0402130 v1, (2004)

[3]. International Journal of Science, Engineering and Technology Research (IJSETR) Volume1, Issue 5, November 2012 Preview on Lock-in Amplifier Bhagyajyoti, Immanuel J, L. S. Sudheer, P.Bhaskar, Parvathi C.S.

[4]. Phase sensitive detection: the lock in amplifier by G. Bradley Armen.

[5]. "Resistance fluctuations and instability in metal nanowires" thesis submitted by Aveek Bid at Department of Physics Indian Institute of Science Bangalore India August 2006

[6]. "Synthesis and photovoltaic properties of twobenzo dithiophene based conjugated polymer" by J Hou et.al. J Phys,Chem, CXXXX,xxx,000

[7]. N Wang, X Bao et.al. org electronics 14(2013), 682-692

Application of Surface Plasmon Resonance (SPR) Technique in Sensing Application

Susheel Kumar Singh, Akash Srivastava, L. K. Dwivedi

Department of Physics and Electronics, KNIPSS, Sultanpur, Uttar Pradesh, India

ABSTRACT

This paper aims to theoretical overview of one type of plasmonic sensors that is Surface Plasmon resonance based sensor which provide higher sensitivity ,faster response, label free sensing and real time analysis from existing biosensors like ELISA and PCR . A biosensor determines the presence and concentration of a specific biological substance in a biological analyte. A biosensor have mainly of three components bio-receptor, transducer and electronics system the detail of each segment and working mechanism discussed in this paper. SPR based technique is not only limited to bio sensing but it have significant contribution in gas sensing as well as chemical sensing application. In an SPR sensor, a variation of the refractive index of the sample under consideration (referred to as the analyte) produces a change of the coupling conditions between incident light and the surface plasmon wave that travels along with the metal- analyte interface. This change can be measured as a variation in one of the characteristics of the output light wave. Various kinds of configuration are useful to excite the surface plasmon like prism based technology like kretschmann configuration and otto configuration similarly by using fiber based technology is trend by using photonic crystal fiber (PCF). Our main focus in this paper is prism based SPR sensor and we have given a theoretical overview of this modern technique.

Keywords: Surface Plasmon Resonance, Kretschmann Configuration, Otto Configuration, Plasmonic Sensor, refractive index

I. INTRODUCTION

As surface plasmon based sensor provides a label free technology so there is no need of fluorescent tagging required, real time monitoring response, so this kind of sensor will be highly beneficial and cost effective in comparison to other existing sensing techniques[1,2]. This kind of sensor is able to detect not only cancer cell but it's expected that it will also useful in other biomedical application in future like to detect virus, enzymes and protein in different bio samples.A biosensor determines the presence and concentration of a specific biological substance in a biological analyte [3].Transducer convert biochemical activity into electrical energy, similarly for gas sensing hazardous gases like methane, carbon di oxide, rogen etc. are sensing element. As defined byinternational union of pure and applied chemistry (IUPAC) a biosensor is "self-containedintegrated device which is capable of providing specific quantitative or semi quantitativeanalyticalinstrumentationusingabiologicalrecognitionelement(biochemicalreceptor)whichis   in

direct spatialcontact withtransducer element[4].Professor Leland C Clark Jnr (1918–2005) known as the "father of Biosensors. In present days glucose sensor, used daily by millions of diabetic patients, based on his research idea [5].
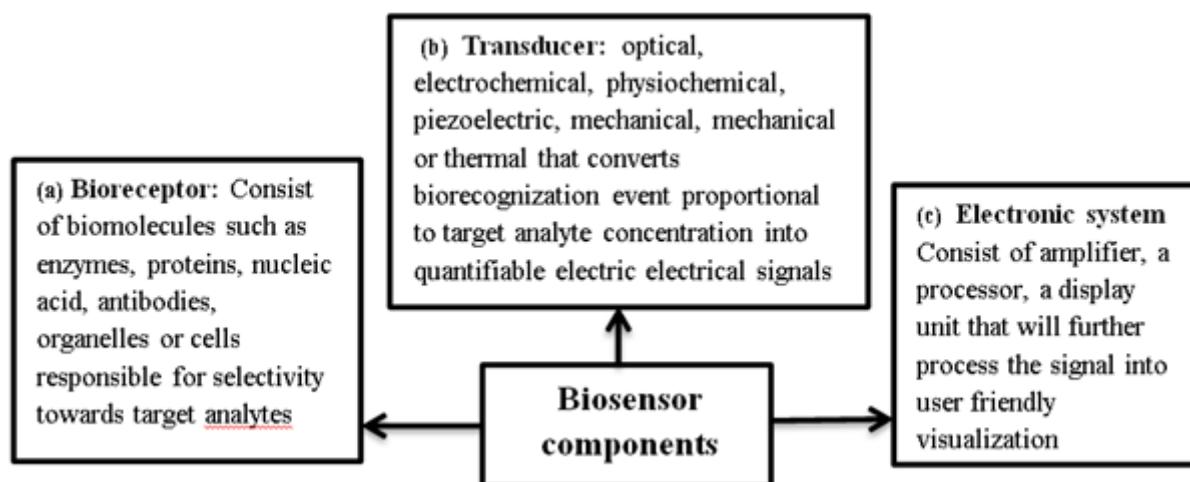
Fig.1Basic blockdiagramof abiosensor

SPRsensorshavegainedanenormousinterestforbiosensingapplicationssuchasthedetection of DNA, proteins, antibody-antigen interactions, cells, and bacteria. The unmatchedquality like real-time monitoring, high sensitivity, and no need for fluorescent labeling andimmuneagainstelectromagneticinterferencesmakeitspecial[6].Abiosensor'soverallperformancereliesuponthefollowingparameterslikesensitivity,precision,cost-effectiveness,utility,simplicity,ruggedness,reliability,speedaccuracy,stability,and easeof Calibration, etc. Surface electrons oscillate against the restoring force of positive nuclei.These collective oscillating electron generate a certain oscillating wave, called surface plasmons wave (SPW) [7]. The first report of SPR phenomenon seen in 1902, by Wood during his experiment. In 1941, Fano first explained Wood's observation by using the surface electromagnetic wave propagating along the interface, which known as SPR phenomenon In 1957, R. H. Ritchie, Powell and Swan discovered that the fast moving electrons lost up its energy when it passing through a thin metal film. Otto (1968) and Kretschmann (1971)[8,9] , developed their own prism coupling configurations respectively to excite SPR by light , based on the "Total internal reflection (TIR)" method. Major issue with conventional SPR sensor is that the metal layer absorption property towards biomolecules is very less, which limits the sensitivity of biosensor[10].Attractive method for improvement of sensitivity of SPR biosensor is to functionalize the metal film with following two dimensional and related nanomaterial like-Graphene, Black phosphorus or related allotropes.Transition Metal Dichalcogenides (TMDs) like MoS_2, $MoSe_2$, WS_2, and WSe_2, Heterostructure of 2D/TMDPerovksite materials like $BaTiO_3$, Sulfosalt like Franckeite, Carbide Nitride materials like MXene[11,12]. There are two advantages of having heterostructure in direct contact with sensing layer. First, an increased adsorption at the surface is achievable due to strong vanderwall force (vdW force) of attraction. Second, the enhancement of field at the interface can be ensured.From last one decade plasmonic sensors are used widely for different kind of sensing

application like biosensing, gas sensing and chemical sensing application. Each area is specific and lots of opportunity for new outcomes. I have aimed to continue my research in biosensing application. On the basis of past work I have observed there is a big scope in this direction which can convert in future research idea. Various research groups like Prajapati Y.K. and Srivastava A. et.al.[13] ,Sharma A and Pandey A. et.al.[14] Pal S.[15] Raghuwanshi S.K.[16], Jha.R et.al.[17] and many more are working on plasmonic sensor and utilizing the property of nanomaterials to enhance the performance of proposed sensors for different application.

II. OPTICAL EXCITATION OF SURFACE PLASMON WAVES

Fast-moving electrons lost up their energy when passing through a thin metal film. As discussed earlier surface plasmon can get excited by either electrons or photons. When an e⁻ beam penetrates the metal a transfer of energy and momentum of electrons from incoming light enables excited the free electrons at the surface of metals. For sensing application however excitation by photons is more suitable. As it's in discussed in an earlier section that Surface plasmon can optically excited under phase-matching conditions (when wavevector of incident light matches to wavevector of surface plasmon). A most common method for optical excitation is prism coupling, grating coupling, and waveguide coupling.

2.1 Prism Coupling:

Otto (1968) and Kretschmann (1971) [18], developed a light prism coupling configuration to excite SPR using the concept of "Total internal reflection (TIR)". Prism-based SPR biosensor is mainly based on two different configurations they are well known as Otto configuration and Kretschmann configuration. Otto arrangement there is an air gap between the metal and the TIR surface Fig. 1(a). Although finding out SPR in solid-phase media could be anappropriatemethodologyhoweverto keep up a distance between the metal and TIR surface is a tedious task and it reduces the SPR potencyconjointlyso thatit'sless useful. Within the Kretschmann configuration, the metal layer is in immediate contact with the prime of the TIR surface that makes it an economical plasmon generator configuration. Fig.1 (b) refers to Kretschmann configuration.
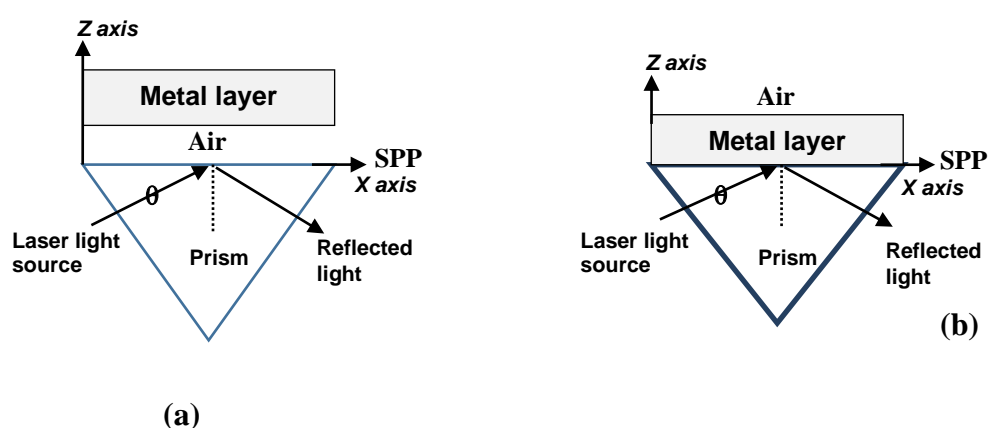
Fig.1 Schematic arrangements of SPR sensor (a) Otto configuration (b) Kretschmann configuration

2.2 Grating coupling

In prism coupling it's shown that prism increases the wavevector of incident light and helpful for wavevector matching and results in surface plasmon excitation. The same phenomenon can be observed by using a diffraction grating. The diffraction grating responsible to scatter the incident light and modifies its in-plane wavevector by an integer multiple of the grating vector G depends on diffraction order. The coupling condition [19] when the mth diffraction is coupled to surface Plasmon can then be expressed as –

$$k_x = k_{ph} + mG = \frac{2\pi}{\lambda_0}n_d sin\theta + m\frac{2\pi}{\Lambda} = Re\{\beta_{sp}\} \qquad (1)$$

Where k_{ph} is wavevector of the incident photon, G is grating scattering vector, m=0, ±1, ±2, ±3…….is diffraction order, Λ is grating period and n$_d$ is the refractive index of the dielectric. Grating coupling provides more angular flexibility in comparison to prism coupling. Depending on grating period and diffraction order m the resonance angle can take on any value from 0 to 90°. Although angle flexibility is the advantage of grating coupling in this case the incident light has passed through the dielectric sample so transparent sample sensing is not possible.

2.3 Waveguide coupling:

Waveguide coupling is also another option for plasmon excitationoffersa good alternative to prism coupling because sometimes it's bulky and difficult to integrate however waveguide coupling is robust, easy to integrate with other optical and electrical components, resist toward EM interference. The light travels in waveguide under TIR condition and generates an evanescent field at the metal-waveguide interface, which excites the SPW likewise prism configuration. The most convenient method for plasmon Excitation is an optical fiber where resonance takes place in a particular region of the fiber cladding under a certain phase-matching condition. As his phase-matching condition satisfied for a short wavelength range, a dip in the transmitted spectrum can be observed. Like prism coupling angle interrogation method is not possible in waveguide coupling hence wavelength interrogation is the only option for sensing purpose. Waveguide-based SPR sensor was first proposed in 1995 by Harris and Wilkinson [20] for a liquid sample medium. Interestingly, the waveguide structure for SP is removed by etching. Waveguide coupling is similar to prism configurations (Otto and Kretschmann-Raether configurations). However, the waveguide-based configuration is a more advantageous technique when compared with the ATR configurations in terms of simplicity, size, interaction strength with the analyte, offers high-resolution measurements than that of the ATR approach. The SP coupling using optical fiber has offered several advantages over the conventional waveguide. First, the cylindrical waveguide of the optical fiber waveguide enables the TE or TM wave considering that polarization lights of any direction easily trigger the SP excitation. Second, one may notice that the total dimension of the fiber optic waveguide-based sensor is small; yet, the active surface sensing area is more extensive because the tube-like surface of the metal as the sensing membrane accommodates more volume of the sample. Nevertheless, a waveguide structure for SP excitation holds drawbacks in the sensitivity performance of random numerical aperture (NA) dependent-incident angle θ. Another significant issue is related to the non-adjustable incident angle which makes polychromatic light the only suitable light source to obtain SPR reflectivity profile. Consequently, the angular interrogation method is not applicable for the sensing approach.

III. METAL LAYER SELECTION

In SPR application choice of metallic film is crucial. The nano thin metal thin layer must be of noble metal. Silver (Ag), Gold (Au), Copper (Cu), Aluminum (Al), Sodium (Na) and Indium (In) Gold (Au) and Silver (Ag) are suitable candidate for SPR sensing application.In is too expensive, Na is too reactive, Cu and Al are too susceptible to oxidation.Gold exhibit higher shift of resonance curve to changes of its surrounding refractive index moreover it's more chemically stable in comparison to silver.Silver is better than gold in terms of FWHM and shows sharp curve in compare to gold, provides large penetration depth.Optimized metal film thickness is 45-50 nm. Comparative analysis between Au and Ag shown in Fig.2 for SPR angle shift analysis.
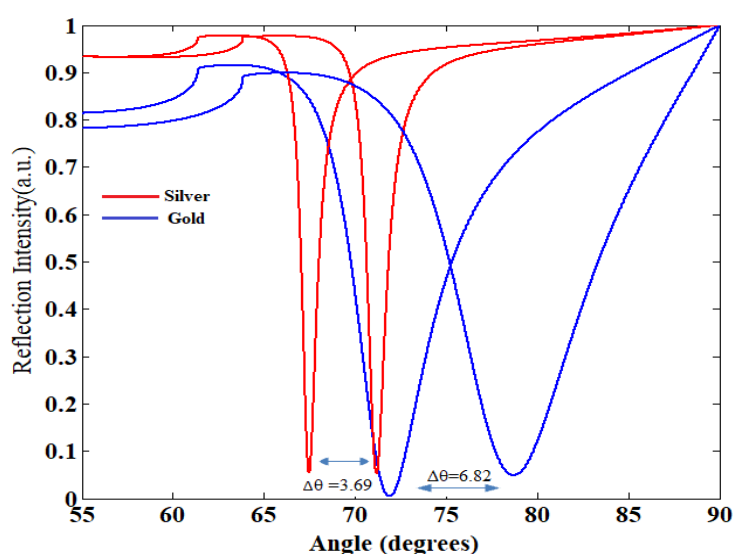
Fig.2 Au vs. Ag SPR angle shift analysis [21]

IV. SELECTION OF PRISM

Prism selection: BK7 prism (also called right angle prism) is preferred due to its low refractive index (n=1.51 at 633nm), as a result, it proves to be a good substrate for high sensitivity. Major issue with low refractive index prism is very short dynamic range As with water the working refractive index span possible from 1.33 to 1.47 so for high refractive index variation SPR shift monitoring is very limited for small range this situation constraints the user for limited sensing application.Higher refractive index prism like Zinc Selenide (n=2.47 at 633nm) is used to overcome this because practically [22] it excites Surface Plasmon as well as reduceθ_{spr}. This will facilitate the user for greater angular span and allow more solvent host to be used (upto 1.33 to 1.7).

At the last of this review article it's concluded that in current technique of virus detection like PCR, RT-PCR, ELISA all are time taking and required specific sample preparation, SPR techniques is label free and real time monitoring scheme.In future for quick detection of covid-19 virus SPR technique can make a cost effective and quick responding detection technique Health monitoring sensor like cancer detection, urine and blood culture, kedney functionality etc. can be made through SPR technique.Hazardous gas monitoring also be

done which influence environment and human body. Various simulation software are useful for SPR sensor performance analysis like MATLAB/Comsol Multiphysics/Winspall etc.

V. CONCLUSION

In this paper author have briefly described about the modern technique of sensing that is Surface plasmon resonance based sensor. Types of SPR sensor, Kretschmann and Otto configuration, how plasmon excitation takes place these phenomenon given in this paper. Application of SPR sensor in biosensing and gas sensing application is a hot topic of research and performance enhancement of sensor get enhance when bio-surface functionalized with nanomaterials in sensor conventional structure. For it we have given a short introduction about various possible 2D materials which exhibits significant quality when used with its monolayer.

VI. REFERENCES

[1].   Yuan Yao, B. Yi, J. Xiao, Z. Li "Surface Plasmon Resonance Biosensors and its Application" IEEE Explore, PP 1043-1046,2007

[2].   J. Homola et al. "Surface Plasmon resonance sensors: review," Sensors Actuators B Chem., vol. 54, no. 1–2, pp. 3–15, 1999

[3].   A. Srivastava and Y. K. Prajapati, "Effect of sulfosalt and polymers on performance parameter of SPR biosensor," Optical and Quantum Electronics, vol. 52, no. 10, Sep. 2020

[4].   P. Suvarnaphaet and S. Pechprasarn "Graphene-Based Materials for Biosensors: A Review" MDPI, Sensors, 2017

[5].   A. Srivastava, Y. K. Prajapati "Performance Analysis of Silicon and BluePhosphorene/MoS2 Hetero-Structure Based SPR Sensor" Photonic Sensors, vol.9(33), pp 1–9, Feb 2019

[6].   X. Wang, Y. Deng, Q. Li, Y. Huang, Z. Gong, K. B Tom and J.Yao "Excitation and propagation of Surface Plasmon Polaritons on a non-structured surface with a permittivity gradient" CIOMP, Light: Science & Applications (2016)

[7].   A. Srivastava, R. Das, and Y. K. Prajapati, "Effect of Perovskite material on performance of surface plasmon resonance biosensor," IET Optoelectronics, vol. 14, no. 5, pp. 256–265, Oct. 2020.

[8].   Richard B. M. Schasfoort, Anna J. Tudos, Handbook of Surface Plasmon Resonance, pp.1-14, Royal society of chemistry, 2008.

[9].   A. Srivastava, Alka Verma, Ritwick Das, Y.K. Prajapati "A Theoretical Approach to Improve the Performance of SPR Biosensor using MXene and Black Phosphorus", Optik - International Journal for Light and Electron Optics Vol.203, pp.1-9,2020

[10].   Canning, J. Qian, and K. Cook, "Large dynamic range SPR measurements using a ZnSe prism," Photonic Sensors, vol. 5, no. 3, pp. 278–283, Jun. 2015

[11].   Y.S. Dwivedi, Anuj K. Sharma, B. D. Gupta "Influence of Design Parameters on the performance of a Surface Plasmon Sensor Based Fiber Optic Sensor", Plasmonics, vol.3, no.2, pp 79-86, Sep.2008.

[12]. A. Srivastava, Alka Verma, Y.K. Prajapati. Theoretical study of hazardous carbon- di-oxide gas sensing using MIM structure-based SPR sensing scheme. IET Opotelectronics. 2021; 1–11. https://doi.org/10.1049/ote2.12035

[13]. S. K. Srivastava, and B. D. Gupta, A multitapered fiber-optic SPR sensor with enhanced sensitivity, Photonics Technology Letters, IEEE, 23(13),923-925, 2011

[14]. Prajapati, Y. K., & Srivastava, A. (2019). Effect of BlueP/MoS2 heterostructure and graphene layer on the performance parameter of SPR sensor: theoretical insight. Superlattices and Microstructures, 129, 152-162.

[15]. Sharma, A. K., & Pandey, A. K. (2018). Blue phosphorene/MoS 2 heterostructure based SPR sensor with enhanced sensitivity. IEEE Photonics Technology Letters, 30(7), 595-598.

[16]. Pal, S., Verma, A., Saini, J. P., & Prajapati, Y. K. (2019). Sensitivity enhancement using silicon-black phosphorus-TDMC coated surface plasmon resonance biosensor. Iet Optoelectronics, 13(4), 196-201.

[17]. Raghuwanshi, S. K., Kumar, M., & Athokpam, B. S. (2016). Analysis of novel class of surface plasmon phenomena having a metamaterial layer between two different metals for sensor application. IEEE Sensors Journal, 16(17), 6617-6624.

[18]. A.K. Sharma and A.K. Pandey "Blue Phosphorene/MoS2 Heterostructure based SPR Sensor with Enhanced Sensitivity" IEEE Photonics Technology Letters vol.30, pp.595-598

[19]. H. Raether "Surface plasmons on smooth and rough surfaces and on grating" Springer Berlin Heidelberg, 1988

[20]. R. D. Harris and J. S. Wilkinson, "Waveguide surface plasmon resonance sensors," Sensors and Actuators B: Chemical, vol. 29, no. 1–3, pp. 261–267, Oct. 1995

[21]. Alka Verma, and Y.K. Prajapati "Effect of 2D, TMD, perovskite, and 2D metal carbide/nitride materials on performance parameters of SPR biosensor" Handbook of Nanomaterials for Sensing Applications, edition-1, chapter 04, pp.57-90, Publisher Elsevier, ISBN 9780128207833,

[22]. Canning, J. Qian, and K. Cook, "Large dynamic range SPR measurements using a ZnSe prism," Photonic Sensors, vol. 5, no. 3, pp. 278–283, Jun. 2015

Art and IVF Labs Are Using Smart Materials and Devices for Infertility Treatments

Ram Dayal[1]*, Ankit Maurya[2]

[1]*Director and Scientist Sr. Embryologist, IRCC IVF Centre, Panchkula, Haryana, India

[2]Department of Mathematics, Shri Lal Bahadur Shastri Degree College, Gonda, Uttar Pradesh, India

ABSTRACT

In terms of technology, smart materials are the most important in the twenty-first century. "Smart Materials" have a crucial role in Assisted Reproductive technology (ART). These innovative materials constitute an important part of infertility treatment. Infertility patients are opting for various type of treatments such as intrauterine insemination (IUI), in-vitro fertilization (IVF), intracytoplasmic sperm injection (ICSI), Intra morphologically selected sperm injection (IMSI), Physiological Intracytoplasmic Sperm Injection (P-ICSI), Laser Assisted Hatching (LAH), Partial Zona Dissection (PZD), Embryo Biopsy and pre-implantation genetic screening (PGS) or Pre-Implantation Genetic Diagnosis (PGD) and other procedures. IUI and IVF is the most common procedure to treat infertility. The adoption of child is another option for infertile couple. The success rate of IVF is high than IUI. All IUI, OPU or Embryo transfer doing under ultrasound guidance. The design of IVF Lab with smart materials involves highly integrated components and requires interdisciplinary knowledge. Smart materials are capable to reducing the dust and VOCs to prevent the infection and improve culture conditions. For best fertilization we can use either conventional IVF or through direct injection of single sperm into the mature oocyte cytoplasm (ICSI). Hera cell 150i (thermos scientific) CO_2 Incubator and bench top incubator are ideal for embryo culture. Micromanipulator help in fine control to the sperm injection and embryo biopsy by applying positive and negative pressure to the joysticks. This mechanical energy is converted into electrical energy and vice versa by smart materials during their functioning. Therefore, smart materials are predetermined and predesigned to severe as sensors and actuators as required. This paper discusses various types of smart equipment's used in the ART and IVF lab to help in treating the infertile couple and achieving their desire of child.

Keywords: Smart IVF Lab, Incubator, Micromanipulator, Laminar Air Flow (LAF), Microscope, centrifuge Machine, Embryo Transfer, USG Machine, Suction Pump, OPU, IVF/ICSI and PGS/PGD.

I. INTRODUCTION

Smart material and devices for sustainable technologies in the ART and In-Vitro Fertilization (IVF) Lab are very important. The ART and IVF Laboratory should have adequate space to follow good laboratory practice. More specifically: The construction of the laboratory should ensure aseptic and optimal handling of gametes and pre-embryos during all phases of the treatment. The location of storage areas and equipment such as

incubators, centrifuges machine and cryo equipment should be logically planned for efficiency and safety within each working area. Separate office space should be provided for administrative work, such as record keeping and data entry. A general wet area in which washing of equipment, sterilization, etc., is performed, should be separate from the embryo laboratory. Moreover, if fixatives are applied, these analyses should be performed in a separate room in a fume-hood. When commissioning the laboratory, thought should be given to the most recent developments in equipment and facilities. Bench height, adjustable chairs, microscope eye height, efficient use of space and surfaces, sufficient air-condition and the amount of daylight, all contribute to a working environment that minimizes distraction and fatigue. Consideration should also be given to local health and safety requirements.

II. INNOVATIVE PRODUCTS TO COMPLETE THE WHOLE IVF PROCESS

ART and IVF clinics can achieve success by combining the use of tried and tested equipment, scientific insights, knowledge of clinical processes, and an informative training and education programme. We are discussed here smart materials and innovative devices which is use in IVF Labs for giving hope for child to childless couples.

III. THE REQUIREMENT AND BENEFITS OF SMART MATERIALS IN IVF LAB

1. **Smart Structures:** Any ART and IVF Labs need to design smart structure with specified floor. Approximately 100 to 200 square feet area is required for IUI / Andrology Lab. The laboratory equipment used should be adequate for laboratory work and easy to clean and disinfect. Critical items of equipment, including incubators and frozen embryo storage facilities, should be appropriately alarmed and monitored.Gas cylindersshould be placed outside or in a separate room with an automatic backup system.

2. **Smart paints:** The walls should also be covered with tiles. Alternately one can cover wall with epoxy paint. 'Ecological' water-based paints are preferred with NO VOC emission. Low-volatile paints with acrylic, vinyl acrylic, or acrylic latex polymers. Epoxy paints emit VOCs (amine) and take several weeks to cure and thus their use should be avoided.Advantage,improved washability and durability. Emission testing on samples is required since amine catalysts can be very persistent. No paint containing formaldehyde, acetaldehyde, isocyanates, reactive amines, phenols and soluble VOCs.

Some examples of smart paints are Benjamin Moore paints, Thomsit, Corian, Lindner, etc., Disadvantage is cost, practical bargain. White coloured, low VOC, low odour epoxy paint with proper burn in period (increased temp and ventilation for a few days initially, with lights on) and assessment for VOCs.

2.1. **Floors:** Large vitrified tiles or vinyl sheets or treated marble is preferred. Impervious, sealed, minimum joints. Edges and corners curved for easy cleaning. Slip resistant, non-staining, non-permeable. Solvent free adhesives/vinyl glues – with low VOC emissions. Changing vinyl flooring in neighbourhood caused dramatic fall in pregnancy rate (PR) due to adhesive vinyl glue (Cohen et al, 1997)

3. **Smart Modular ART Lab:** If anyone wants to be more-strict and is planning to convert the IUI room into an IVF laboratory in future, one can use pressure modules to create positive pressure in the laboratory. however, this is not a must if one is planning just an IUI facility.

3.1. **Doors:** Sliding door in the IVF Lab areas should be avoided.All doors must be tight-fitting with bottom 'sweeps and perimeter seals (top and edges)' making them 'Air-tight'. Doors preferably glass with coated or steel to reduce the VOCs.In sealed doorpass window preferred to overhand the washed semen sample and follicular fluid to the embryologist for screening. If we have AHU to create the positive pressureeasier to maintain if the adjoining operating theatre also has sealed doors and ceiling.Provisions should be made so that doors are wide enough to accommodate large equipment (eg incubators) after the lab becomes permanently sealed and operational.

4. **Smart Andrology:**

Andrology laboratory also need to design modular with metal to avoid the fixing the dust on wall. Modular lab also helps to reducing the VOCs and easier to cleaning. Andrologylab also need to metal cupboard and racks for keeping the files and other things. Super grade computer also needs to equipped in the andrology lab for maintaining the data digitally and easier to trace. In the andrology lab some equipment's are **essential:** Centrifuge, laminar air flow hood, microscope, Incubator, and test tube warmer. Some equipment's are **desirable:**Phase contrast microscope, Makler chamber, CO2 incubator, Experimental-CASA. Neubaeur chamber or the Maklerchamber are commonly used. Use of makler chamber is highly recommended as it is very accurate, though more expensive.

In the andrology lab automatic sperm analyzersystems such as CASA are being routinely used in a large volume of work on semenology is being carried out. However, it is not required to run a routine IUI laboratory.Refrigerator is used to store the various chemicals and culture medias to improve their life and quality. The fridge should not be used for any other activity.

Monocular microscope preferably phase contrast to test the semen for count, motility, morphology and other components such as leukocytes /pus cells. The microscope should have 10x, 20x,40x,and 100x objectives, and a 10x eyepiece.

5. **Smart IVF OT:**

IVF OT preferably modular with wide metal door is recommended. The sterile area includes operation theatre and embryology lab complex.Operation theatre (OT) must have AC and filter system (HEPA) along with emergency recovery equipment for ovum pick-up.

6. **Smart IVF Lab:**

Smart IVF Lab should be made with metal as a modular wall and fitted with HEPA and AHU to create the positive pressure to reduce the air contamination. IVF Lab should have facilities for the control of temperature and humidity and must have filtered air and sterility. Mainly they have:

a. Infrastructure
b. Equipment
c. Manpower (Personnel)

6.1. Location of the building: ART and IVF lab must be avoided near petrol pump, chemical godown, factories emitting fine particles, heavy traffic, parking slots, cement godowns, etc. Enquire whether the building or the surrounding site will undergo renovations or demolition in near future. Basic air sampling & determination of VOCs inside and outside the proposed building must be checked.

For IVF lab first floor is ideal due to less disturbance. We recommend to avoid IVF lab setting in the basement because more chance of moisture and fungal infection. Also need to check for any damp area or water seepage before making the IVF lab. Connectivity with lifts/elevators should be there preferably (transportation of gas cylinders, LN2, etc.). Need to aware in a hospital, should not be near radiation sources like as CT scan, radiotherapy units or near waste disposal areas. It should be away from the exhaust emission areas and the backup power generators. The IVF Lab total area are depending on the expected work load.

Non-sterile and a strictly sterile area: Same space may be used for more than one purpose (no compromise in quality) of service. Sterile and non-sterile cannot be combined. (ICMR ART Regulation bill 2010& 2021)

6.2. Walls & partitions:

In ART & IVF lab walls & partitions should be non-porous inert material. Cladding with a non-porous material such as panels made from aluminium tri-hydrate are expensive but provide an inert (low VOC), hypoallergenic, easy to clean wall. The ceiling must be composed of a contiguous, solid material, e.g. plasterboard, gypsum panels, Gyprock, Sheetrock®, not tiles, and the need for any access panels must be minimized. Essential access panels must have air-tight, silicone gaskets as sealant. False ceilings should be avoided at all points. May be needed to conceal lights and filters should have solid non porous panels.

6.3. Optional: Closed chambers, benchtop incubators, LASER.

6.4. Experimental: IMSI, embryoscope, polscope.

7. Smart Cryobiology Lab:

This lab is also required modular and ventilated with Laminar Air Flow (LAF) fitted with stereozoom microscope. For gamete storage Liquid Nitrogen cylinder mush have and prior use need to fill LN2 and check any leakage to avoid and loss. Nitrogen tanks should be cleaned and sanitized at least every year.

8. Superb AHU:

Air Handling Unit (AHU) use to improve air quality. AHU stands alone units (with/without positive pressure), e.g. Austin Air, United States of America (Lab air purifier). Laminar air flow stations, Inline filters for the gas supply to incubators and filters to be kept in incubators.

9. Smart IVF Work Station

IVF-workstation is used because it offers aseptic atmosphere for handling of gametes and embryos. This is prepared to fresh air as per the need of filtration-illumination and meet up the standard, sound & shuddering free. LAF unit is obtainable with vertical-air flow-arrangement. This is IVF work station with stereozoom microscope, display and heat control also. The smart IVF workstation is dual core and semi closed systems for preventing fluctuation of temperature, air quality and contamination. The major purpose of laminar-flow-cabinets is to filter atmospheric air twice, through HEPA filters with a corrected performance rating of 99.99% with cold-dispersed oil particles (DOP) and 99.97% with hot-dispersed oil particles (HDOP), thus retaining all airborne particles of 0.3-micron or larger. The filters are designed to remove every particle that

hits the HEPA filter. With the help of a technically-balanced blower, you will be able to receive great airflow all around the HEPA filter and on the IVF workstation. The blower is consisting of a ¼ H.P. motor and operates at lowest sound possible (Shivani Scientific, (2020).

10. Smart Incubator

A minimum number of two incubators is recommended. Incubators should be frequently cleaned and sterilized periodically.

11. Smart UPS as a power backup:

All ART and IVF laboratories should have an automatic emergency generator backup in the event of power failure.

12. RI witness:

Correct handling and identification of patients and their gametes and embryos Written procedures should be present describing the various phases of IVF techniques. Rules concerning the correct handling and identification of gametes and embryo samples should be established by a system of checks and, where needed, double-checks. Proper training of all the laboratory staff according to these proceduresis mandatory. ∙ All material obtained from the patients, i.e. tubes with blood,follicular fluid and spermatozoa, should bear unique identification of the treated couple. ∙ Incubators should be organized in order to facilitate identification of embryos, oocytes and spermatozoa. ∙ Verification of patients' identity should be performed at criticalsteps: before ovum retrieval, at semen recovery and embryo transfer procedures. ∙ Double checks need to be considered at least at: insemination of oocytes, replacement of embryos, embryo freezing and thawing. Written validation of all critical steps in each patient's file is essential.

13. Smart Micromanipulators:

This is an inverted microscope which is used to sperm crushing, sperm selection, oocyte holding, micro injection under a microscopic vision, where a level of accuracy of progress is needed that can't be achieved by the without help of human hand. It may normally consist of an input of joystick, a machine for controlling the choice of movement during work and a production division with the resources of asset a holding needle and injection needle to hold for injection or manipulation the gametes as required.

14. Stereo-zoom Microscope:

The stereo zoom microscopeis an optical microscope is planned for small magnification observation of object, searching of oocyte form aspirate of follicular fluid during OPU, usually using beam of light reflected from objectsurface rather than transmitted through it. The stereo-microscope is frequently used to study the surfaces of live sample or to carry-out close-work like as dissection of seminiferous tubule (in case of TESA), micro-surgery, watch assembly, circuit panel production and crack surfaces as in fracto-graphy and [forensic engineering](#).

15. Suction Pump:

Initially oocyte or follicular fluid aspiration was performed by manually using a syringe connected to the needle. This technique was not given suitable and constant pressure which was harmful to the oocyte. Now a day we are using standardized digital suction pump for follicular fluid aspiration in a safest and controlled manner. Suction pump provides a regulated vacuum up to -500 mm Hg for common suction. When press the

pedal then vacuum response is activated on needle tip. We should maintain the suction pressure ideally from 90 – 120 mm Hg and it does depend on clinician personnel experience.

16. Sample Collection Room:

Smart semen collection room need to be equipped with smart LCD andromantic's videos to help in the semen collection to the patients

17. Air Condition (AC):

In any ART and IVF Lab must have AC for maintain the Lab temperature and relative humidity to prevent the bacterial growth / infection.The ideal temperature for an IVF lab is 24 to 27 degrees Celsius, and the ideal relative humidity is 44 to 50%.

18. QC Device:

CO_2 analyser, pH meter, VOC meter and other devices is the key factor for success. IVF Lab results depend upon the strict quality control. Success can be achieved by monitoring air quality, instruments performance, parameter checks. Instruments should also calibrate regularly to achieve success.

We must strict adherence to hygiene at every steps. We follow the protective laboratory clothing & hair nets. We should bear the non-powered gloves and mask during the procedure. Food, gum, drinks and tobacco strictly prohibited in IVF complex. Cosmetic should be minimized and perfumes should be avoided.

19. VOC filter:

Carbon *filters* are specifically designed to remove gaseous elements from the air and may effectively remove *volatile organic compounds and improve embryo quality developments.*

20. Supportiveequipment's:

We must include the supportive equipment like as anti-vibration table, table for incubator and other purposes to improve the work quality. Anti-vibration table is very helpful during micro injection and avoid physical damage of oocyte.

21. Laser for embryo biopsy and assisted hatching:

In the beginning of the LAH has allowed the expansion of accurate methods to drill thethickerzone for easy to hatching and enhancingimplantation rate. LAH can twist in the history of not an achievement of embryos to implant them in uterine cavity.Three methods are being used; the mechanical technique, that is partial zona dissection with glass microneedles (Cohen et al., 1990), the chemical assisted hatching using acidic Tyrode's (Cohen et al., 1992), and the laser assisted hatching (Strohmer and Feichtinger, 1992)

22. Test Tube Warmer:

Commonly this device is used for maintaining a stable heat of follicular fluid aspirates in round bottom tube. One of the main factors to manipulating of gametes and embryos is the maintaining the optimal temperature. Test tube heating machine is needs verification of its ability to keep fluid at the preferred temperature. Itstemperature could differ with fluid quantity and the brand of test tube warming gadget used.

23. Microscope (Basic role of microscope in SA):

Semen-analysis is the firstlevel of screening test during routine-microscopy and leftovers the foundationfor the examination of male-infertility. It gives helpful idea concerning the sperm-count ($x10^6$/ml), sperm-motility, viability or higher leukocytes (pyospermia) of in the ejaculate. Phase contrast microscope is

suggested for routine semen analysis. 50-watt light source for this microscope is recommended, preferably-binocular (have 2-eyepieces 10X), have a phase-condenserand slot for camera attachment.Microscope-should also contain subsequent accessories for semen-examination (Indian fertility Society, 2016):

1. Objective ×10 (with-yellow), ×20 (with-green), ×40 (with-blue) is necessary for evaluation of motility, vitality and counting of sperm and leukocytes.
2. Objective ×100 (white) is oil immersion bright field (for evaluation of sperm-morphology and sperm-vitality)
3. Negative phase-objective ×40 (non-compulsory; for eosin-vitality test)

24. Stripper Handle:

Stripper handle used for oocyte denudation, transferring oocyte one dish to another dish or drop and washing of oocyte or embryos with adding the denuding pipette according to bore size is needed. b. Its volume 0.25 μL to 3.0 μL can be adjusted. c. This handle gives the ideal suction which is ideal for the manipulation of gamete and embryo. d. Denuding pipette handle has available in different models.

25. Centrifuge Machine (SF800):

SF800 is a temperature regulated centrifuge machine which is more suitable for ART laboratory. This machine protects the cold and thermal shock by maintaining ideal temperature, thus designed at improving the recovery of good morphologically selected normal motile sperm pellet and ART results. We can set the program and temperature by manually in SF800. This apparatus has been planned to control and consequently preserve "Critical" inner-chamber-temperature before, during centrifugation and after. This technology for controlling fixed temperature and rotation helps in maintain sperm motility and obtaining good motile sperm pellet (Shivani Scientific, 2020).

26. Role of Micropipettes:

Micropipettes are used in different laboratories like as chemistry lab, biology lab, medicine lab and embryology lab to hold the measure volume. Now micropipettes are commercially availing in a various model and capacity. This device facilitates to measure volume is precise manner at every step (Eppendorf, 2020). Some common pipette used in ART laboratories are: 20 to 200 μl, 10 to 100 μl, 100 to 1000 μl, 2 to 20μl. In these pipettes we use sterile individual packed pipettetips 200 μl and 1000 μl for transferring the media and making the micro drops for micro culture or washing the oocyte or embryos in aseptic manner. We recommend sterilization with ETO or autoclave (if pipettes are autoclavable) before use.

27. Computer and Printer:

Now a days mostly all departments need smart computer for record keeping digitally as a soft copy. Printer also need for printing the report and other documents. Computer use for all the purposes like as email, data entry and storage etc.

28. Construction Materials:

It must be carful about the material using for making IVF Lab. Should follow the ICMR guideline or ESHRE or ASRM or any other good laboratory practice guideline for designing the smart ART Lab.

29. Non-Construction Materials:

All plastics and glass wares are the non-construction materials choose sterile and nontoxic for the gamete and embryos.Glassware and disposable items used for preparation of culture media should be of tissue culture grade and dedicated for this purpose alone.Culture media, or reagents used in their preparation,should be of a purity appropriate for the purpose.

IV. CONCLUSION

Since the procedure began a few years ago, there have been several new techniques introduced. aimed at expanding ART indications: freezing of oocytes and ovarian tissue, in-vitro maturation of oocytes, intracytoplasmic sperm injection, TESA sperm injection, embryo biopsy and physiological ICSI (P-ICSI). Lasers can also be used to improve implantation, especially in frozen thawed embryos, by drilling the zone. To ensure the IVF lab setting place, floor, paints and over all materials are non-toxic to gametes and embryos, we should be aware of this. All culture medias and plastic were should be purchase from authorized vendors with care of IVF Grade material. However, additional studies are needed before establishing an ART and IVF clinic and registration is required from ICMR for the clinic to run properly.

V. REFERENCES

[1]. Cohen, J., Wright, G. and Malter, H. (1990) Impairment of the hatching process following in-vitro fertilization in the human and improvement of implantation by assisting hatching using micromanipulation. Hum. Reprod., 5, 7-13.

[2]. Cohen J, Alikani M, Trowbridge J, Rosenwaks Z. Implantation enhancement by selective assisted hatching using zona drilling of human embryos with poor prognosis. Hum Reprod. 1992, 7, 685–691.

[3]. Eppendorf research plus fixed volume pipettes, Accessed [online] December 2020,https://us.ivfstore.com/products/eppendorf-research-plus-fixed-volume-pipettes?variant=2194995544073.

[4]. Fertility centre of New England, assisted hatching of vitrified embryos, accessed [online], December 2020, https://www.fertilitycenter.com/fertility_cares_blog/laser-assisted-hatching

[5]. ICMR – The Assisted Reproductive Technologies (Regulation) Bill – 2010.

[6]. Makler A. Human Seminology. Chapter 7:115-130, In: Biotechnology of Human Reproduction, Editors: A. Ravelli, I. Tur-Kaspa, JG Holte, M. Massobrio, Parthenon Publising Group, 2003.

[7]. Mobile Nest, Portable Test Tube Warmer, Fornex, Accessed [online], December 2020, https://www.shivaniscientific.com/ivfproducts/mobilenest.htm.

[8]. Operating Instructions CO2 Incubator Heracell 150i / 240i with Decontamination Routine, 50115191 B / 11.2010, Accessed [online], http://stmichaelshospitalresearch.ca/wp-content/uploads/2015/09/HERAcell-150i-240i-with-Decontamination-Routine.pdf.

[9]. SeemaNihalani, Dr.Unnati Joshi, AshishMeeruty; Smart Materials for Sustainable and Smart Infrastructure, Materials Science Forum Submitted: 2018-09-30 ISSN: 1662-9752, Vol. 969, pp 278-283 Revised: 2019-02-12 doi: 10.4028/www.scientific.net/MSF.969.278 Accepted: 2019-02-13 © 2019 Trans Tech Publications Ltd, Switzerland Online: 2019-08-30.

[10]. Semen analysis: Nuts and Bolts, NEXUS, Indian Fertility Society &Origio, India Initiative, Second Issue, Volume: 2 (July, 2016).

[11]. Shivani Scientific, Laminor Air Flow (LAF), (2020). [Online] Accessed, December, https://www.shivaniivf.com/functionwise/functionwise.php?val=16.

[12]. Spermfuge (SF800), Temperature controlled centrifuge machine, Fornax, [online] Accessed, December 2020, https://www.shivaniivf.com/functionwise/functionwise.php?val=1#rgt.

[13]. Suction Pump, Cook Medical, Accessed [online], December 2020, https://www.cookmedical.com/products/wh_mar_5200_webds/

[14]. Strohmer H, Feichtinger W (1992) Successful clinical application of laser for micromanipulation in an in vitro fertilization program. FertilSteril 58:212–214.

[15]. The stripper handle, cooper surgical, fertility and genomic solutions, Accessed [online] December 2020, https://fertility.coopersurgical.com/micropipettes/the-stripper/

[16]. World Health Organization. (2010). WHO laboratory manual for the examination and processing of human semen.Fifth edition.2010, Geneva.

Behaviour of Electric Pressure with Temperature <100>+<111> Tunnelling Model with Electric Field along <111> Direction

D.N.Pandey[1], Jitendra Singh[1], Mukesh Upadhyay[2]

[1]Department of Physics, Sri Lal Bahadur Shastri Degree College, Gonda-271001, Uttar Pradesh, India

[2]Department of Physics, NERIST, Arunachal Pradesh, India

ABSTRACT

In this paper we have study theoretically the variation of electrical pressure with temperature and electric field for <100>+<111> tunnelling model along<111>direction. It may be used to explain various experimental available data and may be also used for further theoretical investigations?

Keywords: Dielectric constant, tunneling model & Electrical Pressure.

I. INTRODUCTION

Diatomic and off-cantered monoatomic impurities alter the properties of host crystal drastically. There has been considerable recent interest in the impurity modes of ions substituted at lattice sites in alkali halide crystals. A small concentration of impurity doped in certain alkali halides cause a large rise in dielectric constant at low temperature.[1].The octahedral potential for the angular motion of the diatomic impurity in solid state matrices was first presented by Devonshire[2].Many experimental results for system such as OH^{-} and CN^{-} ions in alkali halide matrices[3,4] and HCl,HBr etc impurities in rare gas matrices[5] have successfully explained. The effects of externally applied electric field on induced dipole moment of the impurity were studied by Gomez et al[6] using tunnelling models.

II. THEORY

the electric field polarisation for the <110> off cantered model and for the model of simultaneous minima along the direction <110>+<111> has been explained by pandey et al [7,8].Theoretical study of polarisation and dielectric constant fo the various tunnelling models has been given by by Raj Kumar et al[9,10,11,12] . Study of electrical pressure of various tunnelling model has been given by MukeshUpadhyay et al [14,15,16]. In this paper we have to find out the expression for electric pressure for the<100>+<111>tunnelling model along direction <111>.

The expression of dielectric constant is given by

$$\varepsilon = \frac{dP}{dE}$$ 1.1

The expression of electric pressure is given by relation

$$S = \frac{\sigma^2}{2\varepsilon} \qquad \text{.................................. 1.2}$$

Where σ is surface charge density.

The expression of polarisation for<100>+<111> tunnelling model

$$P = N\frac{\left[\sqrt{3}\mu_1\left(e^{x_1/\sqrt{3}} - e^{-x_1/\sqrt{3}}\right) + \mu_2\left(e^{x_2} - e^{-x_2} + e^{x_2/3} - e^{-x_2/3}\right)\right]}{\left[3\left(e^{x_1/\sqrt{3}} + e^{-x_1/\sqrt{3}}\right) + e^{x_2} - e^{-x_2} + 3\left(e^{x_2/3} - e^{-x_2/3}\right)\right]} \text{..................1.3}$$

Where $x_1 = \frac{\mu_1 E}{kT}$, $x_2 = \frac{\mu_2 E}{kT}$

Differentiating equation (1.3) with respect to electric field we get dielectric constant

$$\varepsilon = \frac{N}{kT}\Bigg\{\Bigg[4(\mu_1^2 + 2\mu_2^2) + (\mu_1^2 + 3\mu_2^2)\left(e^{x_1/\sqrt{2}} + e^{-x_1/\sqrt{2}}\right)(e^{x_2} + e^{-x_2}) + (3\mu_1^2 + \mu_2^2)\left(e^{x_1/\sqrt{3}} + \right.$$

$$\left. e^{-x_1/\sqrt{3}}\right)\left(e^{x_2/3} - e^{-x_2/3}\right) + \frac{10\mu_2^2}{3}\left(e^{x_1/\sqrt{2}} + e^{-x_1/\sqrt{2}}\right)\left(e^{2x_2/\sqrt{6}} + e^{-2x_2/\sqrt{6}}\right) - \frac{6\mu_1\mu_2}{\sqrt{3}}\left(e^{x_1/\sqrt{2}} - e^{-x_1/\sqrt{2}}\right)(e^{x_2} -$$

$$e^{-x_2}) - (3 + \sqrt{3})\mu_1\mu_2\left(e^{x_1/\sqrt{3}} - e^{-x_1/\sqrt{3}}\right)\left(e^{x_2/3} - e^{-x_2/3}\right) - 2\mu_2^2(e^{x_2} - e^{-x_2})\left(e^{x_2/3} - e^{-x_2/3}\right)\Bigg]/$$

$$\left[3\left(e^{x_1/\sqrt{3}} + e^{-x_1/\sqrt{3}}\right) + e^{x_2} - e^{-x_2} + 3\left(e^{x_2/3} - e^{-x_2/3}\right)\right]^2\Bigg\} \text{........................... 1.4}$$

Using equation (1.4) in equation (1.2) we have electric pressure

$$S = \frac{\sigma^2 kT}{2N}\Bigg\{\left[3\left(e^{x_1/\sqrt{3}} + e^{-x_1/\sqrt{3}}\right) + e^{x_2} - e^{-x_2} + 3\left(e^{x_2/3} - e^{-x_2/3}\right)\right]^2 / \left[4(\mu_1^2 + 2\mu_2^2) + (\mu_1^2 + 3\mu_2^2)\left(e^{x_1/\sqrt{2}} + \right.\right.$$

$$\left. e^{-x_1/\sqrt{2}}\right)(e^{x_2} + e^{-x_2}) + (3\mu_1^2 + \mu_2^2)\left(e^{x_1/\sqrt{3}} + e^{-x_1/\sqrt{3}}\right)\left(e^{x_2/3} - e^{-x_2/3}\right) + \frac{10\mu_2^2}{3}\left(e^{x_1/\sqrt{2}} + e^{-x_1/\sqrt{2}}\right)\left(e^{2x_2/\sqrt{6}} + \right.$$

$$\left. e^{-2x_2/\sqrt{6}}\right) - \frac{6\mu_1\mu_2}{\sqrt{3}}\left(e^{x_1/\sqrt{2}} - e^{-x_1/\sqrt{2}}\right)(e^{x_2} - e^{-x_2}) - (3 + \sqrt{3})\mu_1\mu_2\left(e^{x_1/\sqrt{3}} - e^{-x_1/\sqrt{3}}\right)\left(e^{x_2/3} - e^{-x_2/3}\right) -$$

$$2\mu_2^2(e^{x_2} - e^{-x_2})\left(e^{x_2/3} - e^{-x_2/3}\right)\Bigg]\Bigg\} \qquad \text{.............1.5}$$

The variation of electric pressure with temperature at steady electic field is given in fig1.1 and the variation of electric pressure with electric field at constant T=10K is given in fig1.2
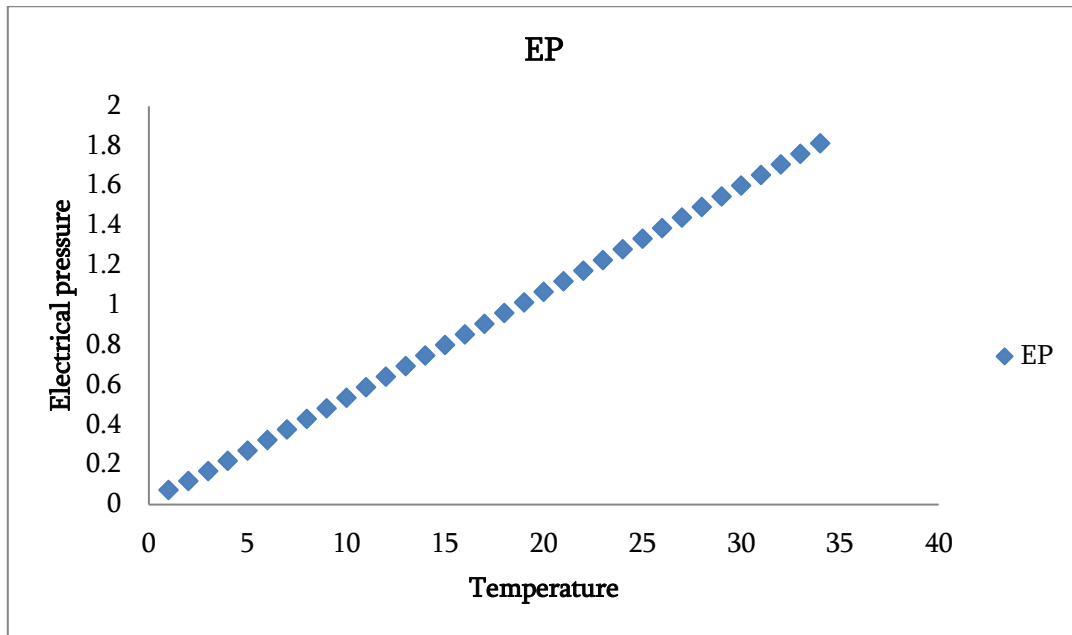
Fig 1.1
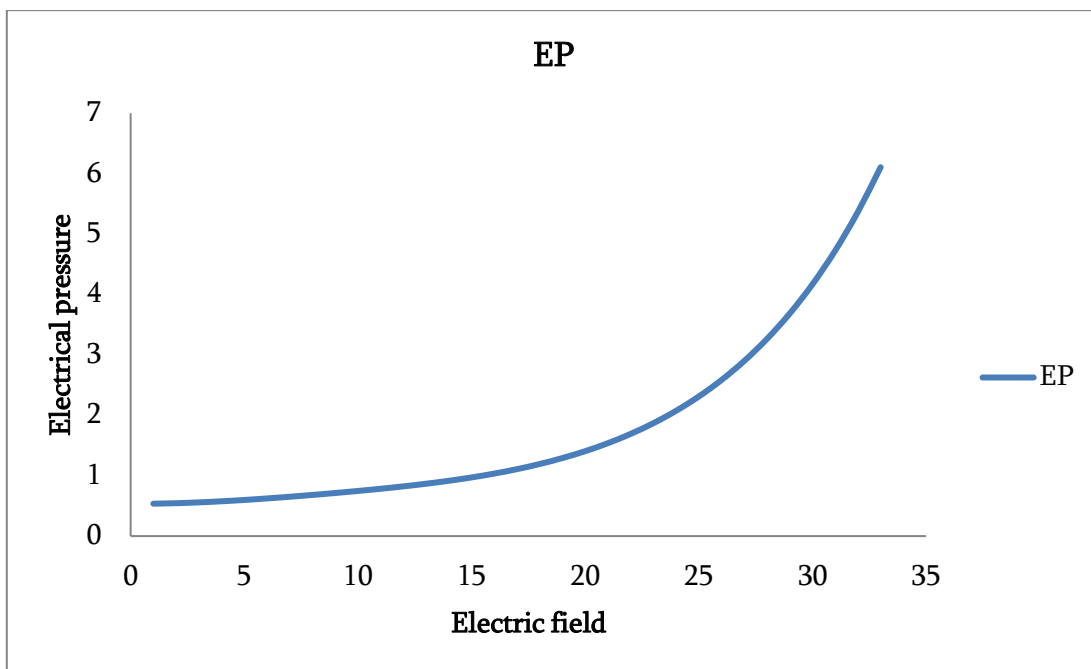
Fig 1.2

III. RESULT AND DISCUSSION

The result of present theoretical investigated for the <100>+<111> tunnelling model along crystallographic direction <111> is given by equation1.5.Fig1.1 and fig1.2 shows the variation of electric pressure with temperature and electric field for<100>+<111> tunnelling model respectively. From fig1.1 it is seen that the

electrical pressure increases with increases of temperature at constant electric field 10^6 V/m.From fig1.2 it is seen that electrical pressure increases slowly with increases electric field but afterward 30×10^6 v/m, electrical pressure suddenly increases with increases electrical field for system<100>+<111>.This theoretical study will be useful in future theoretical as well as experimental investigations.

IV. REFERENCES

[1].   W.Kanzig,H.R.Hart& S.Roberts,Phys.Rev.Lett.13,543(1964)

[2].   A.F.Devonshire,Proc.R.Soc.London A153,601(1936)

[3].   N.Lawless,J.Phys.Chem.Solids 28,1755(1967)

[4].   H .Flygare,J.Chem.Phys.39,2263(1963)

[5].   E.Mann,N.Acquista and D.White.J.Chem.Phys.44,53(1966)

[6].   M.Gomez,S.P.Bowen and Z.A Krumhansl.Phys.Rev.153,1009(1967)

[7].   G.K Pandey,K.L.Pandey,M.Massey&Raj Kumar Phys.Rev.B34,1277(1986)

[8].   G.K Pandey,K.L.Pandey,M.Massey&Raj Kumar Phys.Rev.B39,10300(1989)

[9].   Raj Kumar & P.N.Singh IAPS Vol.IV 2000

[10]. Raj Kumar et al J.Ultra Sci.14(3),545(2002)

[11]. Raj Kumar et al Bulletin of Pure and applied Sciences Vol.22D(No.2),115(2003)

[12]. Raj Kumar et al J.Ultra Sci.18(3),401-404(2006)

[13]. Raj Kumar et al Ultra Sci 20(1),P.131-134(2008)

[14]. Raj Kumar et al Bulletin of pure and applied Science, Vol.31D Physics, Issue2, P219-223, 2012.

[15]. Raj Kumar et al American International Journal of Research in Science,Technology,Engineering & mathematics,8(2),September November,2014,PP.149-151

[16]. MukeshUpadhyay, D.N Pandey et al AIJRSTEM 18- 409; 2018

Compound Push Pull Power Amplifier for Wide Frequency Band Applications Using pair of NMOS and NPN Nanotechnology

Arunendra Nath Tripathi[1], Abhinav Tripathi[1], Raj Kumar Tiwari[2], Monika Tiwari[3], Ganga Ram Mishra[2], Gaya prasad[1]

[1]Research Scholar, Department of Physics & Electronics, Dr. Rammanohar Lohia Avadh University, Ayodhya, Uttar Pradesh, India

[2]Professor, Department of Physics & Electronics, Dr. Rammanohar Lohia Avadh University, Ayodhya, Uttar Pradesh, India

[3]Rajkiya Polytechnic, Gonda, Uttar Pradesh, India

ABSTRACT

In present work we present a new technique to designed compound push pull amplifier using compound NMOS and NPN pair rather than Darlington and other pair. This is a new innovative pair designed by us to exaggerate the performance of the amplifier for Radio Frequency Communications systems. The proposed amplifier using complementary compound pair works for low power consumption 36mW and higher wide band frequency up to Peta Hz at 1mV input supply. It is simulated on 180nm cadence virtuoso tools NMOS and NPN nanotechnology. The proposed circuit shows high voltage gain at low value of inductor in order of Pico Henry and also shows good temperature stability.

Keywords: Frequency Response, NMOS and NPN pair, Push Pull Amplifier, Distortion and Temperature stability.

I. INTRODUCTION

The large signal amplifier as power amplifier is an important building block for all radio frequency communication systems. It provides sufficient power at the output load to drive output power devices. The push pull amplifier is most popular most familiar poweramplifier and its working based on the principal of class B amplifier. It is oftenused over the other power amplifier to spread out high efficiency without any distortion.[1], [2]. In present days basic requirement in electronic market is amplification of very low input voltage signal at very high frequency bandwidth without any distortion. In electronic field, this is major challenging and lure target for the researchers and designers of electronic field. So, to fulfil the above challenge various researcher had been studied and designed power amplifier properly with the help of various topology like cascading of transistors, RC coupled transistor, Transformer coupled transistors, Darlington pair, etc. [3],[4],[5] [6] .These have not to bring to an end the latest demand of electronic market due to efficiency and linearity problems with high band range. Accepting the above critical task, we design wide band push

pull amplifier using RKTANA pair. RKTANA pair is a compound pair designed by in the supervision of Raj Kumar Tiwari and his research scholarsArunendraNathTripathi& Abhinav Tripathi. So, it is called RKTANA pair.

II. COMPLEMENTARY COMPOUND PAIR

This pair is very effetely with low power consumption at very low input power supply to increase the band of signals. the block diagram of RKTANA pair is shown in fig-1.

This pair has been sketch with the help of two NMOS transistor and two NPN transistor. It has three terminals as general transistor like: gate, source, drain. In this innovative work, we used Very low value of inductor at output port, high value of register (100KΩ - 10MΩ) as output load of push pull amplifier which provide increased band width and low power consumption. The W/L ratio of the transistor depends on the maximum power defined by the user [7],[8]. In present case, it was estimated to maximum power 10 dBm with 1mV input supply voltage.
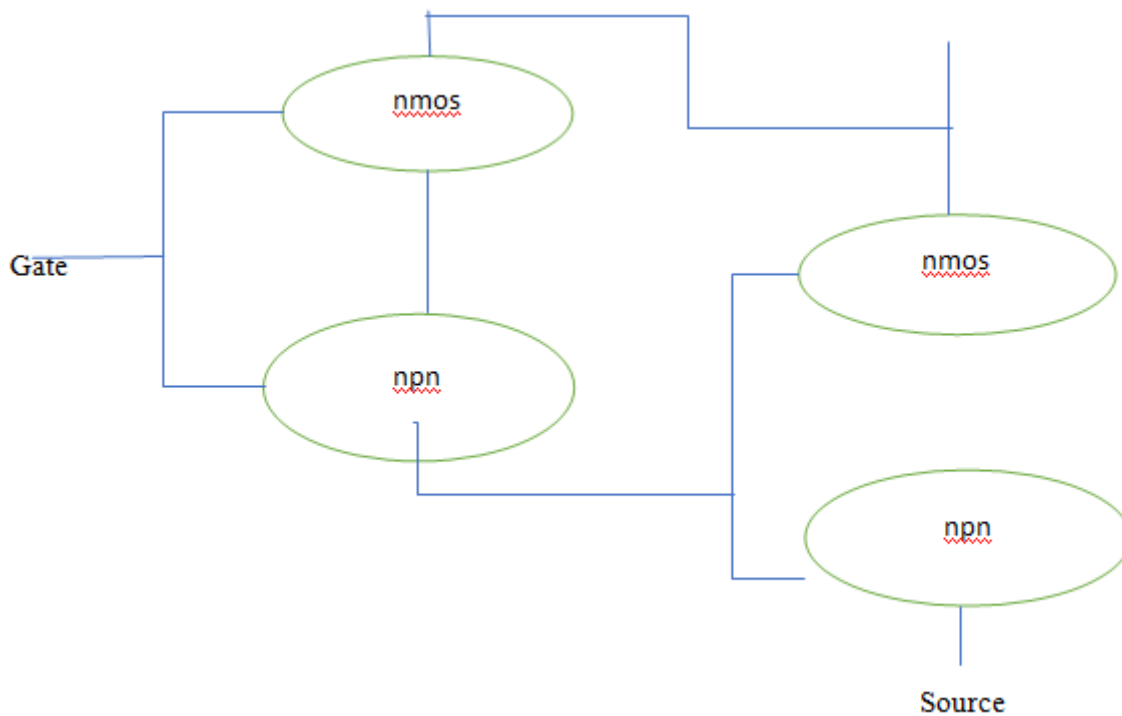

Fig. 1.:Model of compound pair

If a complementary pair is consisting of NPN deriver and PNP output device, then the device act as a simple NPN transistor. If a complementary pair is form as a PNP deriver and NPN output device, then the device act as a simple PNP transistor [9],[10], [11]. RKTANA pair provides very high current gain in the form of β or trans conductance in the form of g_m.

III. EXPLORATORY CIRCUIT

A distortion identified by nonlinearity of the dynamic characteristics may be to extract by using push pull class B power amplifier. When two NMOS inverters are connected in series having an ac input signal and voltage divider biasing with load 100 KΩ shown in fig-2 as a reference circuit. The simulated result of reference circuit with ac analysis is shown in fig-3 which provides narrow band up to KHz. Hence it can be used like tuned amplifier. But it can be increased by instead the NMOS inverter with complementary compound pair and very low value of inductor (pH) and RL (in MΩ) as a output load of power amplifier shown in investigated circuit fig-3. When the value of inductor varies between the 0.5 pH to 10 pH with high output load (1KΩ to Ω), then the maximum low cut off frequency and high cut-off frequency comes out 18.21Hz and 127PHz respectively with the help of proposed amplifier shown in figure- 5 by the ac analysis. While the reference circuit has the band in order of KHz only, it is very low as compare to proposed circuit.
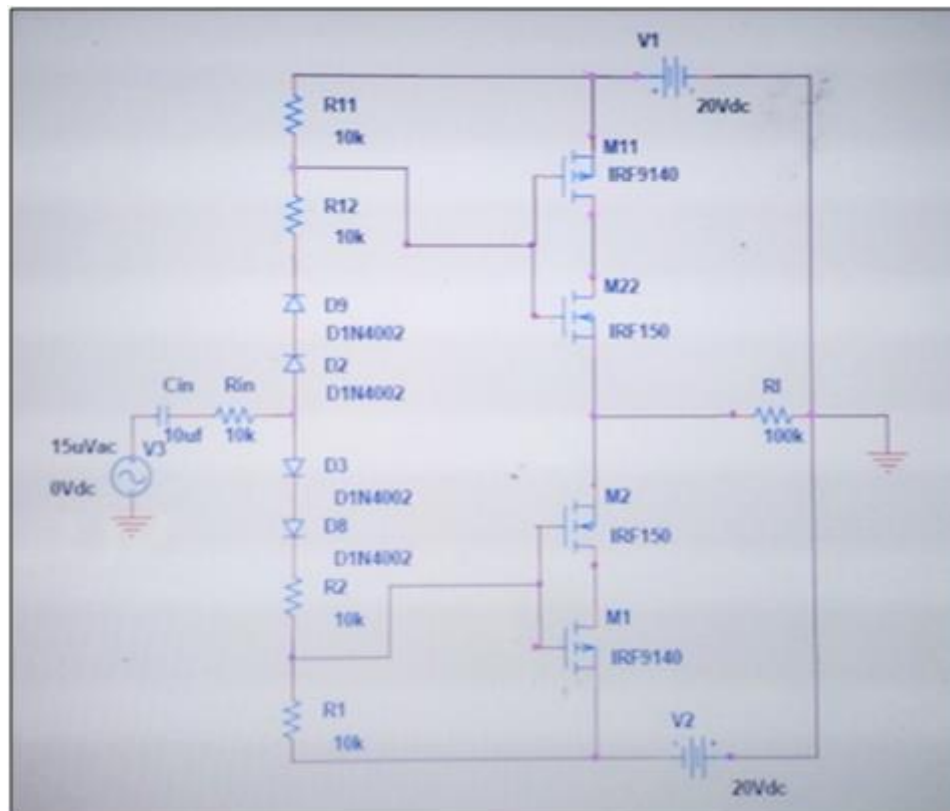
Fig.2
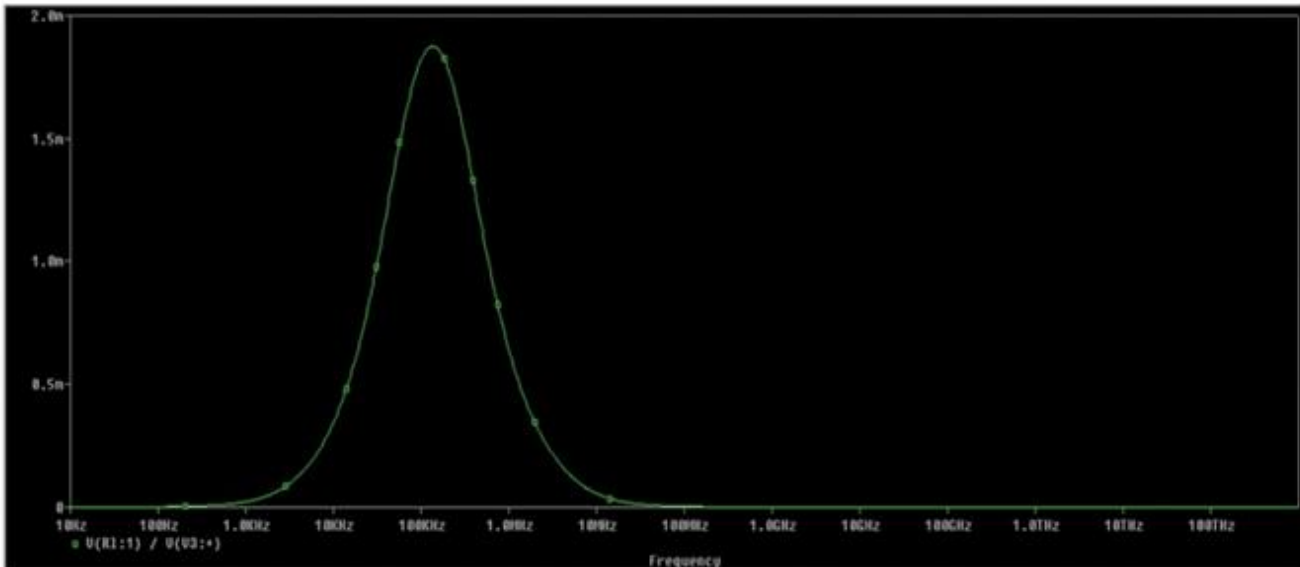
Fig-3 Ac Analysis of CMOS Push Pull amplifier (Reference Circuit)
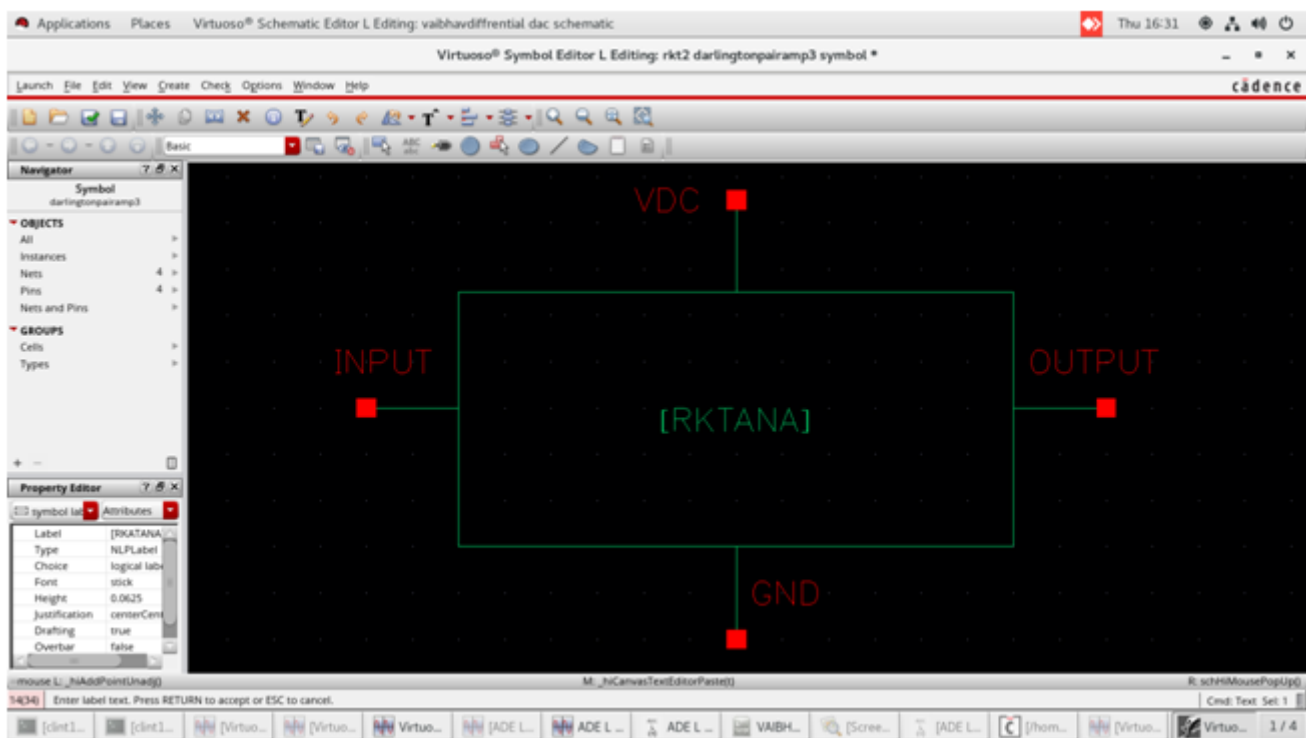
Fig4- Proposed push pull amplifier circuit

Hence, this proposed circuit is very useful for ultra-wide band large signal amplification. Other advantage as like high temperature stability (no temperature effect at high frequency), low output noise at higher frequency. We found 36 mW low power consumption and ultra-wide frequency band at L1=L2=1pH and RL= 1MΩ shown in following simulation results.

IV. SIMULATION RESULTS

Figure -3 shows the frequency response of reference circuit, the minimum frequency range KHz to MHz. So, it can be used for tuned frequency. While, exploratory circuit for the push pull power amplifier can be specialized for ultra- high frequency band Hz to PHz shown in figure –5


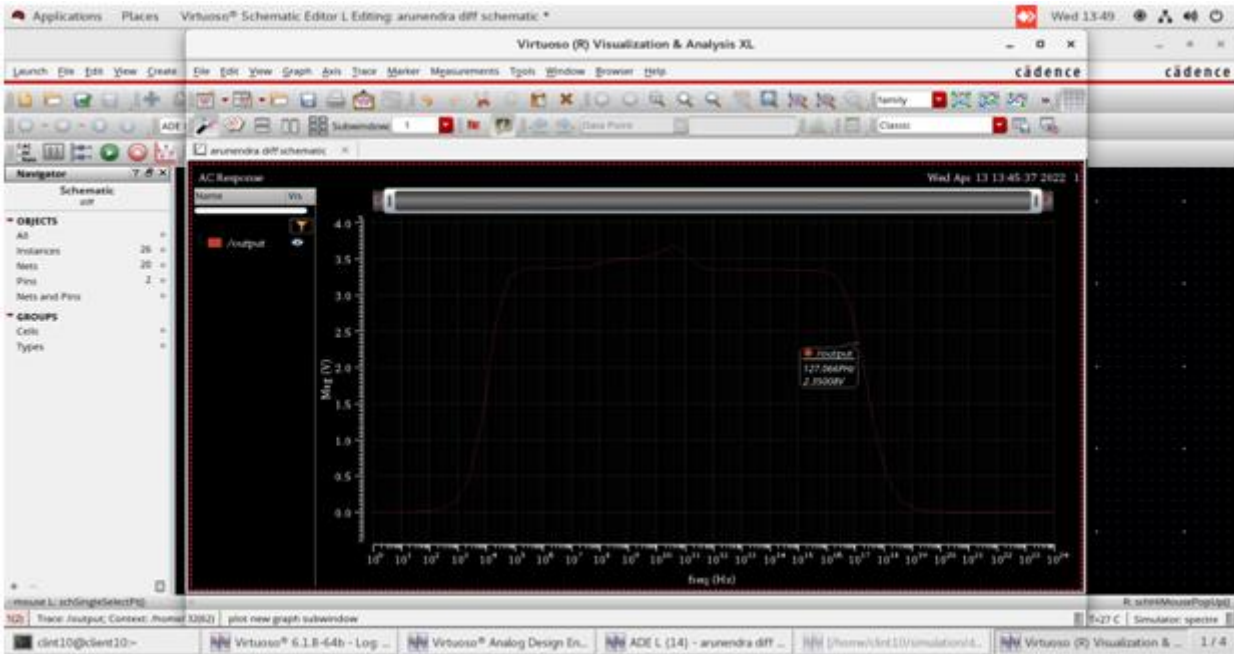**Fig-5 frequency response of proposed push pull amplifier**

The transient's analysis of exploratory circuit (fig-6) with respect to input and output shows that the amplifier has low distortion at output port. The power amplifier has very low power consumption (36mW) at input supply 1V shown in fig-7.
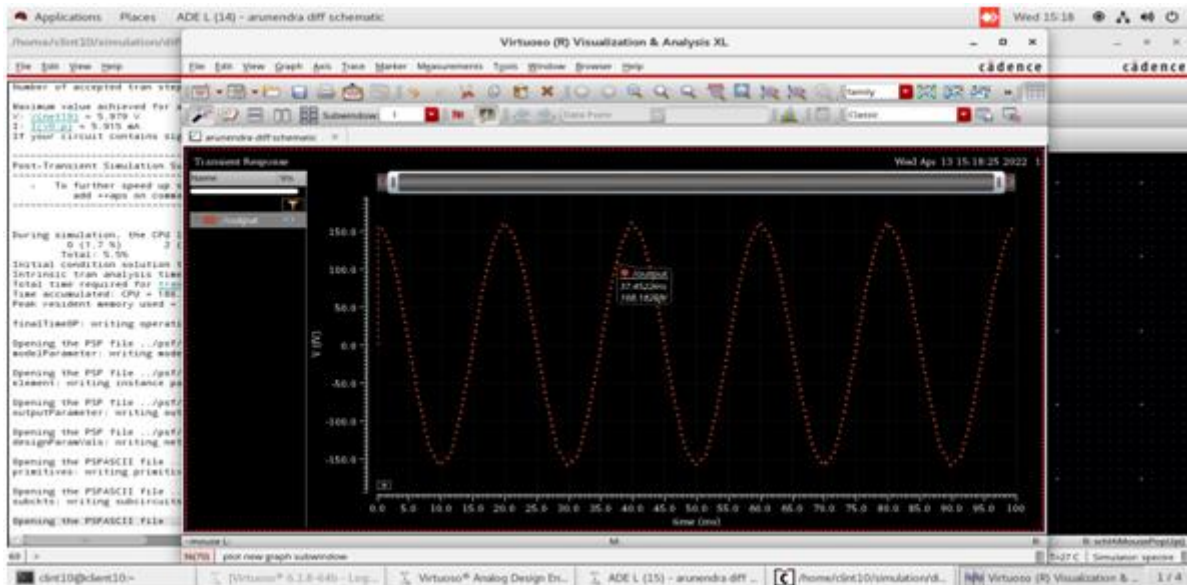
Fig-6Transients analysis of proposed complementary compound push pull amplifier (no distortion)
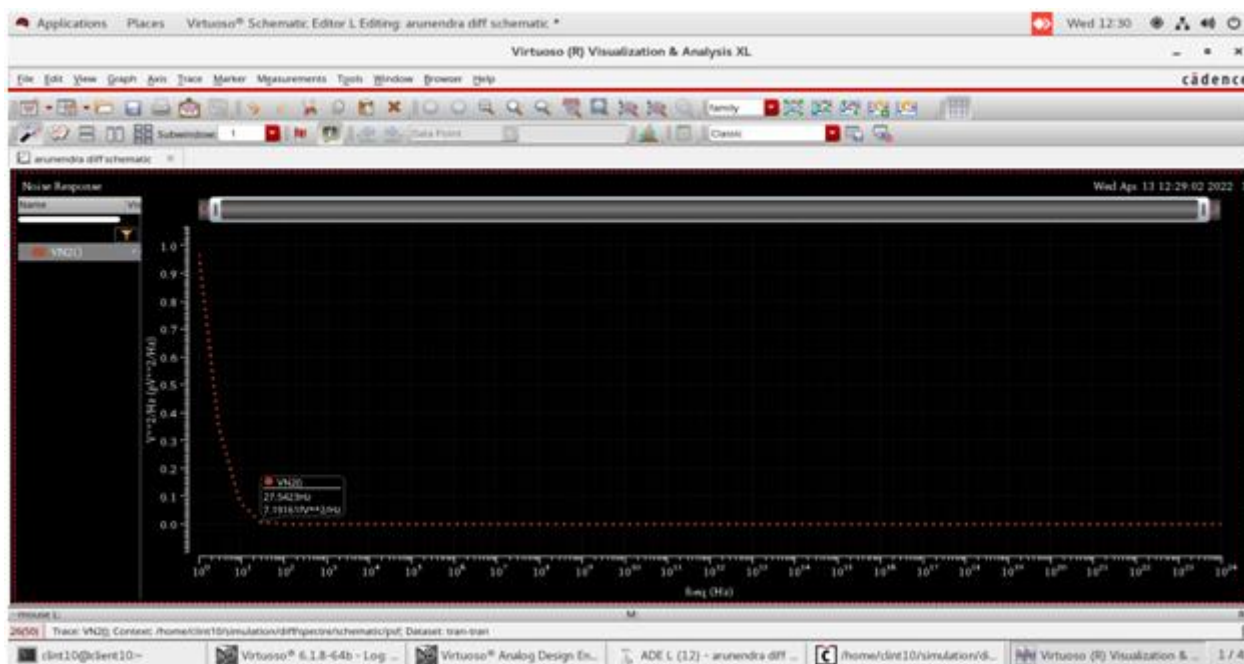
Fig-7The output noise response of proposed push-pull amplifier circuit

This power can be saved moreup to µW by using less than 1mV supply. But its effects the gain and frequency band width both.

V. COMPARISION TABLE

Tools	Technique	Supply voltage	Frequency band	Power consumptions	Voltage gain
65 nm cadence	Three Stage Common Source MOSFET [4]	1V	60GHz	-	8db
45nm Technology	Sub Threshold Region Behavior of Transistor [6]	1V	Up to 5 GHz	0.023mW	-
180nm Technology	CMOS Compund Pair [10]	µV	33.39KHz - 614.65GH z	-	20.9db
Cadence 180nm	CMOS RKTG Pair [13]	1V	100KHz– 6.26ZHz	69mw	14.8db
Cadence 180nm	**This work**	**1mV**	**75HZ-127PHz**	**36mW**	**36.8 db**

VI. CONCLUSION

From above simulation results we conclude that this investigated or designed complementarycompound push pull amplifier is very useful for ultra -wide band approximately 127 PHz at low input voltage 1mV with low value of inductor 1pH and high output load 5KΩ reported first time by our group. From above investigation it

isalso found that in reference circuit power consumption **69 mw** and in proposed circuit **36 mw** and **gain increased** from **14.8db to 36.8** and**bandwidth** approx.**127 PHz** . Band width of propped circuit is **much higherthan** reference circuit.So, we prefer proposed circuit in the place of **RKTG** in radio communications. Our further investigation is to study and measure other parameters by using active high Q CMOS inductor instead of passive inductor of this proposed power amplifier to achieve very high voltage gain with zero power consumption and high efficiency.

VII.   ACKNOWLEDGMENT

VIII. REFERENCES

[1]. Indian patent on CCMOS Compound pair amplifier for wide band amplifier by Raj Kumar Tiwari Shiksha Jain Gaya Prasad & Anurag Jain 2019

[2]. airchild Application Note 77, "CMOS The Ideal Logic Family" 1983.

[3]. S. C. Cripss, RF Power Amplifier for Wirless Communications. Boston, MA: Artech House, 1999.

[4]. D. Chowdhury, P. Reynaert, and A. M. Niknejad, "A 60 GHz 1-volt 12.3 dBm transformer-coupled wideband PA in 90 nm CMOS," in ISSCC Dig. Tech. Papers, Feb. 2008, pp. 590–591.

[5]. SofianeAloui, Eric Kerhervé , Didier Belot, and Robert Plana, "A 60GHz, 13dBm Fully Integrated 65nm RF-CMOS Power Amplifier," Circuits and Systems and TAISA Conference, 2008.

[6]. Raj Kumar Tiwari and Jyotsna Mishra, "A New Circuit Model for Distortionless Push-Pull Amplifier" in Bulletin of pure and applied sciences, An International Journal of Physics, Vol.29D(No.1) JanJune 2010.

[7]. Gauri P. Borkhade, Dr. D. S. Chaudhari, "Ultra- Wideband Low Noise Power Amplifier" International Journal of Advanced Research in Computer Engineering & Technology, ISSN: 2278 – 1323 Volume 1, Issue 4, June 2012

[8]. Raj Kumar Tiwari, Gaya Prasad, and Vineet Tiwari, "A Comparative Study of Multilevel DarligtonFET amplifier", published in Invertis Journal of science and Technology, vol.6, No.4, pp. 205-210, 2013.

[9]. Raj Kumar Tiwari and Gaya Prasad, "A High-Quality Factor Tuned Amplifier Circuit at High Frequency", Published in ActaCienciaIndica, Vol. XXXIX, pp.no.01-05, 2013.

[10]. Raj Kumar Tiwari, Gaya Prasad, "A New Circuit Model Of Low Voltage High Current Gain CMOS Compound Pair Amplifier" IJECET-2014, volume 5,issue 4,April 2014,pp.65-71.

[11]. Raj Kumar Tiwari, Gaya Prasad and Monika Tiwari, "Low Input Voltage High Gain Wideband CMOS Push Pull Amplifier for Tuned High Pass Filter," International Journal of Research in Electronics & Communication Technology, Volume-2, Issue-3, MayJune, 2014, pp. 27-31, ©

[12]. Gaya Prasad, Raj Kumar Tiwari, Shiksha Jain, Ganga Ram Mishra, "Simulation Study Of CMOS Compound Pair Amplifier", ICRISE-18.

[13]. Raj Kumar Tiwari, Gaya Prasad, Shiksha Jain, Ganga Ram Mishra, Monika Tiwari, ParulTrivedi, "RKTG Pair Amplifier with Gain Boosting Stage", AIJRSTEM 19-106; © 2019, ISSN-2328-3491.

[14]. Tiwari, Raj Kumar, Shiksha Jain, and Gaya Prasad. "Complementary Compound Push Pull Power Amplifier for Wide Frequency Band Applications Using CMOS Nanotechnology." In 2020 International Conference on Electrical and Electronics Engineering (ICE3), pp. 402-405. IEEE, 2020.

Ecosystem Rehabilitation Can Be Aided By a Livelihood Security Policy "MGNREGA"

BinodPratap Singh[1], Priya Pandey[2]

[1]Shri Lal Bahadur Shastri Degree College, Gonda, Uttar Pradesh, India

[2]Research Scholar, Dr. Rammanohar Lohia Avadh University, Ayodhya, Uttar Pradesh, India

ABSTRACT

The breakdown of Earth's environment is causing an unexpected environmental collapse. Despite growing involvement in rehabilitation, mostly through the UN Decade on Ecosystem Restoration (Decade), attempts to roll back deterioration have slowly emerged. To accommodate variety of stakeholders, restoration tasks require alternative ideas. However, there is an absence of evaluations of strategies and possibilities that assist to finance reconstruction while enhancing socio ecological results. The Mahatma Gandhi National Rural Employment Guarantee Act (MGNREGA) of India, the nation's biggest livelihood security programme, is used to analyse livelihood security financing and prospects for ecosystem restoration in this paper. The research paper perceives the merits and drawbacks of MGNREGA and broader learning outcomes for a handful of years. MGNREGA obtained major funding flows and a substantial majority of projects across the country that can help with ecological restoration. Also, during the first year of the COVID-19 pandemic, policy formation allowed for the progression and expansion of tasks. Our study results highlight the potential for linking ecosystem restoration with development policies to unlock funds on a national basis.

Keywords: MGNREGA, Sustainable Development, rural development, environmental regeneration.

I. INTRODUCTION

MGNREGA'S Role in Sustainable Development

Sustainable development is regarded as the expansion that meets the current generation's needs without harming succeeding generations' ability to meet their individual needs. It is made up of two fundamental concepts: "wants or needs" and "constraints."The phrase 'wants or needs' especially focuses on the basic requirements of the civilization's poor, which must be prioritized; and the idea of limitations imposed on the ecosphere's capability to meet existing and upcoming expectations by the degree of social and technology framework. Thus, economic and cultural expansion aims must be defined in terms of sustainability at the global level.Brundtland defined sustainable development (SD) in 1987 as "a development and well-being that satisfies the requirements of the current without jeopardizing future generations' ability to satisfy their own needs."Sustainable development is an inherent element in Indian culture, and it is abundantly mirrored in our culture and ancient religion. India accounts for around 18% of the earth's population and is home to approximately 30% of the impoverished and 40% of the earth's illiterate humans. which is a major

impediment to encouraging sustainable development. To attain this sustainability, each nation must offer its best efforts, with India contributing far more than other nations. Sustainable development is an inherent element of Indian ideology and heritage, and it is abundantly mirrored in our society and ancient religion. India accounts for around 18% of the earth's population and is home to approximately 30% of the impoverished and 40% of the world's illiterate people, which is a major impediment to encouraging sustainable development. Due to the terrible impact of the Bhopal gas catastrophe as well as worldwide expansion, a movement in favour of environmental conservation and sustainability started at the beginning of the 1980s in India. During the 1990s, sustainable development was incorporated into the planning phase. The 9th Five-year Plan (1997-2002) openly acknowledged the alignment between surroundings, wellbeing, and growth and outlined the ecological responsibility of such development phase as one of its core objectives through social mobilisation and participation of people in all contexts as one of its main aims. Among the programmes conducted by the government to meet the aims of poverty alleviation and sustainable development were the Community Development Programme (CDP), Integrated Agricultural District Programme (IADP), National Extension Service (NES), High Yielding Varieties Programme, and others. Furthermore, the Government of India has established various policies relating to sustainable development, with an emphasis on socio-eco growth, particularly for people with poor living standards, along with environmental protection. The passage of MGNREGA is one such huge initiative toward protracted sustainability.

The Mahatma Gandhi National Rural Employment Guarantee Scheme (MGNREGS) was successfully launched in 2005. It aims to improve rural people's economic stability by officially giving at least 100 days of compensated employment in each financial year to adult members of families willing to conduct manual unskilled labour connected to public activities. It is the biggest social welfare program in history, including all 626 districts and helping 41 million families.

The programme's aims include

1. Providing job opportunities for the most vulnerable people in rural India to ensure welfare support.
2. Providing long-term consistency to impoverished economic growth through the construction of long-term assets, improved water protection, soil and water restoration, and higher land production.
3. Optimizing flood and drought avoidance in rural India. Through the practice of rights-based legislation, assisting in the empowerment of particularly Scheduled Castes (SCs), and Scheduled Tribes (STs), women.
4. Increasing decentralized, participatory planning by bringing together various anti-poverty and livelihood projects.
5. Strengthening Panchayati Raj Institutions to deepen democracy at the grassroots (PRIs).
6. Increasing openness and accountability in government.

Furthermore, MGNREGA initiatives focus on groundwater recharging, drought-proofing, water collecting, and flood protection activities. Its emphasis on environmental restoration and sustainable living will result in greater land productivity over time, aiding employees in making the transition from wage employment to sustainable employment. Furthermore, almost 80% of MGNREGA initiatives include soil and water

conservation. By definition, MGNREGA strives to boost agricultural productivity, replenish groundwater, and increase water availability. The recent change to the Act to allow MGNREGA to operate on the land of marginal and small farmers, who account for 89% of the farming community, in contrast to SC/ST/BPL/IAY individual land, would increase the implications for agricultural output and household income.

Thus, in order of priority, the scheme's attention will be on the following works:

1. Water harvest and recycling.

2. Drought defences (This includes afforestation and tree planting)

3. Canals for irrigated agriculture, including super micro and minor irrigation infrastructure

4. Irrigation systems, horticulture, planting, and land reform accommodations are required for land owned by households belonging to below-poverty-line families, Scheduled Castes and Scheduled Tribes, or beneficiaries under the Government of India's Indira AwaasYojana, or small farmers or marginal farmers, or beneficiaries of land reforms as described in the Agriculture Department Waiver and Debt Relief Scheme, 2008, or beneficiaries associated to agriculture.

5. Conventional water reservoir rehabilitation, incorporating tank desalination.

6. Transformation of land in the rural area.

7. Operations on flood management and preservation, incorporating disposal in water-logged areas.

8. Remote close connection to facilitate all-weather access, and

9. Any extra task that the Central Government may disclose in collaboration with the State Government.

Thus, tasks were performed under this legislation to revitalize the ecosystems and tackle chronic poverty reasons such as drought, deforestation, soil degradation, floods, and insufficient rural connection; all of which are important parts of sustainable development. This programme of reducing rural poverty and addressing natural resources is strong due to the legal procedures and the premise that it is an Act. The Indian constitution enshrined leadership in strengthening grassroots democratic processes and instilling openness and accountability in rural government. NREGA is intended to eradicate poverty, which is strongly tied to the disruptions such as environmental damage, stability and prosperity, disparities, corruption, a lack of alternatives, and inefficient resource use are all hurdles to attaining ecological growth. Department of Economic and Social Affairs, United Nations, 2008. Poverty eradication provides a conceptual foundation for the process of sustainable development through a normative framework developed from globally recognized Human Rights Standards. Poverty alleviation is thus a necessity for environmental conservation; poverty exacerbates the issues of malnutrition and hunger are further exacerbated by disparities and unequal access of individuals to access food. Furthermore, disparities caused by poverty result in resource waste and hardship, which eventually raises the state's crime rate. MGNREGA, is one aimed at promoting and defending the human rights of people living below the poverty line.

It is also worth noting that the effectiveness of NREGA in avoiding humanitarian calamity during the corona epidemic in rural India has resulted in renewed calls for URBAN NREGA. Without a question, the Covid-19 problem has to light the vulnerabilities that plague the life of the urban poor. They are often less insecure than the rural poor, partially because fallback labour is simpler to obtain in cities, even if it is as simple as pushing a tricycle or distributing tea. Nonetheless, the urban poor remain vulnerable to major eventualities,

both individual (such as sickness and jobless) and social (such as lockdowns, floods, hurricanes, and economic turmoil). Social media platforms, civil society groups, and mutual assistance can all be beneficial, but they have apparent limitations, particularly in times of communal disaster such as the Corona epidemic. As a result, there is a need for improved welfare support in metropolitan regions, encompassing both large and small cities. Aware of the severity of alleviating the economic uncertainty of the urban poor while also revitalizing the urban economic system, Jean Dreze, one of the original NREGA's architects, has drifted a radical proposal—a Decentralized Urban Employment and Training scheme, or DUET, which incorporates government-issued job stamps that can be utilised to employ employees.

II. ENVIRONMENTAL BENEFITS THROUGH MGNREGA

In contradiction to various research studies that have examined the effect of MGNREGS on the economic health and social growth of the country's less-entitled parts, the environmental consequences of the programme have received less attention. The program's possibilities in ecological sustainability are relatively underutilized, which may mirror policymakers' and think tanks' lack of consideration for environmental protection in the midst of the greater clamor for the nation's financial stability and severe obsession for mathematical advancement of GDP, which, in fact, "is an unsatisfactory metric to gauge well-being over time" (Stiglitz et al 2009). It has been commonly stated that a focus on traditional productivity expansion does not bring to alleviate poverty (Peng 2009). Despite apparently unrealistic anchoring of poverty scales, research shows a decline in per capita consumption of grain (Patnaik 2009,2012) or true societal wellbeing under the standard growth economics paradigm. Eradication of poverty is increasingly intimately and comprehensively tied to environmental protection, and policies and interventions must reflect this. The many practices advocated under MGNREGS, such as watershed management and land reclamation, may have a significant impact on environmental stability, ecology, and environmental protection. Indeed, one of the key activities envisaged in NREGA is environmental protection (IAMR2009).

Research undertaken by the Indian Institute of Science in four districts of four chosen states, mainly Chitradurga (Karnataka), Medak (Andhra Pradesh), Bhilwara (Rajasthan), and Dhar (Madhya Pradesh), found that implementing various MGNREGS programmes resulted in significant environmental advantages. The big advantages noted are improvements in water resources (such as rainwater harvesting and extracting projects, water shortages, irrigation procurement, and advancement projects, remodeling of conventional water bodies, enhanced levels of groundwater, additional water provision for irrigated agriculture, enhanced area irrigated by surface and groundwater sources, and lastly, to enhance drinkable water supply for both humans and domestic animals), Environmental advantages and disaster resilience, enlargement of land resources making contributions to optimized soil organic carbon (SOC) content, smaller surface run-off and soil degradation, improvement of agricultural production and crop yields, and beneficial effects on forested areas, plantations, and fruit trees.

Kabeerdham district in Chhattisgarh has accomplished a bunch of labour, planting, and drought-proofing under the supervision of MGNREGS in 2006-07. Limca Book of Records has acknowledged MGNREGS work

for planting 37 lakh seedlings in a single operating day along the side-lines of national highways, state highways, village roads, and deteriorated forest areas. Some communities have begun to practice collaborative reforestation. Jatropha, Gulmohar, bamboo, mango, teak wood, guava, and other plants were picked. It would have been preferable if more native species had been chosen for planting.

III. CONTRIBUTION OF MGNREGA IN BIODIVERSITY

Even if it has been planned underneath MGNREGS to undertake biodiversity protection and improvement projects, the investigation revealed that protecting the environment has yet to be internalized as one of MGNREGS's major aspects. The United Nations Development Programme's (UNDP) prioritized guidelines for MGNREGS, for example, in the report "Greening Rural Development in India" (UNDP 2012), fall short of providing any concrete intervention proposals for biodiversity sustainability should be included in enduring rural development programmes in India. Sustainable green rural development refers to five criteria that do not include biodiversity protection as one of them. It fails to underline the critical relationship between biodiversity protection, ecological security, and regional development in its efforts. The proposed green projects focus on environmental challenges on a wider level.

IV. CONCLUSION

As can be seen, sustainable development does not focus primarily on economic challenges but rather spans three broad policy areas: the environment, the economy, and society. Sustainable development strikes a harmony between diverse human demands, such as the desire for better lives and a sense of well-being, on the one side, and the preservation of natural resources and ecology on the other. Hence, Sustainable Development is the keeper of the various aspects required for the survival of current and upcoming generations. It is widely acknowledged that sustainable development can't be realized without a significant decline in the number of poor people. If we allow poverty to persist in the society of India, the promise will never be realized for sustainable development. Only by addressing the issue of poverty will India achieve long-term development. As a result, MGNREGA is considered to be a rights-based strategy for poverty contraction that has demonstrated how human rights may be sustained by the overall legislative structure and achieved in a sustainable way. Convergence is used as a lever and may be used as a strategic method to eliminate poverty and enhance long-term growth. The opportunity of employment supplied under the head of the MGNREGA scheme may be better employed for the prerequisites of growth. Since the commencement of the MGNREGA, India has achieved great headway in decreasing poverty, hunger, and food uncertainty, which is the initial step toward attaining sustainable development. It is recommended that as members of society, it is our obligation to support sustainable growth by utilizing alternative resources rather than having infinite demands.

Furthermore, the government should take measures to bring together diverse institutions such as commercial, public, and educational bodies for this objective, and should view MGNREGA as a concourse for executing

various policies aimed at attaining sustainability. It is also important to raise awareness among students about the different MGNREGA programmes by including them in their curriculum. The government should not create new policies on sustainable development since they are ineffective; rather, the government should make sufficient efforts to implement current policies. It is up to us to determine if progress means opulence or peace, prosperity, and happiness, and MGNREGA can be a superior approach for achieving development if implemented properly.

V. REFERENCES

[1].   Stiglitz, Joseph E, AmartyaSen and Jean-Paul Fitoussi (2009): "Report by the Commission on the Measurement of Economic Performance and Social Progress", September, available at: http://www.stiglitz-sen-fi toussi.fr/documents /rapport_ anglais.pdf

[2].   IAMR (2009): "All-India Report on Evaluation of NREGA: A Survey of Twenty Districts", prepared with fi nancial support and research inputs from Programme Evaluation Organisation, Planning Commission by Institute of Applied Manpower Research, New Delhi; available at: http://planningcommission. gov. in/ reports/genrep/rep_NREGA.pdf

[3].   UNDP (2012): Greening Rural Development in India, United Nations Development Programme Report, Volume I, available at: http://www. undp. org/ content/dam/india/docs/EnE/greening-ruraldevelopment-in-india.pdf

[4].   World Commission on Environment and Development (WCED), Our common future. Oxford: Oxford University Press,1987 p. 43

[5].   Drèze, Jean, ReetikaKhera and Siddhartha (2008): "Corruption in NREGA: Myths and Reality", The Hindu, available at: http://www.thehindu. com/ 2008/01/22/ stories/2008012254901000. Html

[6].   Patnaik, Utsa (2009): "Origins of the Food Crisis in India and Developing Countries", available at http://monthlyreview.org/2009/07/01/origins-of-the-food-crisis-in-india-and-developingcountries – (2012): "Capitalism and the Production of Poverty", TG Narayanan Memorial Lecture, Asian College of Journalism, Chennai.

[7].   Peng, Aster (2009): "NREGA Significance and Status – Microanalysis on the Status and Implementation of NREGA", Society for the Promotion of Wasteland Development, available at: http://www.spwd.org/wp-content/ uploads/ 2011/11/NAREGA-Signifi cance-andStatus_Aster-Peng_R2009.pdf

[8].   IIS (2013): Synthesis Report on "Environmental Benefits and Vulnerability Reduction through Mahatma Gandhi National Rural Employment Guarantee Scheme", Indian Institute of Science, Bangalore, available at: http://nrega.nic.in/ Netnrega/WriteReaddata/Circulars/Report_ Env_Benefi ts_Vulnerability_Reduction.pdf

[9].   Annual Report 2006-07, ZillaPanchayat, Kabeerdham, CG.

[10]. Planning commission of India

[11]. available at http://www.nrega.nic.in/circular/Convergance_Guidelines.pdf

[12]. available at https://sustainabledevelopment.un.org/content/ documents/Agenda21. pdfhttp//cmsdata.iucn.org /downloads/poverty.pdf

Future Development of Smart Materials Content

Jitendra Singh

Department of Physics, Shri L.B.S. Degree College, Gonda, Uttar Pradesh, India

ABSTRACT

Smart materials are excitation sensitive that constitute a wide range of materials to exploit vibration control such as piezoelectric, shape memory alloy, electro rheological fluid and magneto-rheological fluid. Smart materials show a certain amount of analogy with respect to biological systems. For example, piezoelectric hydrophones which show the similarity of ears by which fish feel vibrations. This review initially discusses a brief summary of the stimuli responsive smart materials above followed by a full description of some of the smart materials.

Keywords: Piezoelectric, Optical fiber, Shape Memory Alloy, Electro-Rheological Fluid and magneto-rheological fluid.

I. INTRODUCTION

Smart content has been extended to materials that receive, transmit, or respond to a stimulus by producing a useful effect that may include an indication that the material is acting on it.Some stimuli that can act on these materials are: strain, stress, temperature, hydrostatic pressure, different types of radiation,chemicals (pH stimuli), electric field, magnetic field, and other forms of stimuli [1].Today the direction of innovation is stronger than ever.New technologies and applications are spreading in all areas of science.As a result, the expectations and needs for engineering applications have increased tremendously, and the prospects of smart technologies to achieve them are very promising[2].

II. CLASSIFICATION OF SMART MATERIALS

The term "smart materials" sometimes are also known as intelligent materials or active materials to describes a group of material systems with unique properties. At this stage, followingmaterials are the active ones:

➢ Piezoelectric materials
➢ Optical fiber,
➢ Shape memory alloys
➢ Magnetostrictive materials
➢ Electrorheological materials
➢ Magnetorheological fluids

Also some materials systems which do not exhibit shape change but others areCritical properties are sometimes called smart materials.Example: electro- and magneto- theologicalfluids. These fluids can change viscosity over several orders of magnitude upon application of an external magnetic or electric field [9].

2.1 PIEZOELECTRIC MATERIALS:

Piezoelectricity, discovered by the brothers Jacques and Pierre Curie in Rochelle Salt 1880, is defined as a change in electrical polarization with a change in applied strain, commonly known as the direct piezoelectric effect.The converse piezoelectric effect is analogous to a change in strain for a free crystal (or strain for a clamped system) with a change in the applied field.Thus the converse piezoelectric effect is commonly used when a physical system is to be constructed using an actuator: Input is a voltage gradient, output a strain. There is a linear relationship between strain and electrical field for low fields. Reversing the field also reverses the direction of the strain[9].Piezoelectric materials can improve the performance of existing products [3].
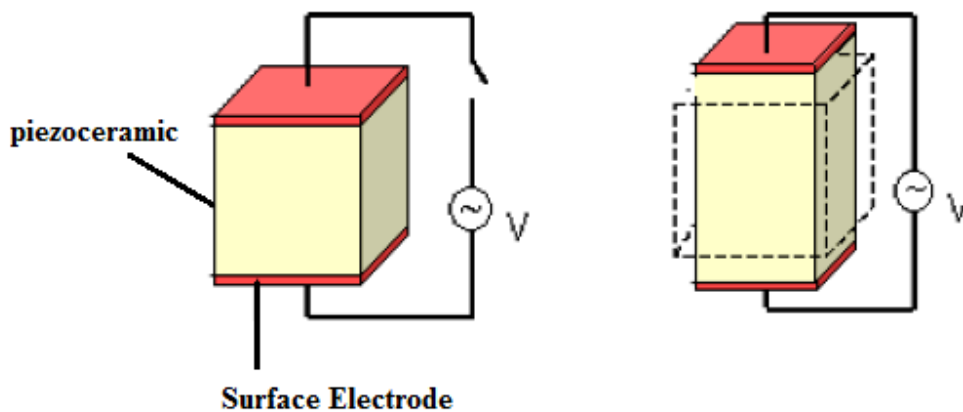

Fig.1: Piezoelectric Materials

2.2 OPTICAL FIBRES:

Optical fibers are often used to transmit light between the ends of the fiber.They are widely used in fiber-optic communications.Mechanical blades, shafts and civil structures are some of the structures that are monitored for variations in stress due to cracks and damage.The most commonly used smart materials for structural health monitoring are fiber-optic sensors and piezoelectric wafer activated sensors. Fiber Bragg grating and fiber-optic polarimetric sensor are the two fiber-optic sensors. Fiber Bragg grating sensor are used for local strain measurement and which can be easily embedded in composite structures for structural health monitoring.Small diameter fiber Bragg gratings have recently been developed to measure internal stress fields that are non-homogeneous.Strain across the entire length of the structure as measured by a fiber-optic polarimetric sensor.Optical fiber can be used to transmit electricity with the help of solar cells.Optical fibers can be used as light guides in medical and other applications.

2.3 SHAPE MEMORY ALLOY:

Shape memory alloy can change in any shape with variation in temperature.One peculiarity that makes it different from other materials is that it can remember its original shape when subjected to external stimuli which is stress.They are also known as intelligent materials.These shape changes occur in two phases from martensites to austenite.The martensite phase is stable at low temperatures and the austenite phase is stable at high temperatures.The occurrence of these thermo mechanical properties of shape memory alloys is due to a reversible solid–solid phase change controlled by temperature and mechanical stress.In terms of phase changes occurring in phase steels are austenite and martensites.
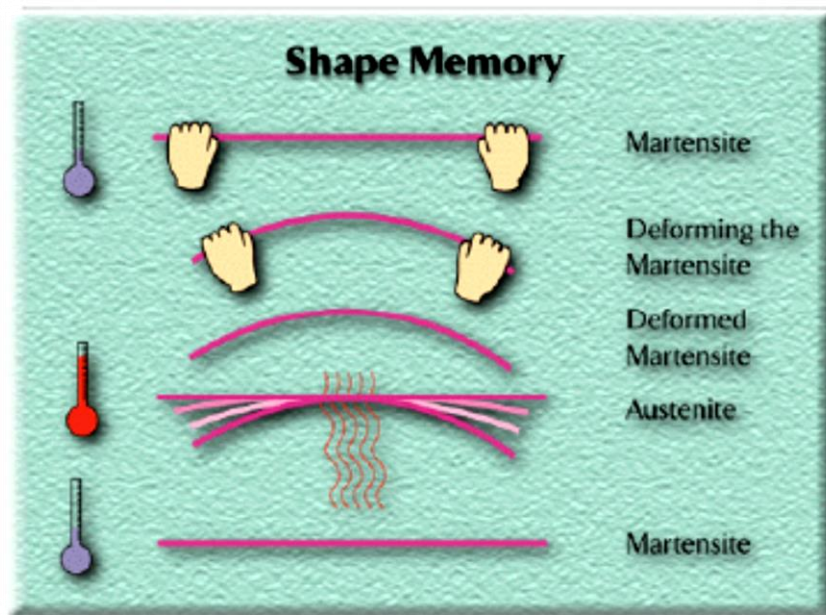

Fig. 2: Shape Memory Materials Proformence

These alloys for commercial use, mostly titanium-nickel alloys, undergo a phase change upon temperature change.This austenitic to martensite transformation can directly lead to sample volume and change size.In addition, if designed properly, materials (such aswire or spring form) can be trained to transform completely reversibly in an exactly reproducible way. Thus represents a micro-motor that can be operated by increasing and decreasing the temperature.Shape memory alloys are a class of novel materials that exhibit two effects: shape memory effect and pseudo-elasticity [9].

2.4 MAGNETORESTRICTIVE MATERIALS:

Magnetorestrictive materials are materials in which the material reacts to mechanical deformation when stimulated by a magnetic field. Also Magnetorestrictiveisapropertyofferromagneticmaterialsthatcausesthemtochangetheirshapeordimensionsduringtheprocessofmagnetization.When these solids are placed in a magnetic field, the repositioning of the domain walls leads to hysteresis between the magnetization and an applied magnetic field.When a ferromagnetic material is heated above its Curie temperature, these effects disappear.The microscopic properties of a

ferromagnetic solid are different from those of a ferromagnetic solid.In a ferromagnetic solid the alignment of dipoles can be parallel or in other directions [4-6].Magnetorestrictive materials are usually inorganic in chemical composition. The most effective magnetorestrictive material is another alloy Terfenol-D developed at the Naval Ordnance Laboratory. It is an alloy of terbium, dysprosium & iron. The whole effect of magnetorestriction occurs in crystalline materials.

2.5 MAGNETO-RHEOLOGICAL FLUIDS

Magneto-rheological fluids will change their rheological properties, such as stress and viscosity, upon application of a magnetic field.Magneto-rheological fluids are also known as magneto-sensitive smart materials [7]. Magneto-rheological elastomers are rubber-like soft particles whose mechanical properties can be changed upon application of a magnetic field.Magneto-rheological elastomers consist of basic components: magnetic particles, non-magnetic elastic matrices and additives.The viscous properties of these materials can be changed by changing the magnetic field.Carbonyl iron is used to prepare magneto-rheological fluids because of its high saturation magnetization. Some of the properties of Magneto-rheological fluids are magnetic property, light in weight, controllable modulus and excellent sound-absorption,visco-elastic in nature.The basic structure of Magneto-rheological fluids was first described in the late 1940's and is shown in Fig.3 [9].
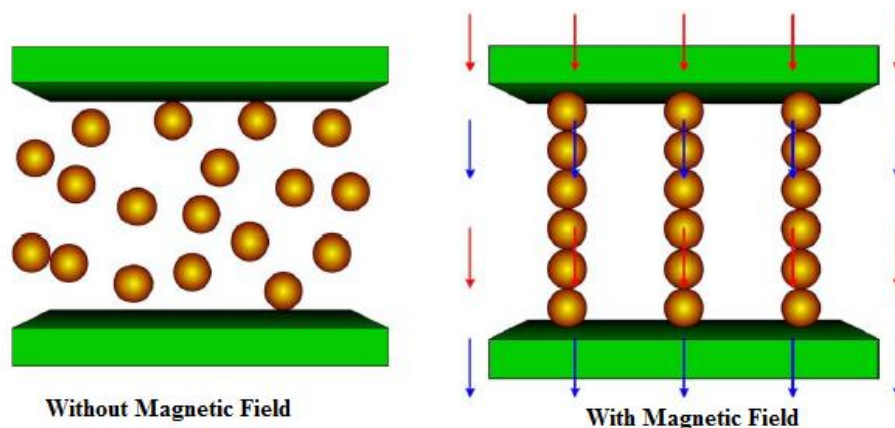

Fig. 3: Basic Structure for Magneto-rheological fluids

2.6 ELECTRO-RHEOLOGICAL FLUIDS:

Electro-rheological fluid is the suspension of very small particles in an electrical insulating fluid. They will rapidly form a solid-like structure in the direction of field when the electric field is applied. They will return from one state to another, i.e. from gel state to liquid and vice versa upon application of an electric field. There are different applications of Electro-rheological fluidin vibration isolators, the automotive industry, shock absorberand clutch. Some properties of electro-rheological fluids arehigh dielectric constant, interfacial bond strength, constable rheology and dielectric in nature, damping coefficient is changed in the electric field.

III. APPLICATION OF SMART MATERIALS

Smart materials are used in a wide range of applications due to their diverse response to external stimuli.Various fields of application can be in our daily life, aerospace, civil engineering applications and mechatronics to name a few.The scope of application of smart materials includes solving engineering problems with immeasurable efficiency and provides an opportunity to create new revenue generating products.The important feature related to smart materials and structures is that they encompass all areas of science and engineering [8].

➢   Medical (Health, Bio-medical)
➢   Smart switches & actuators
➢   Safety device, fuse, alarms
➢   Artificial limbs, blood vessels & muscles (Smart materials Polyurethane-bio compatibility)
➢   Smart clothes (Adaptive to temperature changes)
➢   Smart spoons (Temperature sensitive polymers)
➢   Smart nose & tongue (recognition characteristics)
➢   Food packaging industry-wrappers(adoptability)
➢   NiTiNOLwire-diameterinmm
➢   An"animatedlamp"designed by RomoloStanco that uses shape memory alloy to change its shape whenever it's turned on and off.
➢   StealthBombers"haveferrofluidsontheirouter"skin"tomakethemhardertospotwithradar.
➢   Aircraftwhichwillincorporate"smartmaterials"thatwillallowthewingsof acrafttochangeshapeforoptimalflyingconditions.
➢   Adhesive tapes/bands (time bound adhesive property /painless removal/healing property).

IV. CONCLUSION

The future of smart materials and structures are wide open.It is likely that more interdisciplinary research efforts should be expended. On the other hand, the roles of designers, factories and customers will be redefined significantly as the manufacturing business will be distributed across many different locations such as small workplaces or homes. Understanding and controlling the structure and microstructure of any new material is the ultimate aim of research in this area, and is critical to the production of good smart materials.Insights gained by collecting data on the behavior of the material's crystal internal structure as it heats and cools, deforms and changes, will accelerate the development of new materials for use in a variety of applications.Structural ceramics, superconducting wires and nano-structural materials are good examples of complex materials fashioning nanotechnology.

V. REFERENCES

[1]. J. A. Harvey,Kirk-Othiner Encyclopedia of Chemical Technology, 4thed., Supplement, Wiley, New York,pp. 502–504,1998,.

[2]. Georges Akhras, "Smart Materials and Smart Systems for the Future" Canadian Military Journal, Autumn 2000.

[3]. R.A. Silva-Muñoz, R.A. Lopez-Anido, Structural health monitoring of marine composite structural joints using embedded fiber Bragg grating strain sensors, Compos. Struct.89 224–234, 2009.

[4]. J. A. Harvey,Kirk-Othiner Encyclopedia of Chemical Technology,4th ed., Supplement, Wiley, New York, pp. 502–504, 1998.

[5]. R. E. Newnham,Mater. Res. Soc. Bull.,22(5), 20–34, 1997.

[6]. B. Culshaw,Smart Structures and Materials,Artech House, Boston, pp. 43–45, 117–130, 1996.

[7]. Butera, F., "Shape Memory Actuators", Advanced Materials & Processes, pp. 37-40, 2008.

[8]. SusmitaKamila,   Introduction,Classification   and   applications   of   Smart   materials:An Overview,AmericanJournal of Applied Sciences 10 (8): 876-880, 2013.

[9]. Bohua Sun,Smart materials and structures, Lecture at Swiss Federal Institute of Technology Zurich (ETH),2015.

Micro Structural, Electrical, and Humidity Sensor Analysis of NiO and SnO₂ Nano Particles Synthesized through Co-Precipitation

Vernica Verma[1]*, Priya Gupta[2], Narendra Kumar Pandey[1], Peramjeet Singh[1], Neetu Yadav[1]

[1]Department of Physics, University of Lucknow, Lucknow-226007, Uttar Pradesh, India

[2]Department of Electronics and Communication Engineering, Integral University, Lucknow-226026, Uttar Pradesh, India

ABSTRACT

The present work deals with the synthesis of intrinsic nickel oxide (NiO) and tin oxide (SnO2) nanostructures by co-precipitation synthesis. NiO and SnO2 samples are pelletized and annealed at $400\,^{\circ}C$ and are analyzed on the basis of their humidity sensing, structural, morphological and electrical properties. Powder X-ray diffraction (XRD) results confirms crystalline nature of NiO with cubic structure and SnO2 possesses a tetragonal structure with an average crystallite size of 27.91 nm and 17.32 nm respectively as calculated by Debye-Scherrer's formula. Field emission scanning electron microscopy (FESEM) studies the surface morphology of both the samples. Williamson-Hall (W-H) analysis is employed to evaluate the micro-strains generated in the samples at the nano dimensional scale. Humidity sensing parameters of the prepared NiO and SnO2 nanosensors are observed within 10 %RH to 90 %RH of relative humidity. The SnO2 sensor exhibit high sensitivity of 94.6 %, response/recovery time of 72s/98s with hysteresis error of 0.58. Finally, electrical conductivity measurements are carried using the Four-probe method. The fabricated nanosensors exhibit low hysteresis, less aging and high reproducibility.

Keywords: Co-precipitation, nanostructures, humidity sensor, activation energy.

I.   INTRODUCTION

Almost every industry including agriculture, environment protection, national defense security, and space research organization rely on competent humidity sensing for their efficient and smooth functioning. Numerous effective humidity sensors have been fabricated using different transition metals in their pristine, doped, and composite forms for several research and applications. Various metal oxide semiconductors including WO_3, In_2O_3, Co_3O_4, Cr_2O_3 have been readily employed as humidity sensors. Humidity sensors based on metal oxide semiconductors(MOS) are of much interest as they possess a porous structure for facile adsorption of water molecules through grain boundaries to generate an electrical response. Moreover, nano-scaled MOS exhibit remarkable optical, catalytic, mechanical, and magnetic properties and also give rise to novel attributes. High surface to volume ratio of these nanostructures drastically effects all the surface

interactions thereby enhancing the humidity sensing ability, as for resistive humidity sensors, the dominated sensing mechanism can be described by the resistance change caused by the adsorption of water on surface of MOS. They also fulfill the criterion necessary to be ranked as a humidity sensor such as high sensitivity, stability, reproducibility, quick response and recovery time, easy fabrication, and compactness. The present study intends to analyzenano-dimensional nickel oxide(NiO) andtin oxide (SnO_2) MOS,based on their humidity sensing performance as well as basic morphology, microstructure, and electrical properties.Nanoscaled NiO and SnO_2 exhibit unique size-dependent properties useful fortheir humidity sensing, gas sensing and other useful applications.

Nickel oxide possess a directbandgap from 3.6 to 4.0eVmakes it suitable for optoelectronic applications such as optical switches, photo-cathodes, photovoltaic devices. Moreover, the bandgap can be tailored at nano-dimension making it potent optical limiting and saturable absorption applications. Nano-sized NiO is a potent magnetic material as it exhibits ferromagnetism, super antiferromagnetism, and super-paramagnetism depending on their particle size [i,]. Appreciable electrical properties of NiO cater to its applications as fuel cell electrodes [ii], electrochemical capacitors [iii], and lithium ion batteries [iv].

SnO_2has a direct band-gap of 3.6-3.8eV. It has remarkable optical properties and is commercially used as a transparent metal oxide, and for other optoelectronic applications in the visible and ultraviolet region [v].It exhibits excellent thermal, physical, and chemical stability. Nanoscaled SnO_2 possesses a mesoporous structure making it a suitable candidate for a humidity sensor.Recently much research is focused on the synthesis of various nanostructures and their possible application as resistive type humidity sensors. Earlier research ledbyKaung et. al has reported the synthesis of SnO_2 nanowire based humidity sensor reporting an average response and recovery time of 145s and 40s respectively [vi]. Recently, Gupta et. al reported sol-gel synthesis of NiO humidity sensors with a sensitivity of 47.09% at 90 %RH [vii].Parthibavarmanet. al have reported a response and recovery time of SnO_2nanoparticle humidity sensor to be 32 s and 25 s [viii].

Many techniques have been adopted for the synthesis ofnanostructured NiO and SnO_2including sol-gel, hydrothermal method, micro emulsion technique, microwave irradiation, solvothermal, polymer-matrix assisted synthesis [ix,x,xi]. In this studyco-precipitation and subsequent annealing are schematically followed to produce size-controlled, cost-effective, and a high yield of fine and homogeneous NiO and SnO_2 nanoparticles.

The current work enables to build a better analysis of the microstructures, micro-stress and strains within the nanocrystals,surface morphology, surface states, and humidity sensor parameters of nanostructured NiO and SnO_2 semiconductor metal oxides. Thereby, contributing to the currently available studiesof these semiconductor metal oxides for their structural parameters as well as electrical parameters and humidity sensing application.

II. EXPERIMENTAL

2.1 Chemicals

The precursors utilized for the co-precipitation synthesis of NiO and SnO_2 nanopowdersare nickel nitrate hexahydrate [$Ni(NO_3)_2.6H_2O$, 99% purity], tin chloride dihydrate [$SnCl_2.2H_2O$, 99% purity], sodium hydroxide [NaOH], and ethanol purchased from Loba Chemie and processed without any further purification.

2.2 Synthesis of NiO and SnO2 nanoparticles

NiO and SnO_2 nanoparticles are synthesized by co-precipitation synthesis. Typically, 0.1M homogeneous solution of nickel nitrate hexahydrate [$Ni(NO_3)_2.6H_2O$] is prepared in de-ionized water with continuous stirring for 2 hours on a magnetic stirrer. The pH ofthe above mixture is adjusted to 11 adding 1 M sodium hydroxide solution drop-wise. The addition of sodium hydroxide leads to the formation of a precipitate, which is then filtered and washed several times in ethanoland dried at 150°C for 5 hours. Finally, the product is annealed at 400°C for 2 hours to obtain NiO nanopowder. The same procedure is repeated with tin chloride dihydrate[$SnCl_2.2H_2O$] as a precursor for producing SnO_2nanopowder. The synthesized nanopowders are subjected to a uniaxial pressure of 7 tons in a hydraulic press machine (M.B. Instrument, Delhi, India) to obtain pellets of 10 mm diameter and 2 mm thickness. These pellets are annealed at 200° C for 2 h in an electric muffle furnace for better durability.

III. CHARACTERIZATION AND MEASUREMENTS

The phase and crystallinity of the samplesare studied using the Ultima IV model (Rigaku, Japan) X-ray diffractometer with CuKα Radiation (λ = 1.5406 Å). X-ray diffraction measurements are carried out by fixing the glancing angle at 2° with 2θ varying from 20° to 80° with the step size of 0.02°. Field emission scanning electron microscopy (FE-SEM, FEI Quanta 200) was used to study the surface morphology of the samples. The crystallite size and micro-strains are computed with the help of Scherrer's formulas and various Williamsons-Hall analysis models. Further, the Four-probe method is used to calculate the activation energy of the prepared samples. Finally, the humidity-sensing studies are carried out on the pelletized sensors obtained from the synthesized NiO and SnO_2 nanostructures in a specially designed humidity chamber with a two-probe measuring system.

3.1 Humidity sensing experiment

The humidity sensing measurements are carried out in a specifically designed humidity-sensing chamber. The chamber is sealed and is isolated from the surrounding atmosphere. The humidity within the humidity chamber is increased by introducing a saturated solution of potassium sulfate (K_2SO_4) (humidifier) while it is decreased by using potassium hydroxide (KOH) pellets (dehumidifier). A hygrometer (Huger, Germany, ± 1%RH, ± 1 °C) records the variation of the relative humidity (%RH) and the room temperature and the electrical resistance is measured by using a multimeter (± 0.001MX, model: VC-9808).The NiO and SnO_2

pellets are cross-sectionally placed in between the two plates of copper electrodes to record their electrical resistance variation within a humidity range of 10-90% RH.

IV. RESULTS AND DISCUSSIONS

4.1 XRD Analysis

The crystalline phase and structural composition of the synthesized NiOand SnO_2annealed at 500^0C arecharacterized by an X-ray diffractometer depicted in Fig. 1. Both the samples depict polycrystalline nature. The XRD spectra of the synthesized NiO match with a face-centered cubic structure (JCPDS 03-065-5745) with characterized peaks at37.254, 43.286, 62.878, and 75.413 with (111), (200), (220), (311) orientations respectively. Whereas,SnO_2crystallizes into tetragonalphase of SnO_2, cassiterite structure (space group P42/mnm (136)). Thecharacteristic peaks centered at 26.430, 33.705, 37.750, 51.629 corresponding to (110), (101),(200), and (210) respectively are in agreement with JCPDS 041-1445.No additional phase or peak related to any impurity is observed. The intense and sharp diffractionpeaks of NiO and SnO_2 nanocrystals indicate proper crystallization of the samples. The average crystallite size for pure NiO and $SnO_2$is calculated by using Debye-Scherrer's formula. The XRD data ofboth NiO andSnO_2 nanocrystals is further useful in calculations regarding FWHM, line-broadening, crystallite size, micro-structural strain and through Debye-Scherrer's methods and WH analysis.
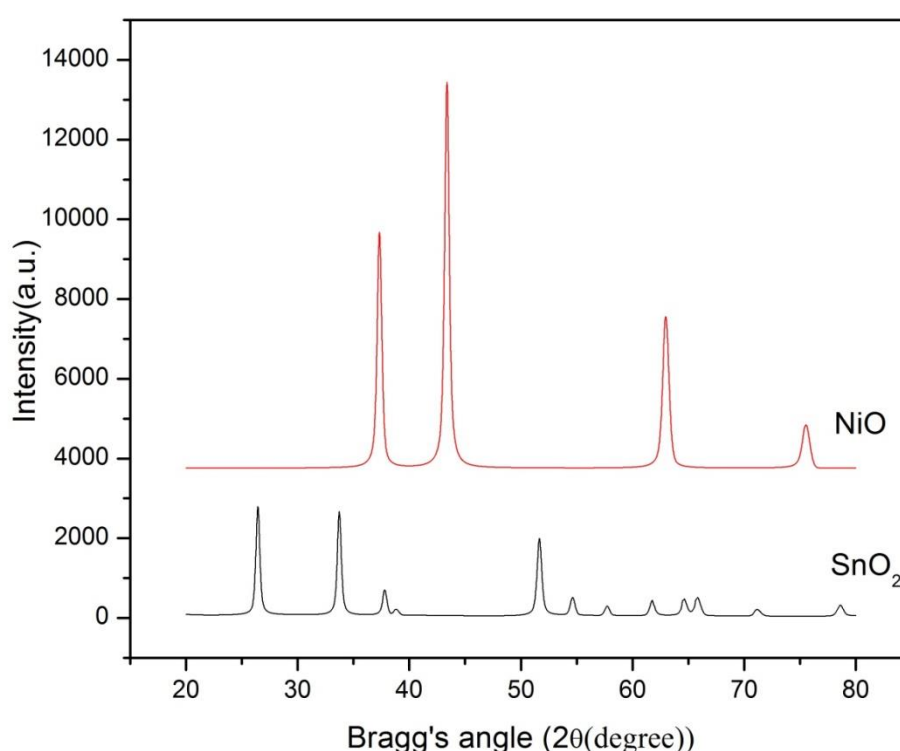

Fig 1.X-ray diffraction spectra of synthesized NiO and SnO_2 nanoparticles.

4.2 Debye-Scherrer Method

X-ray peak broadening is an effective tool to evaluate the crystallite size (D) and micro strains (ε) in the lattice of the prepared NiO and SnO_2 nanopowders. X-ray peak broadening is due to the contribution of crystallite size broadening, micro-strain broadening, and instrumental broadening. The instrumental broadening is eliminated from the recorded peak width to obtain the corrected peak broadening β_{hkl}. For this deconvolution of the instrumental broadening $(\beta_{instrumental})$ and sample-related broadening (β_{sample}) is required.

$$\beta_D = [(\beta_{sample}^2) - (\beta_{instrumental}^2)]^{1/2} \quad (1)$$

Further, we need to take in account the contributions to specimen broadening induced due to crystallite size broadening (β_D) and lattice strain broadening (β_ε) and separate them(described in WH analysis). The average crystallite size (D) is hence estimatedby using the Debye-Scherrer formula as in equation (2);

$$D = \frac{k\lambda}{\beta_D \cos\theta} \quad (2)$$

where, k is the shape factor having value 0.9, λ is the wavelength of CuKα line (1.546 nm), β_D is instrument-corrected Full-width half maxima in radians and θ is the peak position in radians.

The interplanar spacing (d) and lattice parametercorresponding to cubic structure NiO and tetragonalstructure SnO_2samples are calculated from equations (3),(4),(5) respectively. The crystalparameters including crystallite size (D), interplanar spacing (d), lattice constants (a, b, c), unit cell volume (V), are summarized in Table 1.

$$d = \frac{n\lambda}{2\sin\theta} \quad (3)$$

$$\frac{1}{d^2} = \frac{h^2 + k^2 + l^2}{a^2} \quad (4)$$

$$\frac{1}{d^2} = \left(\frac{h^2 + k^2}{a^2}\right) + \left(\frac{l^2}{c^2}\right) \quad (5)$$

Table 1.Lattice parameters of NiO and SnO_2 nanoparticles.

Sample	d(Å)	a(Å)	b(Å)	c(Å)	D (nm)	V (Å)
NiO	2.41	4.16	4.16	4.16	27.91	72.38
SnO₂	3.35	4.76	4.76	3.00	17.32	68.01

4.3 Williamson-Hall Analysis

4.3.1 Uniform deformation model (UDM)

This is an isotropic strain model in which the lattice strain is assumed to be uniform in all the crystallographic directions and all the material properties are independent of the direction along which they are measured. The strainis calculated by using the following equation;

$$\varepsilon = \frac{\beta_\varepsilon}{4\tan\theta_{hkl}} \quad (6)$$

Thepeak width (β_{hkl}) is a function of cosθ corresponding to thecrystallite size and varies as a function of tanθ corresponding to the strain within the crystal.This distinctive property allows crystallite size broadening (β_D) and lattice strain broadening (β_ε) to be additive components of the total integral peak width [xii].

The individual effects of crystallite size broadening and lattice strain broadening on the line broadening can be evaluated by using the following equations (7-9).

$$\beta_{hkl} = \beta_D + \beta_\varepsilon \quad (7)$$

$$\beta_{hkl} = \frac{k\lambda}{D\cos\theta} + 4\varepsilon\tan\theta \quad (8)$$

$$\beta_{hkl}\cos\theta = \frac{k\lambda}{D} + 4\varepsilon\sin\theta \quad (9)$$

As the above equation (9)represents the equation of a straight line, hencethe crystallite size (D) and lattice strain (ε) can be deduced from the linear fit of the data.A graph is plotted between $4\sin\theta$ along the x-axis and $\beta\cos\theta$ along y-axis for all the diffraction peaks of synthesized NiO and SnO$_2$as shown in Fig. 2 (a & b) . The crystallite size is calculated from the y-intercept and strain from the slope of the linear-fit plot.

4.3.2 Uniform stress deformation model (USDM)

Uniform stress deformation model is based on the anisotropic nature of the strainin the crystal lattice.Consideringan infinitesimal strain, Hook's law within the elastic limits can be utilized to obtain the strain from a linear relationship betweenthe stress (σ) and strain (ε) as $\sigma = Y_{hkl}\varepsilon$. Hence, the WH equationis modified to incorporate the anisotropic strain in the second term of the equation (9) as follows;

$$\beta_{hkl} = \frac{k\lambda}{D} + \frac{4\sigma\sin\theta}{Y_{hkl}} \quad (10)$$

Where, Y_{hkl} is the anisotropic Young's modulus perpendicular to (h, k, l) planes [xiii].The uniform deformation stress(σ) and crystallite size are obtained from the linear-fit of a plot between $\frac{4\sin\theta}{Y_{hkl}}$ on the x-axis and $\beta\cos\theta$ on the y-axis. The intercept on the y-axis gives the crystallite size and the slope of the linear-fit is used to calculate the uniform deformation stressusing Fig. 2(c & d).

4.3.3 Uniform deformation energy density model (UDEDM)

A Uniform deformation energy density model is employed to calculate the energy density(u) of the crystal. This model also assumes the inhomogeneous and anisotropic of the crystal properties. Hook's law in this case

is no more a linear relation of the stress and strain rather it is related as $Y_{hkl} = \dfrac{2u}{\varepsilon^2}$. Based on this relation, equation (9) can be further modified as the following equation;

$$\beta_{hkl}\cos\theta = \frac{k\lambda}{D} + 4\left(\frac{2u}{Y_{hkl}}\right)^{1/2}\sin\theta \qquad (11)$$

The values of $4\sin\theta$ and $\beta_{hkl}\cos\theta$ are plotted on the x-axis and y-axis respectively. The linear fit to the data plot in Fig. 2(e & f) is used to calculate the crystallite size from the y-intercept and the slope of the plot gives the energy density of the system.

4.3.4 Size-strain plot (SSP)

Strain size plot is a peak profile analysisof the integral breadths of broadened X-ray diffraction peaks. It is based on the assumption that size broadening is Lorentzian while strain broadening is Gaussian in nature. Whereas, in the WH analysis, size and strain related broadening have their respective angular dependence on diffraction angle (2θ) as 1/cosθand tanθ. The XRD peak profile is thus considered as a convolution of the Lorentzian and Gaussian functions [xiv]in SSP.The total peak broadening$\left(\beta_{hkl}\right)$ in SSP expressed as;

$$\beta_{hkl} = \beta_L + \beta_G \qquad (12)$$

Where β_L is size-induced peak broadening (Lorentzianfunction) and β_G is strain-induced peak broadening (Gaussianfunction).

SSP provides precise results for the isotropic broadening by considering the low reflection angles. The SSP calculations are done based on the following equation [xv];

$$\left(d\beta_{hkl}\cos\theta\right)^2 = \frac{K\lambda}{D}\left(d^2\beta_{hkl}\cos\theta\right) + \frac{\varepsilon^2}{4} \qquad (13)$$

A liner-fit graph is plotted $\left(d\beta_{hkl}\cos\theta\right)^2$ along the x-axis and$\left(d^2\beta_{hkl}\cos\theta\right)$ along the y-axis corresponding to each diffraction peak. The crystallite size is extracted from the slope of the linear fit of the plot and the lattice strain from the intercept of Fig. 2(g &h). The crystallite size, strain, stress and energy density obtained from the calculations based on the isotropic UDM and anisotropic USDM and UDEDM models as well as SSP are in absolute accordance with the crystallite size deduced for NiO and SnO₂ crystal from the Debye-Scherrer formula and are mentioned in Table 2.

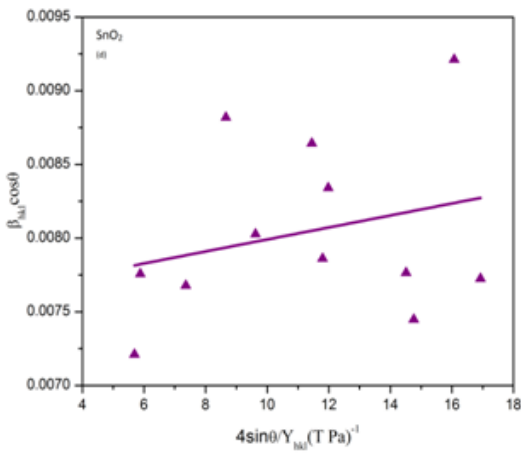**Table 2 Geometric parameters of NiO and SnO₂ nanoparticles.**

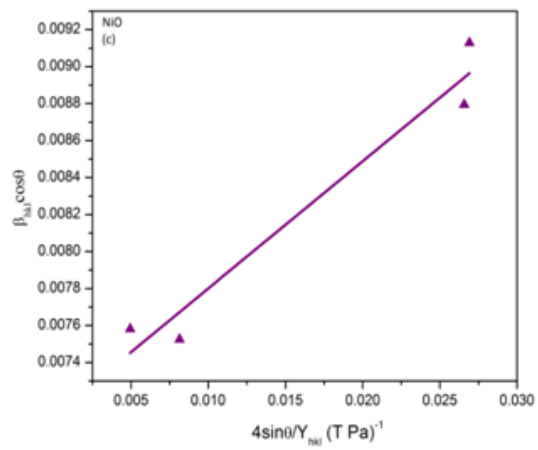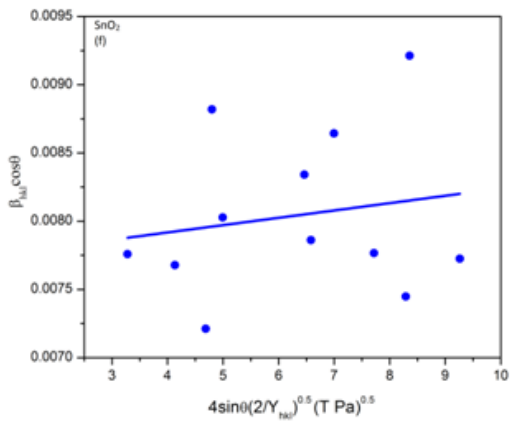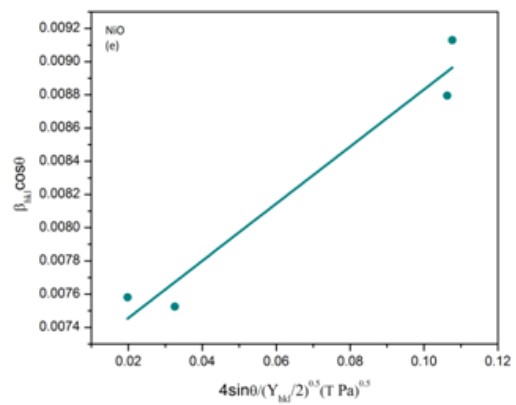| Sample	UDM		USDM		UDEDM		SSP	
	D(nm)	$\varepsilon \times 10^{-3}$	D(nm)	σ (M Pa)	D(nm)	u (KJm^{-3})	D(nm)	$\varepsilon \times 10^{-3}$
NiO	27.17	151	25.15	172	24.72	0.000231	21.06	168
SnO₂	17.26	40.72	18.28	53.73	18.00	0.004132	17.74	17.7

(a)

(b)

(c)

(d)

(e)

(f)

(g)   (h)
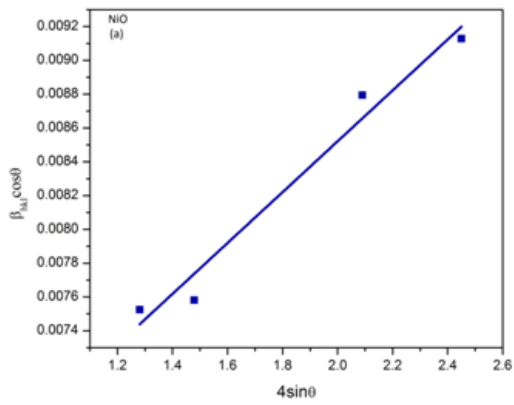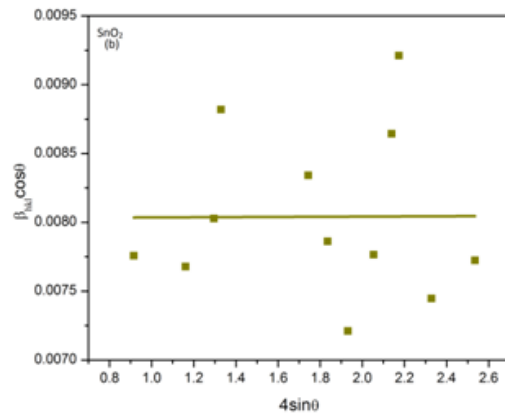
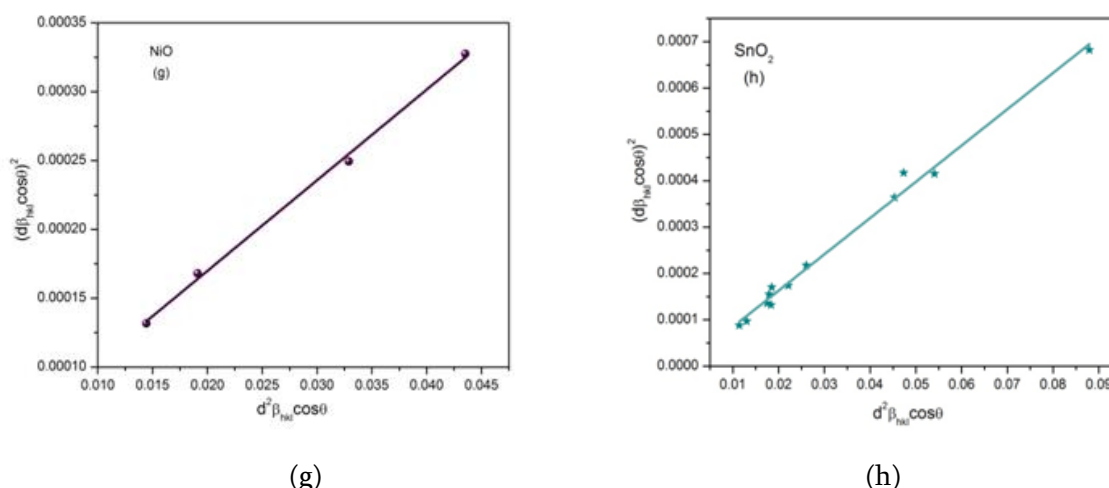Fig 2 (a &b) UDM plot for NiO and SnO$_2$, (c &d) USDM plot of NiO, SnO$_2$ (e&f) UDEDM plot of NiO and SnO$_2$and (g & h) SSP plot for NiO and SnO$_2$.

4.3.5 Dislocation density(δ)

The dislocation density is a measure of the concentration of dislocations or the defects present within the crystal structures. Dislocations exist in most of the crystalline structures due to stress-induced during the formation of the crystals. The micro-mechanisms responsible for the dislocation density is measuredas dislocations intersecting the unit area of a crystal. Thesmallerthe grain size, the larger is the area of the grain boundaries, which obstruct dislocation motion by attractive or repulsiveinteractions. The smaller grain size implies a larger dislocation density is which usually seen to improve the strength [xvi] of the nanostructures. The dislocation densities of the co-precipitated NiO and SnO$_2$ nanocrystals are obtained by using equation (14) and their values are summarized in Table 3;

$$\delta = \frac{1}{D^2} \qquad (14)$$

where, δ is the dislocation density and D is the particle size in nm.

4.3.6 Specific surface area (SSA)

The specific surface area of the synthesized NiO and SnO$_2$ nano-samples is an important parameter material property. It depends on the size and porosity of the nanomaterials and is a key feature of various surface reactions and interactions including absorption, adsorption, and desorption. Nanomaterials, in general, are supposed to possess large SSA which includes the total surface of the nanoparticles comprising its pores aswell.Specific surface area (SSA) is related to the particle size (D) by the Sauter formula [xvii] in equation (15).

$$SSA = \frac{6000}{D \times \rho} \qquad (15)$$

Where, ρ is the density of the material.The SSA of NiO and SnO$_2$nanoparticles are mentionedin Table 3.

Table 3. SSA and Dislocation density of NiO and SnO$_2$ nanoparticles.

Sample	SSA (m²/g)	δ (line m^{-2})x10^{16}
NiO	33.31	0.001283
SnO$_2$	49.84	0.003333

V. FESEM

The microstructural and morphological analysis of the samples is done based on FESEM images taken at 30,000 x magnification shown in Fig. 3(a).FESEM image of NiO reveals a non-uniform distribution of large size agglomerated grainsformed from smaller grainswhereas, SnO$_2$nanoparticles in Fig. 3(b) are fine and uniformly distributed all over the cross-section accompanied by a network of pore channels which are supposed to promote water adsorption and hence the humidity sensing of SnO$_2$ sample.Both the samples comprise the pores present at the grain boundary separating the grains. However, The SnO$_2$ nanostructure shows more porosity.
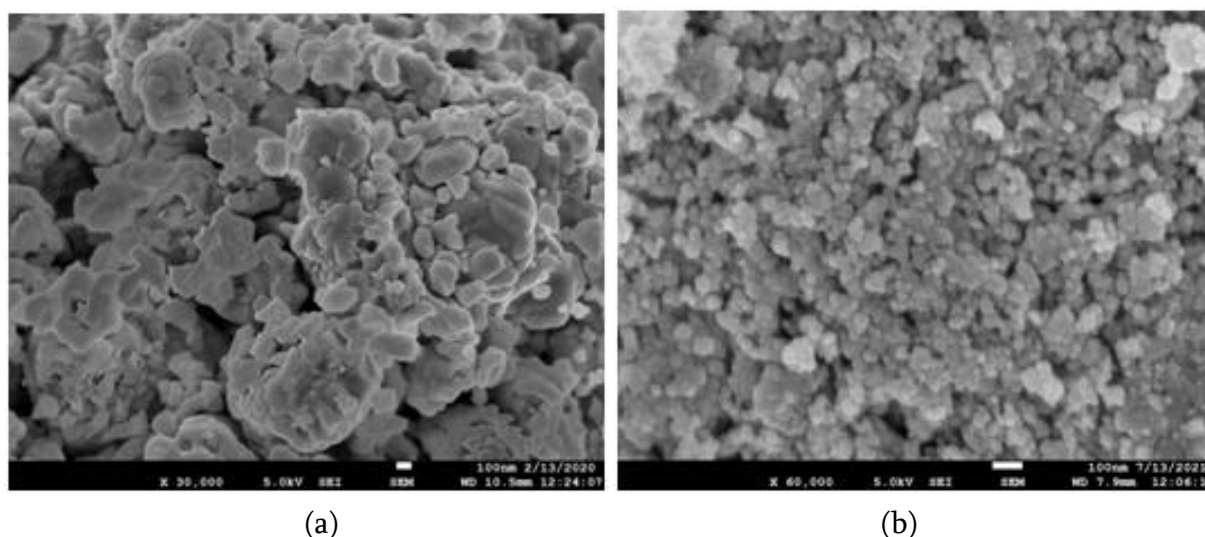

(a)   (b)

Fig. 3 FESEM images of (a)NiO and (b)SnO$_2$nanoparticles.

VI. HUMIDITY SENSING

Fig. 4(a) shows the dependence of impedance on varying relative humidity %RH for NiO and SnO$_2$nanosensors. With an increase in the relative humidity (%RH) from 10 to 90 %RH the NiO shows an insignificant change inthe electricalresistancewhereas, the resistance for SnO$_2$ nanosensor drops remarkably.In the SnO$_2$ sensor for the variation of relative humidity from 10 % to 90 % RH, the impedance decreases by at least three orders of magnitude (10^8~10^6).The NiO sample supports only limited humidity sensingas this sensor shows very small variation in the resistance when subjected to different humidity values, which may be due to an agglomerated morphology and insufficient electron transport [xviii]. Although the SnO$_2$sensor exhibits quick and stable electrical response with the %RH variation. Thisbetterhumiditysensing

of SnO₂ nanosensors can be attributedto its morphology with lessagglomeration and more porous network.The metal oxide surface responds differently to different relative humidity (%RH). For relatively low humidity, the water molecules gets chemisorbed on the metal oxide surface and get instantly dissociated into hydroxyl ions (OH⁻) and protons (H⁺), and ions due to self-ionization.The dissociatedhydroxylions bondwiththe metallic sites to form Ni-OH/ Sn-OH bonds thereby releasing H⁺ ionsand conduction occurs via proton hopping[xix]. With the further increase in water content on the surface, continuum water layer physisorbed on the previously chemisorbed layer, encouraging the proton transfer through Grotthuss mechanism [xx]. Further rise in relative humidity leads to percolation of water molecules through capillary pores thereby creating an aqueous medium for electrolytic conduction responsible for decrease in the impedance of NiOand SnO₂nanosensors with theincrease in%RH from 10 % to 90 % RH.

Humidity sensing performanceis dependent on the sensitivity of the sensors, their response/recovery time,hysteresis and stability. All these parameters are studied in the humidity range of 10-90 %RH at room temperature by alternately exposing the samples to the lowest and highest relative humidity for four consecutive cycles.Fig. 4(d) is the response and recovery curves for NiO and SnO₂nano-sensors as the relative humidity switches between 10 to 90% RH. The responseandrecoverytime are the two performances determiningfactorsof a humidity sensor, calculated against 90% of the total resistance change in a sensor during adsorption and desorption respectively. NiO basedsensordisplays a response and recovery timeof135 s and 164 s.Whereas, SnO₂ nano-sensorhas response and recovery time of 72s and 98s, suggesting that NiO based sensor takes a longer time to achieve a stable state than SnO₂ sensor.As SnO₂ nanostructuresshow more pore channels formed by the interspaces and voids and accelerates the steady-state formation for high %RH values. Hysteresis is a crucial parameter in determining the credibility of the synthesized NiO and SnO₂humidity sensors. It may be estimated by the amount of deviation introduced in the output resistance during the adsorption and desorption cycle of thehumidity sensor. The hysteresis of the synthesized nanosensors is obtained by switching the sensors from 10 to 90 %RH and reverting from 90 to 10 %RH.The hysteresis error (Hₑ) is calculated using the following expression;

$$H_e = \pm \frac{\Delta H_{max}}{2F_{fs}} \qquad (16)$$

Where, ΔH_{max} the difference of the increasing and decreasing humidity cycle measurements and F_{fs} is the full-scale output. The calculated hysteresis error of the NiO (Fig. 4a) and SnO₂(Fig 4b) sensors are19.04 and 0.58 respectively. The sensitivity of NiO and SnO₂ nanosensorsareestimated from the value of S% which is calculated by using equation (17);

$$S\% = \left(\frac{R}{R_o} - 1 \right) \times 100 \qquad (17)$$

Where R is the resistance for all %RH (10% to 90% RH), R_o is the resistance for 10% RH [xxi]. The sensitivity of the NiO and SnO₂ nanosensors are 18.5% and 94.6% respectively. The sensitivity values ofboththesamples make it obvious thatSiO₂ based metal oxide semiconductor is a much better humidity sensor as compared to NiO humidity sensor.The high electron density of SnO₂facilitates charge transport [xxii], improves the

conductivity and hence its humidity sensing performance. The superior performance of the SnO_2 nanosensor may also be attributed to its better morphology in terms of smaller grain size, more surface to volume ratio, availability of sufficientpores, and less agglomeration [xxiii]. Generally, a large surface area provides active site for adsorption of water molecules and numerouspores help percolation of water for better humidity sensing performance. Furthermore, the stability and aging effects of fabricated sensors are observed to ensure their efficiency.Fig. 4(e) is the stability graph of the sensors for electrical response corresponding to 10 % RH, analyzed over a period of 60 daysfor several cycles,where the samples exhibit a stable responseand less aging.
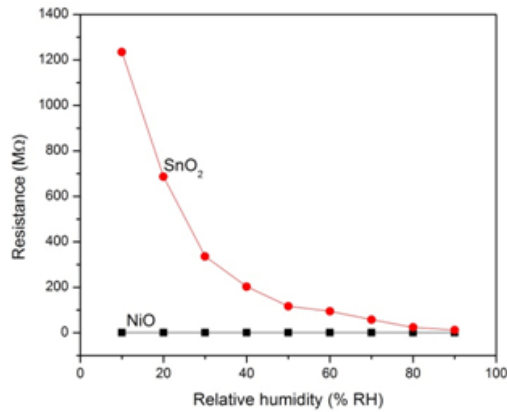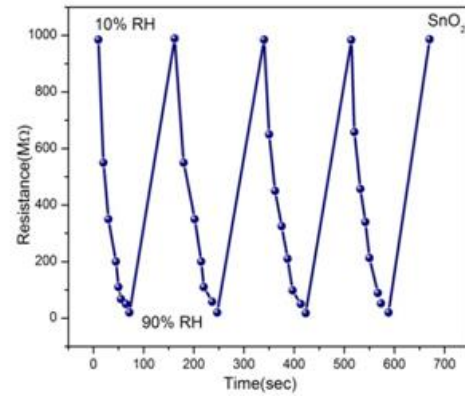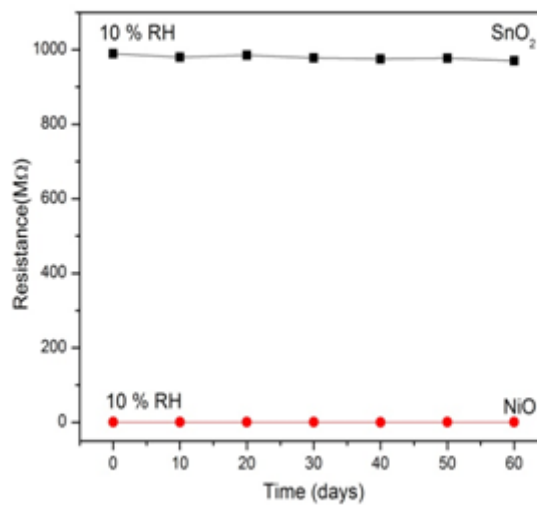
(a)
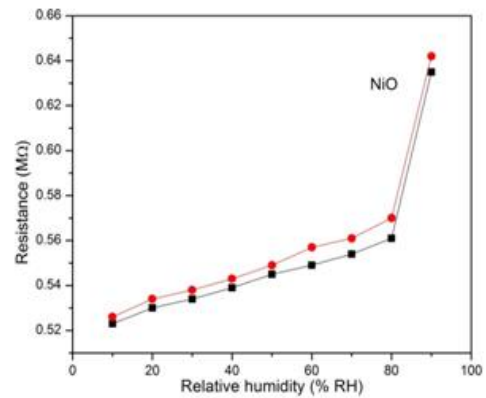
(b)
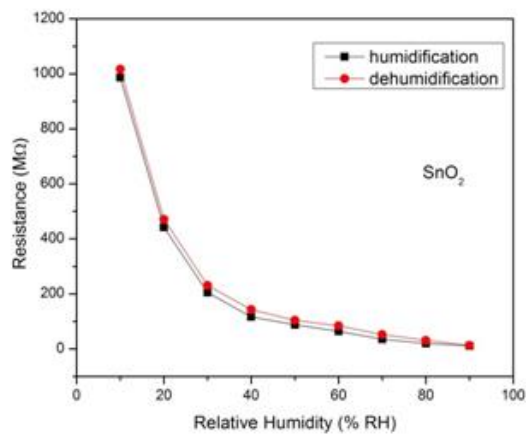
(c)

(d)

(e)

Fig.4 (a) Resistance of variation with relative humidity for NiO & SnO₂ (b) Hysteresis curve of NiO nanosensor (c) Hysteresis curve of SnO₂ nanosensor (d) Response and recovery curve of SnO₂ nanosensor (e) Stability plot of NiO and SnO₂ nanosensors.

VII.   ELECTRICAL CONDUCTIVITY

The electrical conductivity of the NiO and SnO₂ nanomaterials is measured using the four-probe setup within the temperature range 303-403 K.The measurements are recorded by placing the surface of NiO and SnO₂ pellets in contact with the four electrical contacts. The current is supplied to the two outer probes through a high impedance current source and the voltage is measured between the two inner probes by a voltmeter. The obtained values of electrical conductivity are used to evaluate the activation energy (E_a) [xxiv] of the samples using equation (18).

The conductivity of a semiconductor is related as;

$$\sigma = \sigma_o \exp\left(-\frac{E_a}{kT}\right) \quad (18)$$

Where σ is the conductivity at an absolute temperature in $(\Omega cm)^{-1}$, σ_o is a constant, E_a is the activation energy (eV), k is the Boltzmann constant (8.6×10^{-5} eVK^{-1}), and T is the absolute temperature(K). On taking log on both sides of equation (18) we obtain;

$$\log \sigma = C - \left(\frac{1}{2.3026 \times 10^3} \times \frac{E_a}{k}\right)\left(\frac{1000}{T}\right)$$

$$(19)$$

$$Slope = \left(\frac{E_a}{2.3026 \times 10^3 \times k} \right)_{(20)}$$

$$E_a = \left(k \times 2.3026 \times 10^3 \times slope \right)(\text{eV}) \qquad (21)$$

Byplotting a graph between $\log_{10}\sigma$ and 1000/T, the activation energy values for nickel oxide and tin oxide nanostructures can be calculated from the slope of the Arrhenius plot over the entire temperature range (303-403 K) shown in Fig. 5 (a) and (b). Thecalculated values of activation energies for NiO and SnO$_2$ are 0.3429 eV and 0.0394eV respectively.

TheArrhenius plot relates the electrical conductivity to the absolute temperature and to the mobility of charge. The higher electrical conductivity of SnO$_2$ nanostructures can be supported by the higher carrier concentration of SnO$_2$ in comparison to NiO as the electrical conductivity for semiconductor metal oxide is the product of mobility and the carrier concentration. A better crystal structure and sharp grain boundaries in SnO$_2$ reduces structural defects and also reduces the carrier scatterig from such defects and lead to enhancement of free carrier concentration and therefore higher mobility.
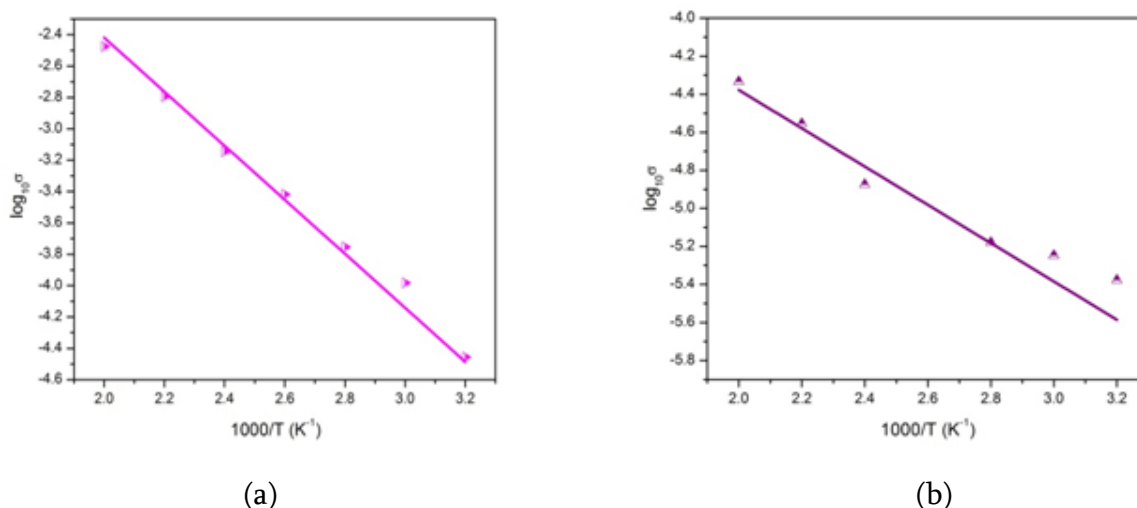

(a)   (b)

Fig. 5 Plot of(a)NiO and (b) SnO$_2$for 1000/T vs. log σ.

VIII.   CONCLUSION

NiO and SnO$_2$ nanoparticles are successfully prepared through co-precipitation synthesis. The NiO nanoparticles exhibit cubic structure and SnO$_2$ exhibit tetragonalstructure. The calculated crystallite for NiO is 27.91 nm and 17.32 nm for the SnO$_2$ sample. The WH analysis of the samples provides the values of average crystallite size and lattice strains in NiO and SnO$_2$nanocrystals. Surface morphology of NiO and SnO$_2$based on the SEM images reveals large particle size distribution of NiO nanoparticles whereas fine and uniform particle distribution can be observed for SnO$_2$nanoparticles. The humidity sensing properties of the SnO$_2$samples are found to be much better in comparison to NiO sample. For SnO$_2$sample, a variation of at least 3 orders of impedance with a response and recovery time of 72s and 98 s respectivelyis recorded. This sample exhibits a

minimum hysteresis error of 0.58 and a sensitivity of 94.6%. Whereas, for NiO the resistance change is negligible within the humidity range 10-90 %RH with hysteresis error of 19.04 and a sensitivity of 18.5%.The response and recovery time is recorded to be 135 s and 164 s. The electrical conductivity measurements shows that SnO_2has better electrical conductivity with activation energy 0.0394eV over NiO with activation energy 0.3429 eV. The conductivity of the NiO sample is too small to be put in use as a humidity sensor in pristine form. Whereas, the SnO_2 sample exhibit appreciable humidity sensing properties and prove to be practically better humidity sensor.To conclude, NiO-based humidity nanosensors have limited performance as compared to SnO_2 humidity nanosensors.

IX. ACKNOWLEDGMENTS

X. REFERENCES

[1]. Rui Zhanget. al, Rational design and tunable synthesis of Co3O4 nanoparticle-incorporating into In2O3 one-dimensional ribbon as an effective sensing material for gas detection.Sensors and Actuators B, 310, 127695 (2020). https://doi.org/10.1016/j.snb.2020.127695.

[2]. Qi Wang et.al, A Flexible Humidity Sensor Based on Co3O4 Nanoneedles with High Sensitivity and Quick Response, Journal of Nanoelectronics and Optoelectronics, 15(7), 870-874 (2020), DOI: https://doi.org/10.1166/jno.2020.2788

[3]. Suman Pokhrel, K.S. Nagaraja, Solid State Electrical Conductivity and Humidity Sensing Properties of Cr2O3–MoO3 Composites., 25 October 2002, https://doi.org/10.1002/1521-396.

[4]. Brouriet. al, Interplay effects of humidity and UV light sensitivities of Zn0.9Mg0.1Onanogranular thin films, Applied Surface Science 353 (2015) 933–938, ttp://dx.doi.org/10.1016/j.apsusc.2015.07.033.

[5]. Physical properties of La-doped NiO sprayed thin films for optoelectronic and sensor applications. Ceramics International, 42(5), 5963-5978 (2016).https://doi.org/10.1016/j.ceramint.2015.12.144.

[6]. Karthikeyan et. al, Wet chemical synthesis of diameter tuned NiO micro rods: microstructural, optical and optical power limiting applications. Cryst Eng. Comm, 18, 601-607(2016). DOI: 10.1039/c5ce02232k.

[7]. S. A. Makhlouf, F. T. Parker, F. E. Spada and A. E. Berkowitz, Magnetic anomalies of NiO nanoparticles, J. Appl. Phys. 81 5561-5563 (1997).

[8]. Y. Ichiyanagi, N. Wakabayashi, J. Yamazaki, S. Yamada, Y. Kimishima, E. Komatsu and H. Tajima, Magnetic properties of NiO, Physica B 329 862863 (2003). https://doi.org/10.1016/S0921-4526%2802%2902578-4

[9]. Li F, Chen HY, Wang CM, Hu K., A novel modified NiO cathode for molten carbonate fuel cells. J ElectroanalChem 2002;531:53–9.

[10]. Nathan T, Aziz A, Noor AF, PrabaharanSRS. Nanostructured NiO for electrochemical capacitors: synthesis and electrochemical properties. J Solid State Electrochem, 2007;12:1003-9.

[11]. N. Srivastava and P. C. Srivastava, Synthesis and characterization of (single- and poly-) crystalline NiO nanorods by a simple chemical route, Phys. E, 2010, 42, 2225–2230. https://doi.org/10.1016/j.physe.2010.04.023

[12]. LinaXu, Joseph C. Fanguy, KrunalSoni, and Shiquan Tao, Optical fiber humidity sensor based on evanescent-wave scattering, Optics Letter, 29(11), 1191-1193 (2003).

[13]. Q. Kuang, C.S. Lao, Z.L. Wang, Z.X. Xie, L.S. Zheng, High-sensitivity humidity sensor based on a single SnO2 nanowire, J. Am. Chem. Soc. 129 (2007) 6070–6071.

[14]. Priya Gupta , Savita Maurya, N. K. Pandey, and Vernica Verma, Structural, electrical and humidity sensing properties of nano-structured nickel oxide prepared by sol–gel method.

[15]. M. Parthibavarman, V. Hariharan, C. Sekar, High-sensitivity humidity sensor based on SnO2 nanoparticles synthesized by microwave irradiation method. Material science and engineering : C, 31(5) 840-844 (2011).

[16]. Gupta et. al, Effect of annealing temperature on highly sensitive nickel oxide based LPG sensor operated at room temperature. App. Phy, A, 127:289 (2021).

[17]. Yu Du et, al, Preparation of NiO nanoparticles in micro emulsion and its gas sensing performance. Materials Letters 68, 168-170(2012).https://doi.org/10.1016/j.matlet.2011.10.039

[18]. Haixia Xia et. al, Solvothermal synthesis of highly crystalline SnO2 nanoparticles for flexible perovskite solar cells. Materials Letters 240, 311-314 (2019). https://doi.org/10.1016/j.matlet.2018.09.117

[19]. M. Birkholz et. al, Thin Film Analysis by X-Ray Scattering, Journal of applied crystallography, 39(6),925-926 (2006). https://doi.org/10.1107/S0021889806034698.

[20]. Heryanto, B Abdullah, D Tahir and Mahdalia, Quantitative analysis of X-Ray diffraction spectra for determine structural properties and deformation energy of Al, Cu and Si.J. Phys.: Conf. Ser. 1317 012052(2019).

[21]. M.A. Tagliente, M.Massaro, ―Strain-driven (0 0 2) preferred orientation of ZnO nanoparticles in ion-implanted silica‖ Nucl. Instrum Methods Phys. Res. B. 266, 1055 -1061 (2008).

[22]. V.D. Mote, Y. Purushotham, B.N. Dole, Williamson-Hall analysis in estimation of lattice strain in nanometer-sized ZnO particles, J. Theor. Appl. Phys. 6, 6–14 (2012)

[23]. Sirdeshmukh DB, Sirdeshmukh L, Subhadra KG. Micro- and Macro-Properties of solids: Thermal, Mechanical and Dielectric properties. Springer, New York. 2006.ISBN:9783540317852.

[24]. Priya Gupta, N. K. Pandey, Kuldeep Kumar, B. C. Yadav, Structural, optical and LPG sensing properties of zinc oxide doped nickel oxide pellets operated at room temperature, Sensors and Actuators A, 319, 112-484 (2021).

[25]. P. Pascariu, A. Airinei, N. Olaru, I. Petrila, V. Nica, L. Sacarescu, F. Tudorache, Microstructure, electrical and humidity sensor properties of electrospun NiO–SnO2 nanofibers. Sens. Actuators B, 222, 1024–1031 (2016).

[26]. Kannanet. al, A highly sensitive humidity sensor based on DCreactivemagnetronsputtered zinc oxide thin film, Sensors and Actuators A 164 (2010) 8–14, doi:10.1016/j.sna.2010.09.006.

[27]. Verma et. al, Humidity sensing enhancement and structural evolution of W doped ZnO nanosensors fabricated through co-precipitation synthesis. Physica B, 619 (2021) 413224. https://doi.org/10.1016/j.physb.2021.413224

[28]. D. Tolomanet. al , Reduced graphene oxide decorated with Fe doped SnO2 nanoparticles for humidity sensor, Applied Surface Science 402 (2017) 410–417.

[29]. W.D. Zhou, D. Dastan, J. Li, X.T. Yin, Q. Wang, Discriminable sensing response behavior to homogeneous gases based on n-ZNO/p-NIO composites. Nanomaterials 10, 785 (2020).

[30]. X.-T. Yin, P. Lv, J. Li, A. Jafari, F.-Y. Wu, Q. Wang, D. Dastan, Z. Shi, S. Yu, H. Garmestani, Nanostructured tungsten trioxide prepared at various growth temperatures for sensing applications. J. Alloy. Compd. 825, 154105 (2020).

[31]. Suneet Kumar Misra, Narendra Kumar Pandey, Analysis on activation energy and humidity sensing application of nanostructured SnO2-doped ZnO material, Sensors and Actuators A 249 (2016) 8–14

[] S. A. Makhlouf, F. T. Parker, F. E. Spada and A. E. Berkowitz, Magnetic anomalies of NiO nanoparticles, J. Appl. Phys. 81 5561-5563 (1997).

[ii] Li F, Chen HY, Wang CM, Hu K., A novel modified NiO cathode for molten carbonate fuel cells. J   ElectroanalChem 2002;531:53–9.

[iii] Nathan T, Aziz A, Noor AF, PrabaharanSRS. Nanostructured NiO for electrochemical capacitors: synthesis and electrochemical properties. J Solid State Electrochem, 2007;12:1003-9.

[iv] N. Srivastava and P. C. Srivastava, Synthesis and characterization of (single- and poly-) crystalline NiO nanorods by a simple chemical route, Phys. E, 2010, 42, 2225–2230. https://doi.org/10.1016/j.physe.2010.04.023

[v] LinaXu, Joseph C. Fanguy, KrunalSoni, and Shiquan Tao, Optical fiber humidity sensor based on evanescent-wave scattering, Optics Letter, 29(11), 1191-1193 (2003).

[vi] Q. Kuang, C.S. Lao, Z.L. Wang, Z.X. Xie, L.S. Zheng, High-sensitivity humidity sensor based on a single SnO2 nanowire, J. Am. Chem. Soc. 129 (2007) 6070–6071.

[vii] Priya Gupta , Savita Maurya, N. K. Pandey, and Vernica Verma, Structural, electrical and humidity sensing properties of nano-structured nickel oxide prepared by sol–gel method.

[viii] M. Parthibavarman, V. Hariharan, C. Sekar, High-sensitivity humidity sensor based on SnO2 nanoparticles synthesized by microwave irradiation method. Material science and engineering : C, 31(5) 840-844 (2011).

[ix] Gupta et. al, Effect of annealing temperature on highly sensitive nickel oxide based LPG sensor operated at room temperature. App. Phy, A, 127:289 (2021).

[x] Yu Du et, al, Preparation of NiO nanoparticles in micro emulsion and its gas sensing performance. Materials Letters 68, 168-170(2012).https://doi.org/10.1016/j.matlet.2011.10.039

[xi] Haixia Xia et. al, Solvothermal synthesis of highly crystalline SnO2 nanoparticles for flexible perovskite solar cells. Materials Letters 240, 311-314 (2019). https://doi.org/10.1016/j.matlet.2018.09.117

[xii] M. Birkholz et. al, Thin Film Analysis by X-Ray Scattering, Journal of applied crystallography, 39(6),925-926 (2006). https://doi.org/10.1107/S0021889806034698.

[xiii] Heryanto, B Abdullah, D Tahir and Mahdalia, Quantitative analysis of X-Ray diffraction spectra for determine structural properties and deformation energy of Al, Cu and Si.*J. Phys.: Conf. Ser.* 1317 012052(2019).

[xiv] M.A. Tagliente, M.Massaro, ―Strain-driven (0 0 2) preferred orientation of ZnO nanoparticles in ion-implanted silica‖ Nucl. Instrum Methods Phys. Res. B. 266, 1055 -1061 (2008).

[xv] V.D. Mote, Y. Purushotham, B.N. Dole, Williamson-Hall analysis in estimation of lattice strain in nanometer-sized ZnO particles, J. Theor. Appl. Phys. 6, 6–14 (2012)

[xvi] Sirdeshmukh DB, Sirdeshmukh L, Subhadra KG. Micro- and Macro-Properties of solids: Thermal, Mechanical and Dielectric properties. Springer, New York. 2006.
ISBN:9783540317852.

[xvii] Priya Gupta, N. K. Pandey, Kuldeep Kumar, B. C. Yadav, Structural, optical and LPG sensing properties of zinc oxide doped nickel oxide pellets operated at room temperature, Sensors and Actuators A, 319, 112-484 (2021).

[xviii] P. Pascariu, A. Airinei, N. Olaru, I. Petrila, V. Nica, L. Sacarescu, F. Tudorache, Microstructure, electrical and humidity sensor properties of electrospun NiO–SnO2 nanofibers. Sens. Actuators B, **222**, 1024–1031 (2016).

[xix] Kannanet. al, A highly sensitive humidity sensor based on DCreactivemagnetronsputtered zinc oxide thin film, Sensors and Actuators A 164 (2010) 8–14, doi:10.1016/j.sna.2010.09.006.

[xx] Verma et. al, Humidity sensing enhancement and structural evolution of W doped ZnO nanosensors fabricated through co-precipitation synthesis. Physica B, 619 (2021) 413224. https://doi.org/10.1016/j.physb.2021.413224

[xxi] D. Tolomanet. al , Reduced graphene oxide decorated with Fe doped SnO2 nanoparticles for humidity sensor, Applied Surface Science 402 (2017) 410–417.

[xxii] W.D. Zhou, D. Dastan, J. Li, X.T. Yin, Q. Wang, Discriminable sensing response behavior to homogeneous gases based on n-ZNO/p-NIO composites. Nanomaterials **10**, 785 (2020).

[xxiii] X.-T. Yin, P. Lv, J. Li, A. Jafari, F.-Y. Wu, Q. Wang, D. Dastan, Z. Shi, S. Yu, H. Garmestani, Nanostructured tungsten trioxide prepared at various growth temperatures for sensing applications. J. Alloy. Compd. **825**, 154105 (2020).

[xxiv] Suneet Kumar Misra, Narendra Kumar Pandey, Analysis on activation energy and humidity sensing application of nanostructured SnO2-doped ZnO material, Sensors and Actuators A 249 (2016) 8–14

Note on the X-ray Satellite Systematization

Nand Kumar[1], Jitendra Singh[2]

[1]Department of Physics, Jawaharlal Nehru Memorial P.G. College, Barabanki, Uttar Pradesh, India
[2]Department of Physics, Shri L.B.S. Degree College, Gonda, Uttar Pradesh, India

ABSTRACT

The X-ray satellites are very weak lines. These lines are measured generally in the close vicinity of the strong diagram line. Difficulty involved not only in the measurement but also identification of their origin. The frequency of the X-ray satellite line may not fit in the normal energy level diagram of particular element. These lines are produced when a single transition occurs in doubly ionised atom. Many attempts on their systematization procedure and identification of origin have been put forwarded by researchers. The aim of present paper note is to summarize various theory of the systematization and identification of X-ray satellite lines.

Keyword: X-ray satellite, systematization, identification, origin, transition.

I. INTRODUCTION

The X-ray spectrum lines are emitted due to the transition of the atom from one energy level to another. The emitted X-ray lines are called diagram lines. Some weak lines are also emitted closed to diagram lines which frequency may not be fitted in the normal energy level diagram of atoms. Therefore these weak lines are called "non-diagram" lines or satellite lines of a strong parent line (diagram line). Siegbahn and Stenstrom [1] were first time discovered the existence of the satellites of $K\alpha_1$ diagarm line for Z=11 to 31.Druyvestyen [2],Stenstrom [3] observed these lines in L and M spectrum respectively. Many satellite lines have been observed for the K, L, and M spectra throughout the atomic numbers Z=3 to 92.Cauchois and Senemaud [4] have compiled wavelengths data of various satellites of K, L, and M series with few exceptions [5].Most recent data tables of Cauchois and Senemaud [4] for X-ray satellites wavelengths compilation are revealed the some facts : (i) Some of satellites are non-identified (ii) Some satellites are reported by more than one researchers but Cauchois and Senemaud included only the latest wavelengths (iii) Several satellites have been tabulated only their wavelengths without identification (iv) Several satellites have not been listed though their wavelengths had been reported in the literatures (v) Many satellites have been listed with interrogation marks and their identification not sure and (vi) Some satellites have been given more than one wavelength value without assigning any reason.X-ray satellites can be classified in two broad group one is called high frequency satellite(HFS) which are observed on the higher energy side of the their parent (diagram) line. Other class of satellites are observed lower energy side of their strong parent (diagram) line called low

frequency satellite(LFS).However HFS and LFS both are observed corresponding to a single parent line. Except the HFS and LFS some hyper satellites are also observed.

Since these X-ray satellites are weak lines therefore difficulty arises in their measurements and also identification of their origin [5].Several theories have been put forwarded for the explanation of their origin. The high energy satellites origin hypothesis known as Wentzel-Druyvestyen theory [5] is only accepted. According to the Wentzel-Druyvestyen explanation on the origin of high energy satellites, these lines are emitted due to the single electron transfers in atomic energy level in which two or more electrons have been removed from the inner shells of the atoms and finally atoms goes in doubly ionized states. It is not necessary that two or more electrons will be ejected from the same level and that may be occurred from different inner levels. The transition mechanism of the emission of a satellite can be represented as the transition $AX \rightarrow XB$ where A, X,B are denoted for involved energy levels in emission process.However energy level 'X' here known as spectator. The assignment $A \rightarrow B$ is represented for parent (diagram) line. Whereas $AX \rightarrow XB$ for the doubly ionized atom. However the concept of multiplicity of the energy levels must be considered which was not taken into account in this theory and modification for multiplicity first was introduced by Ray in 1929[6].This may possible when Auger transitions are considered. Auger electrons transitions [7] are arised due to a two step non radiative process. The first step is that the incident photon ionized atom in inner shell(A) resulting a hole which is filled through any outer level electron(B) and thus a X-ray photon corresponding to energy hv=E_A-E_B releasing. The second process is "radiation less" in which energy of $E_A \rightarrow$ E_B transition is utilized to ejection of another electron (say C) and thus finally atom goes into doubly ionized state as represented here $A \rightarrow BC$ or [ABC].Thus Auger process of transitions gives double ionization of atom and consequently X-ray satellite emission possible.A simple expression for the kinetic energy of Auger type electron can be written as E_{kin}=$(A)_z$ -$(B)_z$ -$(C)_{z+\Delta z}$ where Z is atomic number of atom and Z+ΔZ is a nuclear charged in order to the increased nuclear pull due to hole in the energy level B.Finally $(A)_z$,$(B)_z$ and $(C)_z$ are the binding energies of electrons of involved energy levels. For the sake of simplicity ΔZ=1 is considered.

II. DIFFERENT METHOD AND RESULT DESCRIPTIONS

Many procedures on the systematization of X-ray satellites spectra have been suggested by workers and these are discussed below:

2.1 Various procedures for the identification of parent line of X-ray satellites are suggested which are listed:

(i) Semi Moseley law given by Richtmyer[8] and according to which $(v_s - v_p)^{(\frac{1}{2})}$ vs. Z is linear (ii)$(v_s - v_p)$ vs.Z is linear law and was given by Idei[9] and (iii)$(\sqrt{v_s} - \sqrt{v_p})$ vs. Z is linear plot and known as Deodhercriterion[10].Here v_s and v_p denoted as satellite and parent line frequencies respectively .The identifications of parent line of satellites can be desided with the help of above linear plotting graphs.

2.2 To determine the energy of X-ray satellites there are only two procedure are established one is known as Moseley law[11] and other is iterative self-consistentprocedure[12],[5] these are discussed below.

2.2.1   Moseley Law:

The existence of Moseley law first time established by Misra and Kumar in satellite spectra [12].Further Tewari et al. [13] applied this law for the calculations of Lα satellites in the atomic number range 31 to 38.This law is summarize in brief as the square root of energy of satellite line increases with the increase of atomic number of atoms and can be represented as √E(ev) vs. Z plot is linear .This can be mathematically represented as [√E(ev) – (AZ+B)] where Z is atomic number of the atoms and A and B are constants of a particular straight line. The energy of missing element of particular line can be determined. However energy values which obtained are not too much precise and reliable in X-ray satellite spectra because more than one line each are observed in closed vicinity.

2.2.2   Iterative Procedure:

Misra et al. [14] have established first an empirical method which is based on the Moseley law and known as iterative self consistent doubly modified Moseley plot. A detail description of the method can be found in literatures (5, 12, 14).This procedure first applied by Kumar [5] in the systematization of the L X-ray satellites in (α, β, γ) series for $39 \leq Z \leq 80$.Various erroneous identification of L X-ray satellites have been removed in the study. Many satellites which have not been observed were calculated and their values found in close agreement to experimental wavelengths. The main drawback of iterative method is at least five experimental satellite data of line is required in the particular atomic number range which are in under consideration. Therefore various lines in different atomic number ranges may not be systematized.

III. CONCLUSION

It is clear from the above discussion that no any suitable method is established so far the energy value calculations as well as identifications of satellite line. Therefore it is strong need now to develop appropriate procedure for same purpose and also modify the X-ray satellites wavelengths data table.

IV. REFERENCES

[1].   M.Siegbahn and W.Stenstrom, Z.Physik 17, 48(1916) and Z.physik 17,318(1916).

[2].   M.J.Druyvesteyn, (1928), Het Rontgenspectrum vande tweede soort.Dissert, Groningen.

[3].   W.Stenstrom, Ann.der Phys.57, 347(1918).

[4].   Y.Cauchois and C.Senemaud, Longueurs d'onde des Emission X et des Discontinuities d'absorption X.2nd Ed, (Pergamon, Oxford) (1978).

[5].   N. Kumar, PhD. thesis, university of Lucknow, India,(2002).

[6].   B.B.Ray, Phil. Mag. 6, 64(1929).

[7].   P.Auger, C.R.Acad. Sci (Paris) 180, 65(1925).

[8].   F.K. Richtmyer, Phil. Mag. 6, 64(1928) and J. Franklin Inst.208, 325(1929).

[9].   S.Idei, Sci. Rep. Tohuku. Symp.Univ. I, A 13,382(1930a) and A 19,559(1930b).

[10]. G.B. Deodher, Proc.Roy.Soc. , London 131,476(1931).

[11]. H.G.J. Moseley, Phil.Mag.26, 1024(1913) and Phil. Mag. 27,703(1914).

[12]. U.D.Misra and N.Kumar, Indian J. of Pure and Applied Physics Vol. 42,891(2004) and Indian J. of Pure and Applied Physics, Vol.43, 83(2005).

[13]. Int.J. of Recent Technology and Engineering (IJRTE), vol.8, 5275(2019).

[14]. U.D.Misra et al., Z.phys.D.37, 127(1996).

On The Identification of Lα₄ and Lαˣ Satellite Lines

Nand Kumar[1], Sameer Sinha[2]

[1]Department of Physics, Jawaharlal Nehru Memorial P.G. College, Barabanki, Uttar Pradesh, India
[2]Department of Physics, G.S.P.G. College, Sultanpur, Uttar Pradesh, India

ABSTRACT

X-ray satellites are very weak lines in X-ray emission spectra. X-ray satellite lines are measured in the close approximation of the strong diagram lines which is called parent line of the satellite. The frequency of these X-ray satellite lines cannot be fitted in the normal energy level diagram of particular element. These lines are produced through a single transition in atom when atom goes in doubly ionized state. The measurement of their wavelengths and identifications for their origin are very difficult. Similar problem is in the identification of their parent line also. Various procedures on the identification of their origin and parent line have been put forwarded by researchers. The aim of present paper is to identify the Lα₄ and Lαˣ satellite lines.
Keyword: X-ray satellite, diagram lines, origin, identification, Moseley law.

I. INTRODUCTION

Electrons, ions and charged particles are most commonly used method for the excitations of target atoms. When target atoms go in excitations, mainly two events can takes place (i) A continuous X-ray spectrum occurred and (ii)if at least one of inner electrons from the target atom removed a vacancy is created in inner shell. An electron from any other shell jumps into inner shell and fills up the vacancy and a quantum of X-ray photon of energy hν $=E_i-E_f$ is emitted (ν is frequency , h is Planck's constant ,E_i is initial energy andE_f is final energy of levels involved).These observed spectrum from different combinations of E_i and E_f is called line emission spectrum which is characteristics of the target atom and called characteristic emission spectra. The emitted X-ray lines are called X-ray diagram lines which are originated from singly ionized atoms. Early in the development of X-ray spectroscopy some weak lines were also observed to close approximations of diagram lines which frequency did not fit in the natural energy level diagram of the particular atom and they were called " non-diagram lines" or X-ray satellite line of two related parent line(diagram line).On the basis of the their occurrence X-ray satellites can be classified generally in two broad groups one is called high frequency satellite(HFS) which is observed higher energy side of strong parent line and other is called low frequency satellite(LFS) which is observed lower energy side of parent line.The transition mechanism of X-ray satellites were explained by wentzel-Druyvestyen [1].According to the theory the emission of X-ray satellite may be represent as$PX \rightarrow XQ$ where 'X' acts as a spectator (P, X and Q denote energy level).Thus a X-ray satellite is emitted when a transition $PX \rightarrow XQ$ occurs in doubly ionised atom and the single level transition $P \rightarrow Q$ represents the parent line. Variousprocedure of their systematizations, identification of

parent line and their origin of emission have been put forwarded by researchers [2].Cauchois and Senemaud [3] have compiled wavelengths data of X-ray satellites of K,L and M series for almost atomic number of elements. The L series various satellite lines of Lα from atomic number 27 to 92 have been compiled in their tabulations. $L\alpha_4$ satellite line wavelengths are compiled for atomic number 27 to 56 and $L\alpha^x$ satellite line wavelengths are compiled for atomic number 62 to onwards with few exceptions [2].Present investigation is based on the identifications of $L\alpha_4$ and $L\alpha^x$ satellites for their same origin.

II. METHODOLOGY AND RESULT DESCRIPTION

Moseley law (1913, 1914) [4] is used for the identification of $L\alpha_4$ and $L\alpha^x$ satellite lines. This law is summarized as the characteristic X-ray emission spectra (diagram line spectraandsatellite line spectra [2] both),the frequency of the characteristics X-ray emission line are increased with the atomic numbers of the emitting atoms and this can be represented as $\sqrt{v/R}$= A(Z-σ) where A and σ are constants. This means than the under roots of energy of emission line is linearly proportional to the atomic number (Z) of atoms. The linear variation of the $\sqrt{v}$ or $\sqrt{eV}$ as a function of atomic number has made it possible to determine the relative energy positions of several elements by drawing as the so called Moseley plot$\sqrt{eV}$ versus Z. The existenceandthevalidity of this law in the case of X-ray satellite line spectra were first establishedby Misra and Kumar [5].Compilation of data of wavelengths of X-ray satellite in the Cauchois and Senemaud table have been used for the identification of $L\alpha_4$ and $L\alpha^x$ satellite lines with few exceptions. $L\alpha_3$,$L\alpha_4$ and$L\alpha_5$ satellite lines experimental data have been considered for the atomic number 39 to 56 and $L\alpha^x$satellite data taken for the atomic numbers range 57 to 80 with some missing data .Some wavelength of $L\alpha^x$satellite data for atomic number 58, 59, 60,   63 and 67 have been taken from literatures which were not compiled by Cauchois and Senemaud.Experimentallyobserved wavelengths data of these satellite lines are tabulated in X.U. which have been converting in eV to$\sqrt{eV}$ by using the conversion factor [6],λ (X.U.)*V (KeV) =12372.42.The $L\alpha_3$,$L\alpha_4$ and$L\alpha_5$satellites wavelengths (X.U.) and their$\sqrt{eV}$ values are listed in Table 1 for the atomic number range 39 to 56 and in Table 2 $L\alpha^x$ satellite line data are tabulated for the atomic number range 57 to 80 with few exceptions. The Moseley plots ($\sqrt{eV}$ vs Z) of $L\alpha_3$,$L\alpha_4$ and$L\alpha_5$for the atomic range 39 to 56 and also $L\alpha^x$ satellite line plot for the atomic number range 57 to 80 have been shown in figure 1and 2.This is reflected in the graph that L α_4 and L α^x lines are meeting at the same point on atomic number 57 on the extrapolation .Thus it is cleared from the graphsthat $L\alpha_4$ and $L\alpha^x$ satellite lines both are originated from same origin and the nomenclature of $L\alpha^x$satellite line from atomic number 58 to onward is wrong and which must be assigned to as $L\alpha_4$line. This is the first time the Moseley law is using for the identification of X-ray satellite line. Further investigation is needed from other theory.

Table 1. Experimentally Observed wavelengthsof $L\alpha_3$, $L\alpha_4$ and $L\alpha_5$ satellite lines for atomic number range 39 to 56 and their $\sqrt{eV}$ values.

Satellite Lines	Experimentally Observed $L\alpha_3$	Experimentally Observed $L\alpha_4$	Experimentally Observed $L\alpha_5$

Atomic Number(Z)	λ(X.U.)	$\sqrt{eV}$	λ(X.U.)	$\sqrt{eV}$	λ(X.U.)	$\sqrt{eV}$
39	6416.2	43.913	6410.8	43.931	6405.4	43.95
40	6038.5	45.265	6032.5	45.288	6026.5	45.31
41	5695.4	46.609	5689.6	46.632	5684.6	46.653
42	5383.3	47.941	5380	47.955	5374.8	47.978
43	-	-	-	-	-	-
44	4822.8	50.65	4817.8	50.676	4813.3	50.7
45	4575.4	52.001	4571.1	52.026	4566.6	52.051
46	4347	53.35	4342.7	53.376	4338.1	53.404
47	4134.7	54.702	4131	54.727	4126.5	54.757
48	3937.2	56.057	3933.8	56.082	3929.6	56.112
49	3753.7	57.411	3750.6	57.435	3744.6	57.481
50	3584.5	58.751	3579.7	58.79	3575.8	58.822
51	-	-	3419.6	60.151	3416.2	60.18
52	-	-	3270.9	61.503	3267.7	61.533
53	3138	62.791	3132.4	62.848	3129	62.882
54	-	-	-	-	-	-
55	2882.1	65.52	2879.1	65.554	-	-
56	2767.6	66.871	2760.4	66.949	2758	66.978

Table 2. Experimentally Observed wavelengthsofLα^xsatellite line for atomic number range 57 to 80 and their $\sqrt{eV}$ values.

Satellite Line ➜	Experimentally Observed Lα^x	
Atomic Number (Z)	λ (X.U.)	$\sqrt{eV}$
57	-	-
58	2544.5[7]	69.731
59	2447.6[7]	71.098
60	2354.9[2]	72.484
61	-	-
62	2189	75.18
63	2108[2]	76.611
64	2035.7	77.96
65	-	-

66	1898.1	80.736
67	1834.5[2]	82.214
68	1774.4	83.503
69	-	-
70	1662	86.28
71	1609.7	87.671
72	1560.11	89.053
73	1512.85	90.434
74	1467.25	91.828
75	1424.08	93.209
76	1383.07	94.581
77	1343.17	95.976
78	1305.23	97.361
79	1268.68	98.753
80	1233.38	100.156
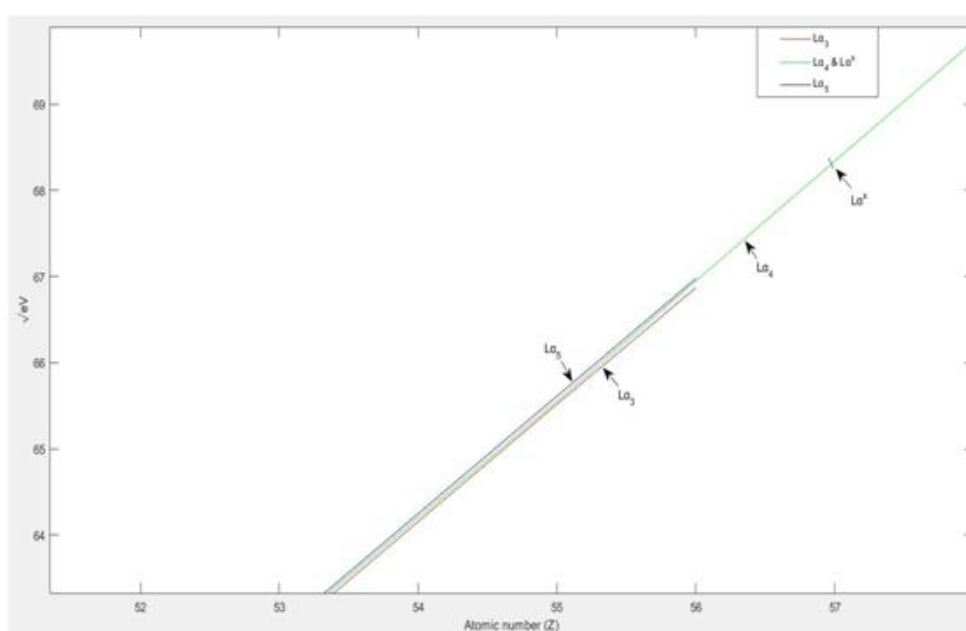
Fig.1: Moseley Plot of $L\alpha_3$, $L\alpha_4$ and $L\alpha_5$ satellite lines and $L\alpha^x$ satellite line for atomic number range 51 to onwards. Clearly $L\alpha_3$ and $L\alpha_5$ lines are reflected distinct to $L\alpha_4$, and $L\alpha_4$ and $L\alpha^x$ meet at a point Z=57 on extrapolation.
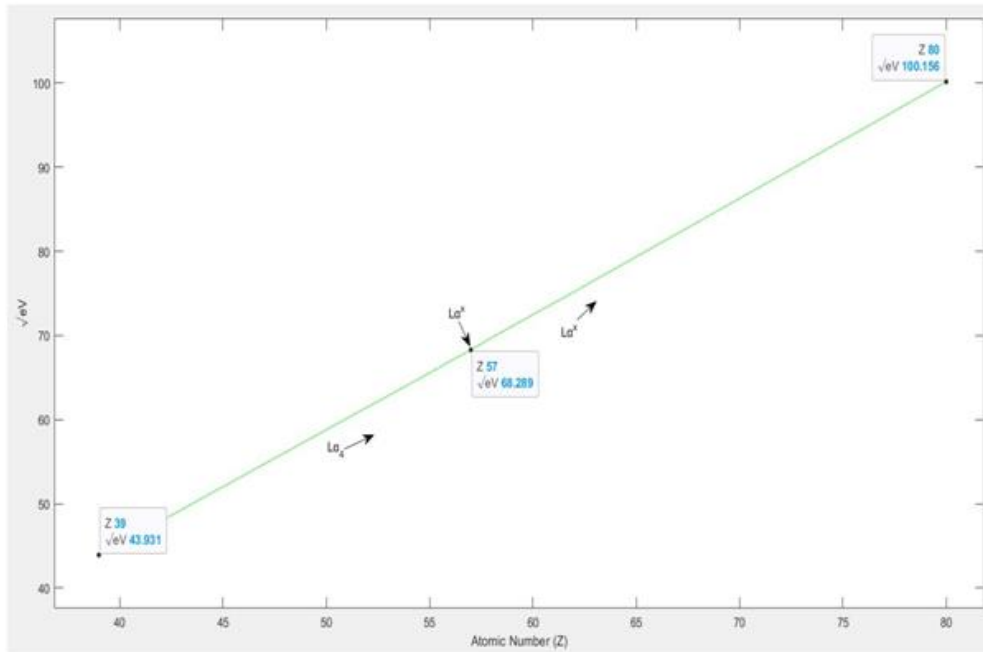
Fig. 2:Lα_4 and Lα^x satellite lines meet on the single straight line at Z=57.

III. REFERENCES

[1]. G.Wentzel, Ann.derPhysik, LPZ 66, 437(1921) and M.J.Druyvesteyn, Z.Phys, 43, 707 (1927).

[2]. N. Kumar,Ph.D. Thesis, University of Lucknow, India (2002).

[3]. Y.Cauchois and C. Senemaud, Longueursd'onde des Emission X et des Discontinuities d'absorption X.2nd Ed,(Pergamon,Oxford)(1978).

[4]. H.G.J.Moseley, Phil Mag 26, 1024(1913) and Phil Mag 27, 703(1914).

[5]. U.D.Misra and N.Kumar, Ind. J. of Pure and Applied Physics, 42, 891(2004) and 43,83(2005).

[6]. J.A. Bearden and A.F. Burr, Atomic Energy Levels,U.S. Atomic Energy Commission Report,NYO-2543-1,35(1965).

[7]. B.D.Srivastvaetal.Phys. Letters A 110(6) 323-326(1985).

Operational Transconductance Amplifier Based Universal Active Filter for Biomedical Signal Processing Unit

Syed Shamroz Arshad[1], SachchidaNand Shukla[1], Jitendra Singh[2]

[1]Department of Physics & Electronics, Dr. Rammanohar Lohia Avadh University, Ayodhya, Uttar Pradesh, India

[2]Department of Physics, Shri L.B.S. Degree College, Gonda, Uttar Pradesh, India

ABSTRACT

In this paper, design and analysis of OTA based universal active filter at 180nm technology is done. It employs two OTAs and two capacitors with three input terminals and one output terminal. With this filter, low pass, high pass, band pass and band reject filters can be realized by the proper combination of input signal. These filter circuits have been simulated in Cadence virtuoso tool under Spectre simulation. Simulation results show that theses filters, based on their cut-off frequencies, may be used in cost-effective radio frequency appliances and pre-amplifier stages of EEG signal acquisition unit. With low total power consumption in mW range, proposed filter circuits are found to operate excellently within temperature range -50℃ to +50℃. Less number of active components also make the proposed filter circuit easy for IC fabrication.

Keywords: OTA, Universal active filter, EEG, Candence.

I. INTRODUCTION

Universal active filters are widely used in various communication systems. Different types of active filters have been realized using different types of active devices viz., Op-Amp, OTA [1]. Operational transconductance amplifier (OTA), on the other hand, are frequently employed to configure universal active filters because it has large transconductance gain, simple circuit and can be tuned electronically [2]. Furthermore, OTA based filters have no passive components in their circuitry (ex. resistor, capacitor and inductor), therefore they can be suitable for IC fabrication [3]. In addition, these filters employ minimum numbers of active devices and passive devices, thus they reduce total power consumption and chip area of the circuit when they undergo IC fabrication [4]. While designing the OTA based universal active filter for biomedical signal processing, two things must be kept into consideration— (i)To determine the topologyof the filter appropriately which mainly depends on bandwidth, total harmonic distortion and signal to noise ratio and (ii) To determine that a given block used to design this filter satisfy the need of such signal processing system. In analog filter design THD and SNR are frequently used to describe the quality of the filter circuit [5]-[10].

In this article, a universal active filter based on operational transconductance amplifier has been designed which are found to be used in cost-effective radio frequency appliances and pre-amplifier stages of bio-

medical signal processing unit [11]-[14]. These filters employ two OTAs and two capacitors with three input terminals and one output terminal. Minimum numbers of active and passive components present in the circuit also make it highly suitable for IC fabrication. In this filter, proper combination of input signals result in different types of filters such as low pass, high pass, band pass and band reject filters [14]-[19].

Rest of the paper is organized as follows- circuit description is given in section II, results and discussion is explained in section III and finally conclusion is drawn in section IV.

II. CIRCUIT DESCRIPTION

Operational Transconductance amplifier (OTA) is basically a voltage controlled current source (VCCS) whose differential input produces an output current [1]. Basic circuit diagram of OTA and its symbol is shown in Figure 1.
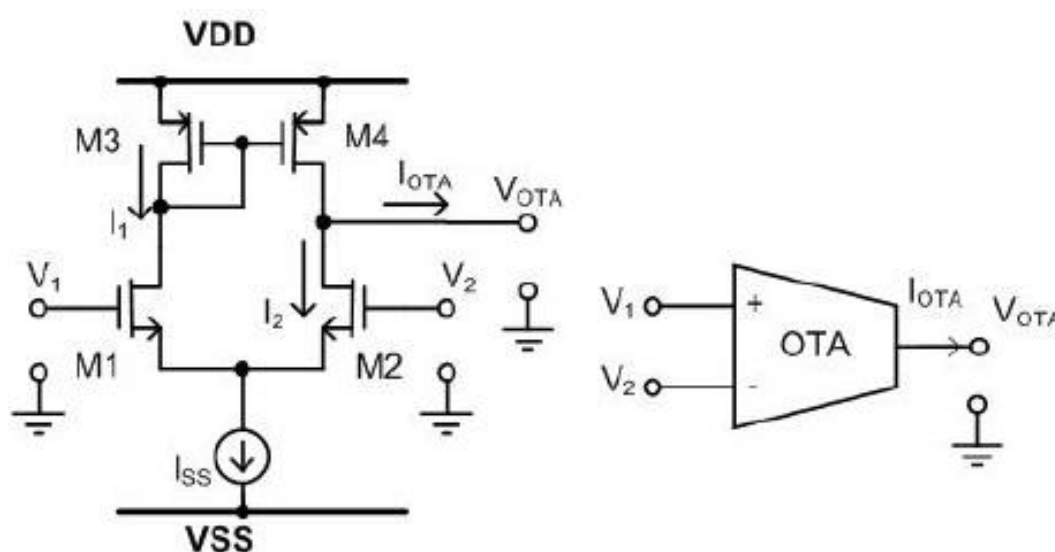
FIGURE 1: CIRCUIT DIAGRAM AND SYMBOL OF OTA

The ideal characteristics of an OTA can be given by the following expression—

$$I_{OUT} = (V_{IN+} - V_{IN-}) \times g_m$$

Where V_{IN+} is the voltage at positive terminal, V_{IN-} is the voltage at negative terminal and g_m is the transconductance of the amplifier. The Universal active filter based on OTA has been presented in Figure 2. Each filter circuit consists of two OTAs and two capacitors [2]-[8]. These filter circuits employ three input terminals and one output terminal. Basic circuit structure of all the filters is same. However, different input signals are used to realize different filter circuits. These combinations of input signals are listed in TABLE 1.

TABLE1: **INPUT SIGNAL COMBINATIONSTO REALISE FILTERS**

Filter Circuits	V₁	V₂	V₃
Low Pass Filter	Input Signal	0	0
High Pass Filter	0		Input Signal
Band Pass Filter	0	Input Signal	0
BandReject Filter	Input Signal	0	Input Signal

The aspect ratio of NMOS transistor is w/l = 5µ/1µ whereas for PMOS transistor, it is w/l = 10 µ/1µ. Different circuital components of all the filters with their respective values have been listed in TABLE 2.

TABLE2: **DESCRIPTION OF CIRCUITAL PARAMETERS**

Circuit Components	Low Pass Filter	High Pass Filter	Band Pass Filter	Band Reject Filter
Input Voltage at terminal, V_1	10 mV at 1KHz	--	--	10 mV at 1KHz
Input Voltage at terminal, V_2	--	---	1 V at 1 KHz	--
Input Voltage at terminal, V_3	--	2 V at 1 KHz	--	10 mV at 1KHz
Source Supply voltage, V_{SS}	-1.25 Volt	-1.25 Volt	-0.8 Volt	-1.25 Volt
Drain Supply Voltage, V_{DD}	+1.25 Volt	+1.25 Volt	+0.1 Volt	+1.25 Volt
Input Capacitance, C_1	10 pF	10 pF	1 µF	10 pF
Output Capacitance, C_2	10 pF	10 pF	1 µF	10 pF
Base Current, I_{DC}	50 µA	50 µA	50 µA	50 µA

Schematic of low pass filter, high pass filter, band pass filter and band reject filter has been depicted in figure 2.1, 2.2, 2.3 and 2.4 respectively. These filter circuits have been realized in Cadence virtuoso tool at 180nm technology under Spectre simulation.
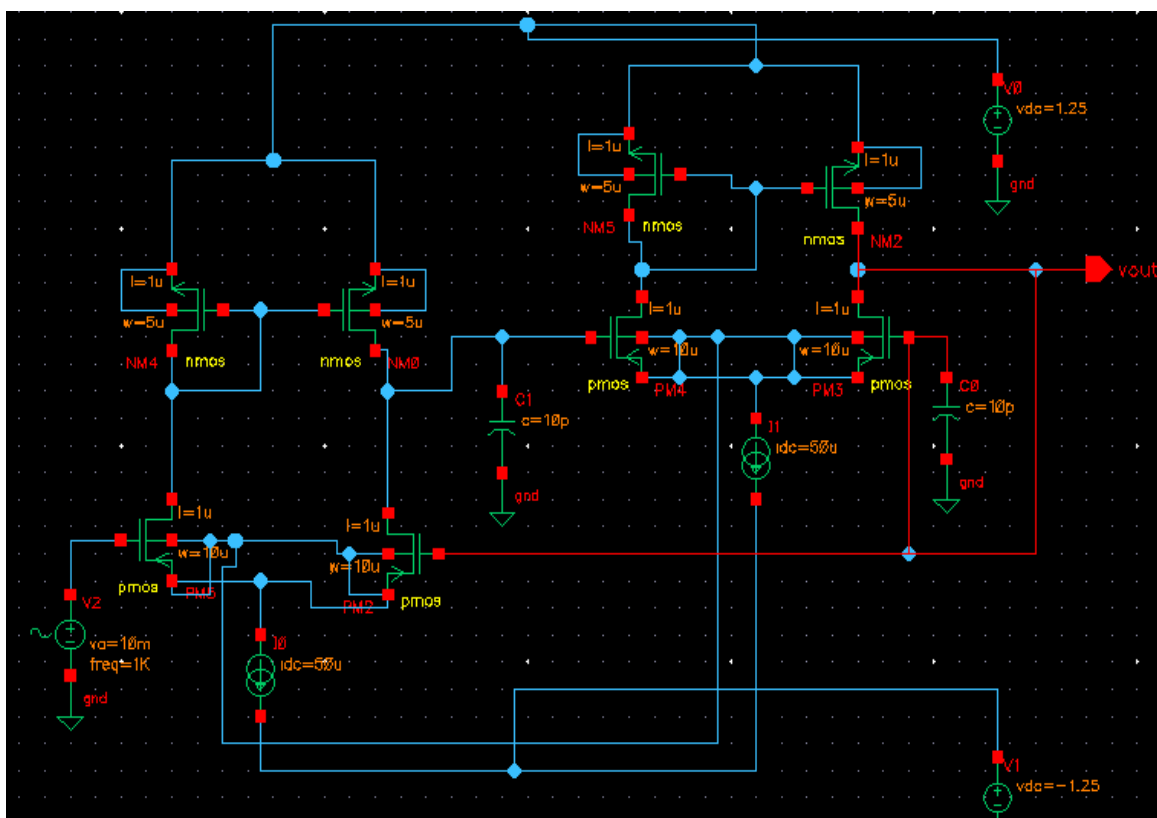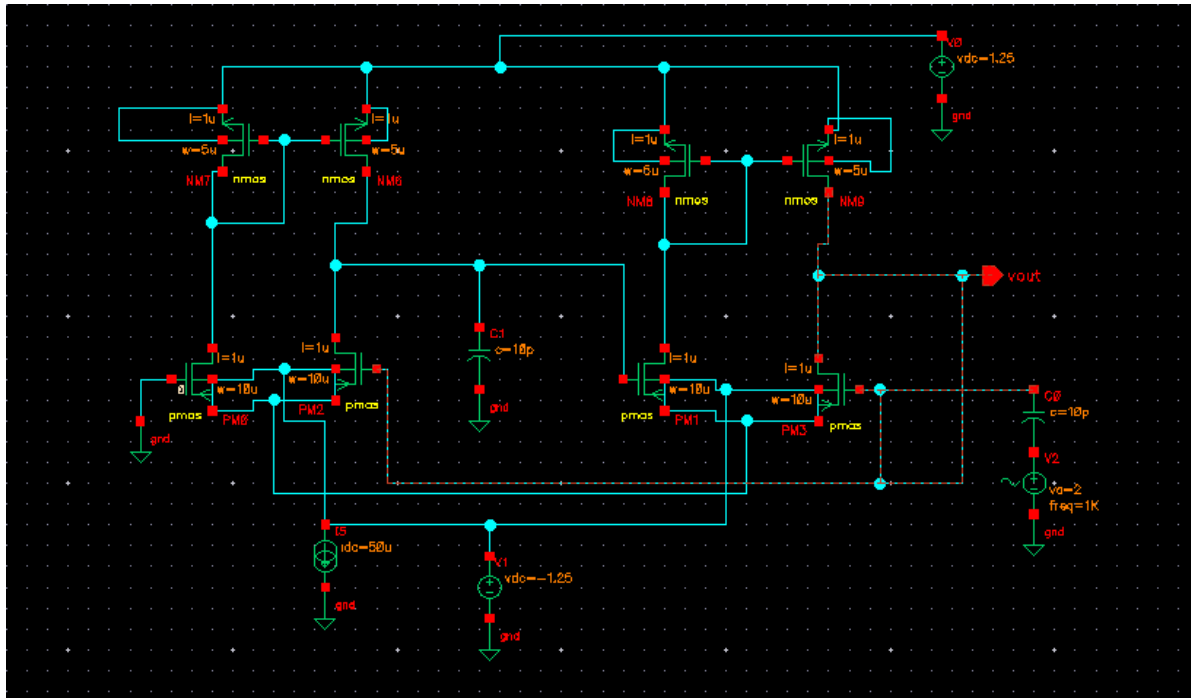

FIGURE 2.1: SCHEMATIC OF LOW PASS FILTER

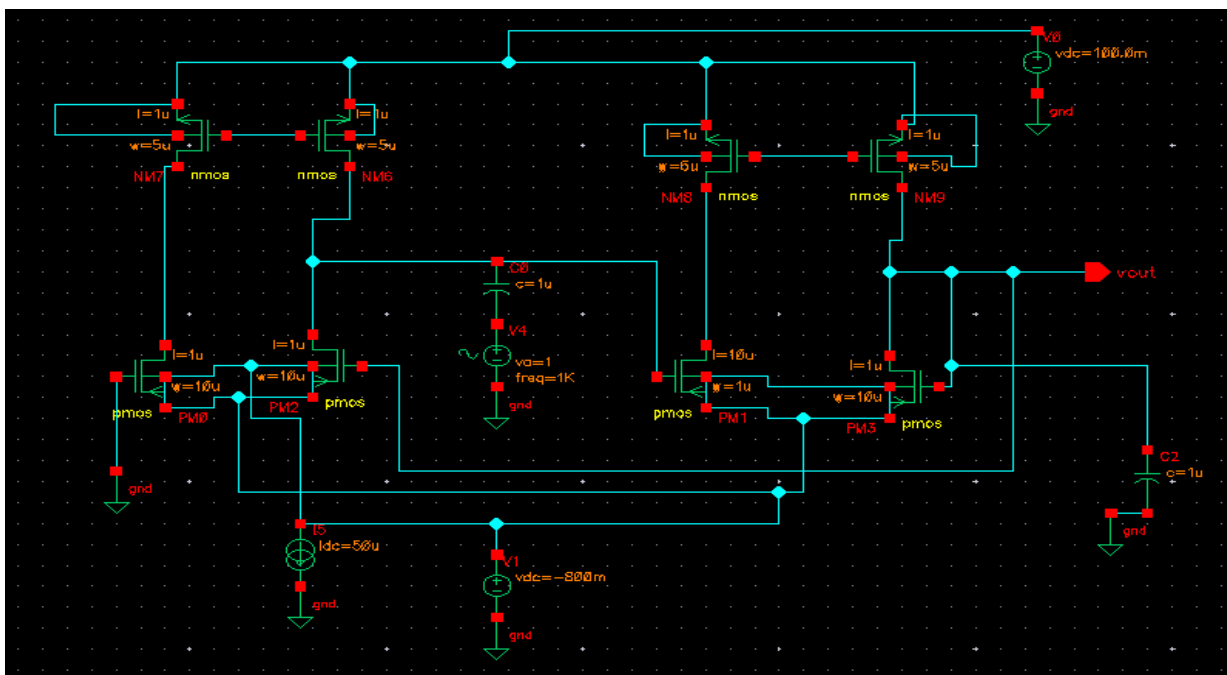FIGURE 2.2: SCHEMATIC OF HIGH PASS FILTER
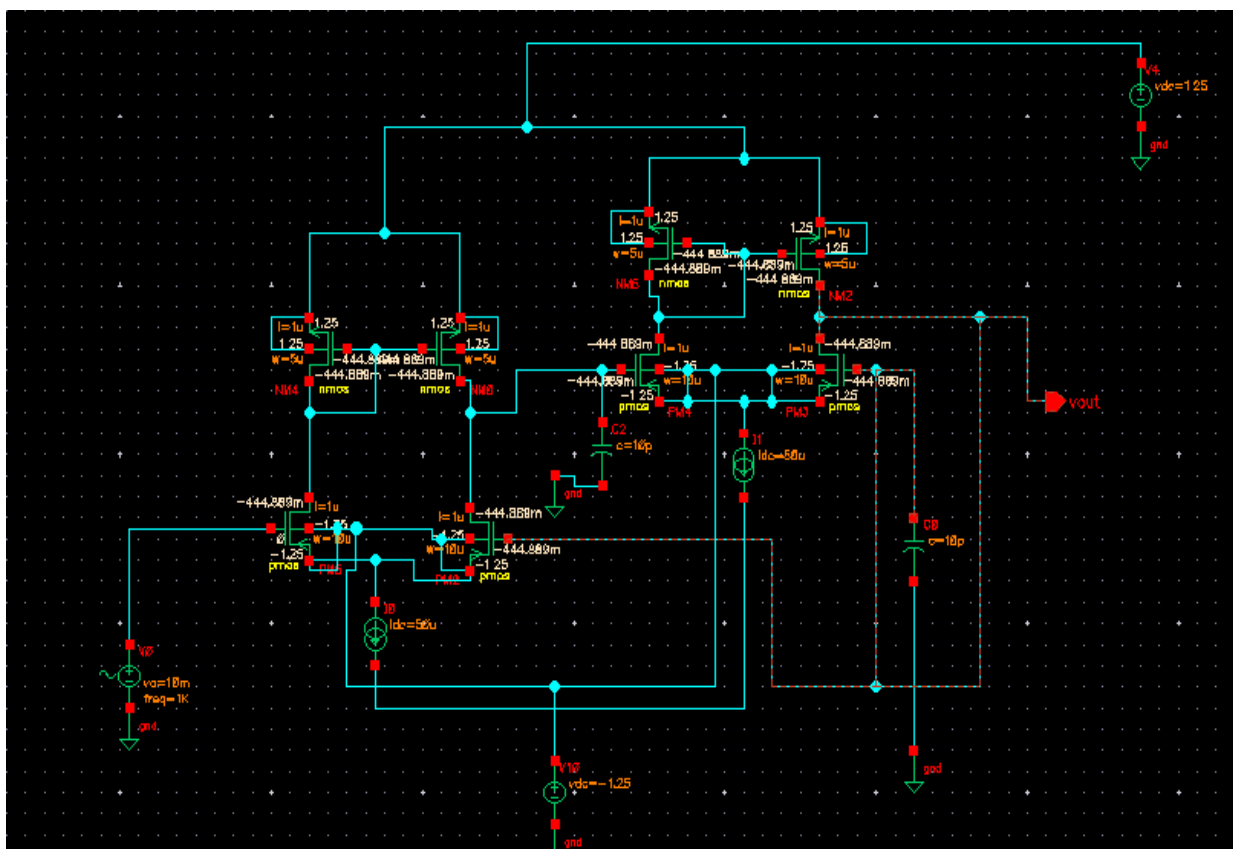

FIGURE 2.3: SCHEMATIC OF BAND PASS FILTER

FIGURE 2.4: SCHEMATIC OF BAND REJECT FILTER

III. RESULTS AND DISCUSSION

The proposed filter circuits are simulated using cadence virtuoso tool in 180nm technology at room temperature and respective cut-off frequencies and output voltages are recorded in TABLE 3.

TABLE3: **CUT-OFF FREQUENCY OF THE FILTER CIRCUITS**

Filter Circuit	Cut-off Frequency (Approx.)	Output Voltage
Low Pass Filter	0.3 MHz	60 mV
High Pass Filter	52.1 GHz	56.8 mV
Band Pass Filter	98 Hz - 26 Hz	415.5 nV
Band Reject Filter	40 Hz - 50.6 Hz	0.8 V

Refer Table 3. Low pass and high pass filter circuit produces high cut-off frequencies (under MHz and GHz ranges); thus, they may be used in cost-effective radio frequency appliances [9]. Similarly, band pass and band reject filter circuit generate low cut-off frequencies (≤100 Hz), hence they may be used in pre amplifier stages of EEG/ biomedical signal processing circuit as shown in Figure 3 [10]-[16].

Frequency response curve of low pass, high pass, band pass and band reject filters are depicted in Figure 4.1, 4.2. 4.3 and 4.4 respectively. It is also found that these filters produce excellent temperature stability over - 50℃ to +50℃ and dissipates low power in mW range [17]-[19].
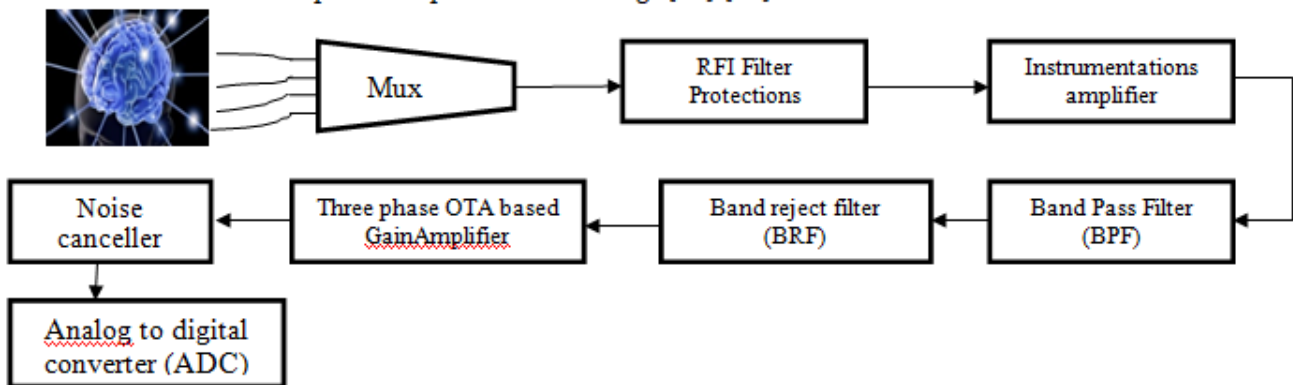

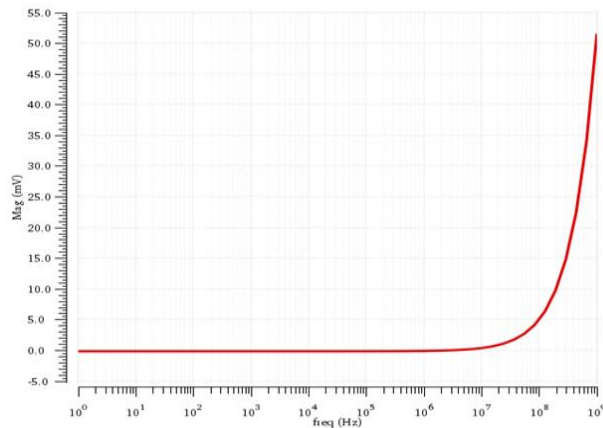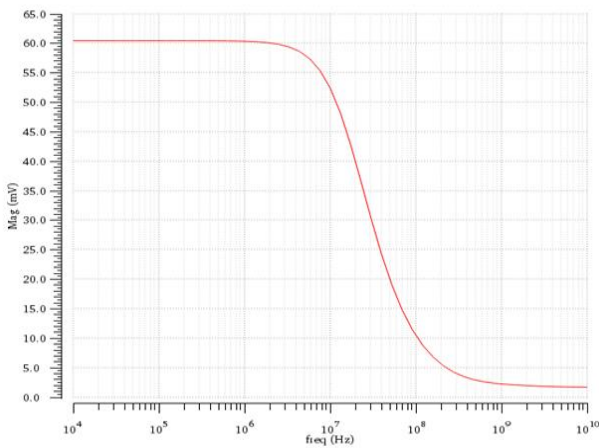FIGURE 3: BLOCK DIAGRAM OF NEURAL SIGNAL PROCESSING

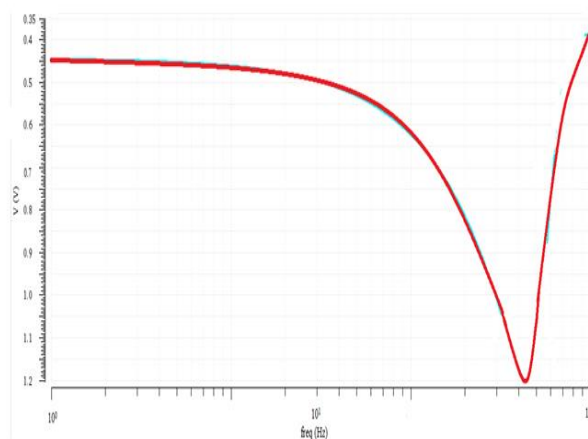FIGURE 4.1: RESPONSE CURVE OF LOW PASS FILTER FIGURE 4.2: RESPONSE CURVE OF HIGH PASS FILTER
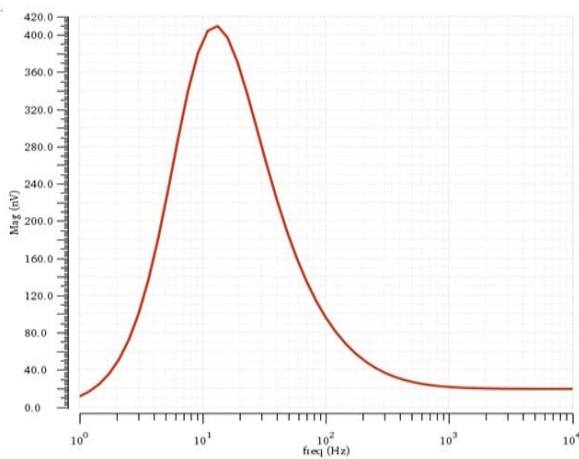

FIGURE 4.3: RESPONSE CURVE OF BAND PASS FILTER FIGURE 4.4: RESPONSE CURVE OF BAND REJECT FILTER

IV. CONCLUSION

In this article, a universal active filter based on OTA has been proposed and analyzed using Cadence virtuoso tool at 180nm technology. Different input signal combinations have been used to realize different filters viz., low pass, high pass, band pass and band reject filters. Theses filters employ two OTAs and two capacitors having three input terminals and one output terminals. It is found that band pass and band reject filters, having cut-off frequency less than 100 Hz, could be used in EEG or biomedical signal processing unit whereas low pass and high pass filter, with cut-off frequency in MHz-GHz range, could be used in cost-effective radio frequency appliances.It is also found that these filters produce excellent temperature stability over -50℃ to +50℃ and dissipates low power in mW range. In addition, minimum number of active components present in the filter also make it easy for IC fabrication.

V. REFERENCES

[1]. Rahul Kumar, D. S. Ajnar, P. K. Jain, "Design of biquad universal filter using operational transcondictance amplifier in 180nm technology", International Journal Of Engineering Research And Application, Vol. 4, Issue 5 (Version 2), May 2014, pp. 120-125.

[2]. Moradi, Marzieh, MassoudDousti, and PooyaTorkzadeh. "Designing a Low-Power LNA and Filter for Portable EEG Acquisition Applications" IEEE Access, Vol. 9, 2021, pp. 71968-71978.

[3]. Mohammad ArifSobhanBhuiyan, MasturaBinti Omar, Mamun Bin IbneReaz, Noorfazila Kamal and Sawal Hamid Md Ali, "A Complementary metal oxide semiconductor (CMOS) band-pass filter for cost-effective radio frequency applinaces", Journal of Engineering Research, vol. 4, no. 3, pp. 114-127, September 2016.

[4]. Lee, Shuenn-Yuh, and Chih-Jen Cheng. "Systematic design and modeling of a OTA-C filter for portable ECG detection." IEEE Transactions on Biomedical Circuits and Systems, Vol. 3, no. 1, 2009,pp. 53-64.

[5]. F. Khateb, P. Prommee and T. Kulej, "MIOTA-Based Filters for Noise and Motion Artifact Reductions in Biosignal Acquisition," IEEE Access, vol. 10, 2022, pp. 14325-14338, doi: 10.1109/ACCESS.2022.3147665.

[6]. Rodriguez-Villegas, Esther, Alexander J. Casson, and Phil Corbishley. "A subhertznanopower low-pass filter." IEEE Transactions on Circuits and Systems II: Express Briefs, Vol. 58, no. 6, 2011 pp. 351-355.

[7]. Liu, Zexue, Yi Tan, Heyi Li, Haoyun Jiang, Junhua Liu, and Huailin Liao. "A 0.5-V 3.69-nW complementary Source-Follower-C based low-pass filter for wearable biomedical applications." IEEE Transactions on Circuits and Systems I: Regular Papers, Vol. 67, no. 12, 2020 pp. 4370-4381.

[8]. Chien, Chao-Liang, Chung-Chih Hung, and Chia-Wei Chen. "A pseudo-differential OTA with linearity improving by HD3 feedforward." In 2009 IEEE Asian Solid-State Circuits Conference, , 2009, pp. 237-240.

[9]. Sergio Solis Bustos, Jose Silva Martinez, Franco Maloberti and Edgar Sanchez-Sinencio, "A 60-dB Dynamic-Range CMOS SixthOrder 2.4-Hz Low-Pass Filter for Medical Applications", IEEE

Transactions on Circuits and Systems, vol. 47, no.12, December 2000,pp. 1391- 1398, doi: 10.1109/82.899631.

[10]. Mahmoud, Soliman A., Ahmed Bamakhramah, and Saeed A. Al-Tunaiji. "Low-Noise Low-Pass Filter for ECG Portable Detection systems with Digitally Programmable Range." Circuits, Systems, and Signal Processing, vol. 32, no. 5, 2013,pp. 2029-2045, doi: 10.1007/s00034-013-9564-9.

[11]. SachchidaNandShukla, SyedShamrozArshad and GeetikaSrivastava, "NPN Sziklai pair small-signal amplifier for high gain low noise submicron voltage recorder",International Journal of Power Electronics and Drive Systems, Vol. 13, No. 1, March 2022,pp. 11-22, DOI: 10.11591/ijpeds.v13.i1.pp11-22

[12]. SachchidaNandShukla, GeetikaSrivastava, and SyedShamrozArshad, "Study of Low-Noise Wide-Band Tuned Sziklai Pair Small-Signal Amplifier", Research Trends and Challenges in Physical Science, Vol. 1, August 2021,pp.1-16, DOI: 10.9734/bpi/rtcps/v1/4064F

[13]. Sergio Solis Bustos, Jose Silva Martinez, Franco Maloberti and Edgar Sanchez-Sinencio, "A 60-dB Dynamic-Range CMOS SixthOrder 2.4-Hz Low-Pass Filter for Medical Applications", IEEE Transactions on Circuits and Systems, vol. 47, no.12, December 2000, pp. 1391- 1398, doi: 10.1109/82.899631.

[14]. Mahmoud, Soliman A., Ahmed Bamakhramah, and Saeed A. Al-Tunaiji. "Low-Noise Low-Pass Filter for ECG Portable Detection systems with Digitally Programmable Range." Circuits, Systems, and Signal Processing, vol. 32, no. 5, 2013,pp. 2029-2045, doi: 10.1007/s00034-013-9564-9.

[15]. Karimi-Bidhendi, Alireza, OmidMalekzadeh-Arasteh, Mao-Cheng Lee, Colin M. McCrimmon, Po T. Wang, AkshayMahajan, Charles Yu Liu, ZoranNenadic, An H. Do and PayamHeydari. "CMOS Ultralow Power Brain Signal Aquisition Front-Ends: Design and Human Testing", in IEEE Transactions on Biomedical Circuits and Systems, vol. 11, no. 5, Oct. 2017,pp. 1111-1122, doi: 10.1109/TBCAS.2017.2723607.

[16]. Prommee, Pipat, KhunanonKarawanich, Fabian Khateb, and Tomasz Kulej. "Voltage-mode elliptic band-pass filter based on multiple-input transconductor." IEEE Access, vol. 9,pp. 32582-32590, 2021.

[17]. Kumngern, Montree, Fabian Khateb, Tomasz Kulej, and Costas Psychalinos. "Multiple-Input Universal Filter and Quadrature Oscillator Using Multiple-Input Operational Transconductance Amplifiers." IEEE Access, vol. 9,pp. 56253-56263, 2021.

[18]. F. Khateb, P. Prommee and T. Kulej, "MIOTA-Based Filters for Noise and Motion Artifact Reductions in Biosignal Acquisition," in IEEE Access, vol. 10, 2022,pp. 14325-14338,doi: 10.1109/ACCESS.2022.3147665.

[19]. Garcia-Alberdi, Coro, Antonio J. Lopez-Martin, Lucia Acosta, Ramon G. Carvajal, and Jaime Ramirez-Angulo. "Tunable class AB CMOS Gm-C filter based on quasi-floating gate techniques." IEEE Transactions on Circuits and Systems I: Regular Papers, vol. 60, no. 5,pp. 1300-1309, 2012.

IJSRST

National Conference
on
"Smart Materials and Devices for Sustainable Technologies"

Organized By
Department of Physics & IQAC
Shri Lal Bahadur Shastri Degree College, Gonda, U.P.
(Affiliated to Dr. R.M.L. Avadh University Ayodhya, U.P.)
Co-Sponsored by
Satya Saroj Foundation, Gonda
&
State Bank of India, Main Branch, Gonda